

**Polyaniline Coated**  
**Short Nylon Fiber/Elastomer Composites:**  
**Electrical and Microwave Characteristics**

**Saritha Chandran A.**

Submitted by: Saritha Chandran A.,  
36/569 A, Pothannoor Sudhalayam,  
St. Francis Xavier Church Cross Road,  
South Kaloor, Ernakulam,  
Cochin- 682 017.  
sarithachan@yahoo.co.in  
sarithachandran@gmail.com

Supervisor: Prof. (Dr.) Sunil K. Narayanankutty  
sunil@cusat.ac.in  
<http://psrt.cusat.ac.in/sunil/index.html>

**Subject headings:** conducting polymer composites / polyaniline / polyaniline coated  
short nylon fiber / natural rubber / chloroprene rubber / etching / *in situ*  
polymerization / mechanical properties / electrical conductivity / dielectric properties  
/ microwave characteristics

Being multidisciplinary, the work described in this dissertation was carried out at the Dept. of  
Polymer Science and Rubber Technology, the Magnetism lab of the Dept. of Physics and CREMA  
of the Dept. of Electronics of Cochin University of Science and Technology. The research was  
funded by the Cochin University of Science and Technology.

Cover: Electromagnetic interference shielding by conducting elastomer composite  
Designed by: Saritha Chandran A. and K. Ajith Kumar

**Polyaniline Coated  
Short Nylon Fiber/Elastomer Composites:  
Electrical and Microwave Characteristics**

*Thesis submitted to*

**Cochin University of Science and Technology**

*in partial fulfillment of the requirements for the award of the degree of*

**Doctor of Philosophy**

*under the*

**Faculty of Technology**

*by*

**Saritha Chandran A.**



**Department of Polymer Science and Rubber Technology  
Cochin University of Science and Technology  
Cochin- 682 022, Kerala, India  
<http://psrt.cusat.ac.in>**

**July 2008**



**Dept. of Polymer Science and Rubber Technology  
Cochin University of Science and Technology  
Cochin-22, Kerala**

**Ph: 0091 484 2575723**

**Fax: 0091 484 2577747**

**Dr. Sunil K. Narayanankutty  
Professor**

### **Certificate**

Certified that, the thesis entitled **‘Polyaniline Coated Short Nylon Fiber/Elastomer Composites: Electrical and Microwave Characteristics’** being submitted to Cochin University of Science and Technology under the Faculty of Technology, by Ms. Saritha Chandran A., is an authentic record of the original research carried out by her under my supervision and guidance. The thesis has fulfilled all the requirements as per regulations and no part of the results embodied has been submitted to any other institution for any other degree/diploma.

Cochin  
28<sup>th</sup> July 2008

Sunil K. Narayanankutty



## Declaration

I hereby declare that the thesis entitled **‘Polyaniline Coated Short Nylon Fiber/Elastomer Composites: Electrical and Microwave Characteristics’** being submitted to Cochin University of Science and Technology under the Faculty of Technology is based on the original research carried out by me under the supervision of Dr. Sunil K. Narayanankutty, Professor, Dept. of Polymer Science and Rubber Technology and that no part of the results presented has been submitted to any other institution for any other degree/diploma.

Cochin  
28<sup>th</sup> July 2008

Saritha Chandran A.



*....To he who paved the way, for his firm conviction and  
unreeling support throughout....*

## *Acknowledgements*

---

This is a moment of great satisfaction, to realize that I have reached this point; acknowledging all those who have extended support to this successful venture. It is with a medley of emotions that I remember all of them. I have seen my seniors at this stage; I have seen their face glow with great happiness, confidence and satisfaction. Hardly could I understand their emotions then. Little did I realize that I would ever walk to this juncture to follow their heart fully.

My guide and mentor, Dr. Sunil K. Narayanankutty is an amazing person with a positive attitude to others. I feel a warmth entering his room. I can chat with him as freely as I do with my friends; rarely do I realize that I am talking to my supervisor. All through these four years of association with him, there has never been a moment that he went mad at me; not because that I was flawless, but because that he had so much patience. I wish to express my gratitude and love to you, Sir.

I wish to express my gratitude to Dr. M. R. Anantharaman, Dept. of Physics and Dr. P. Mohanan, Department of Electronics, Cochin University of Science and Technology for permitting me to carry out the dielectric and microwave measurements. Two chapters of this thesis were entirely molded at their labs. I extend my gratefulness to Dr. K. T. Mathew, Dept. of Electronics, for allowing me to use the network analyzer and his willingness to clarify my doubts.

I am thankful to all the faculty members of PSRT; Dr. K. E. George, Dr. Rani Joseph, Dr. Thomas Kurian, Dr. Philip Kurian, Dr. Eby Thomas Thachil and Ms. Jayalatha Gopalakrishnan for their whole-hearted support and well wishes. A special word of thanks to the office staff of PSRT for their prompt support with the administrative formalities.

### *Acknowledgements*

---

I recall some of the first faces I saw when I joined this department: my seniors Dr. Aswathy P. V., Dr. Lity Alen Varghese, Dr. Rinku Mariam, Dr. Soney Varghese, Dr. Thomas N. Abraham, Dr. Vipin Rajan and Dr. Ushamani. They have offered me a very comfortable atmosphere at PSRT. I would like to thank Dr. Lovely Mathew who used to take me around with special love and care. She was very supporting and tried to boost up my confidence, especially when I was totally down and confused. Dr. Honey John is another person whom I want to thank, for her enthusiasm in my work and for the useful suggestions. I had a very jovial relationship with Dr. Maya. Dr. Nisha Radhakrishnan is a close pal of mine, who talks on and on ..... and on.....

The best friend is one, whose face flashes in your mind when in a crisis or need. And the face that comes to my mind is yours, Anoop. Though I deny to you, I learnt a lot from you. I honestly appreciate your concern about making my thesis impeccable. You often remind me of my Dad; you sound just like him at times, you too always look for that “style and standard” and you are as authoritative as him. Well... after all, you are “the incredible Anoop”!!

My heart-felt gratitude to my fellow researchers: Bipin, who was always willing to extend a hand of assistance to me, Julie, Leny, Raju and Reshmi. With immense pleasure, I thank Ansu, Bhuvaneswary, Parameswaran and Vijayalekshmi for the marvelous companionship; I had some rocking moments with you. I express my appreciation to Abhilash, Dhanya, Priya, Sreekanth and Vinoj for being so affable. I am grateful to the ‘FIPs’, Dr. Joshy, Jude, Mary, Prema (for the valuable tips), Sreenivasan and Dr. Unnikrishanan for being so friendly. I cannot help recalling Rajesh. He used to be a good friend of mine and showed a lot of interest in my work. The well wishes of the new members of PSRT; Ajilesh, Anna, Jinesh, Neena, Nimmy and Vidya are highly appreciated.

My sincere acknowledgements are to be expressed here to Deepu, Praveen, Robin and Sujith, Dept. of Electronics, for helping me with the microwave measurements. I could enjoy the benefit of excellent support and assistance from Vijutha, Magnetics lab, Dept. of Physics in the tedious dielectric measurements. I offer my deepest sense of gratitude to her. I would also like to thank Harikrishna Reghunathan (NCL, Pune)

### *Acknowledgements*

---

for XPS spectra. A special thanks to James for supplying me with necessary literature, Sareena and Sreedevi for the wonderful friendship.

I am greatly indebted to my parents for their endless inspiration, moral support and immense patience. Hadn't been for them, I would never have reached this phase of life. I thank my father for providing me with all the facilities and fulfilling all my genuine necessities with utmost care. He has always kept himself updated on my progress. I take this opportunity to express my love to my dear brother Appu.

I thank my Dad and Uma aunty for their kind concern and love. I adore you the way you are, Dad. Though you couldn't be with me always, you catch up my mind more easily. And that's why I love you.

I bow my head to His Almighty who has always showered blessings upon me for the successful completion of this research.

*Saritha Chandran A.*

## *Contents*

---

<b>Preface</b>	<b>I</b>
<b>Chapter 1 General Introduction</b>	<b>1</b>
1.1 Polyaniline	2
1.1.1 The birth and growth	3
1.1.2 The structure	4
1.1.3 Doping	6
1.1.4 Charge storage and conduction	7
1.1.5 Synthesis	10
1.2 Polyaniline/polymer blends and composites	11
1.2.1 Conducting fibers	12
1.2.2 Conducting elastomer composites	15
1.2.2.1 State-of-art research	16
1.3 Conduction processes	20
1.4 Dielectric spectroscopy	23
1.4.1 Polarization	24
1.5 Microwave technology	27
1.5.1 Electromagnetic shielding	29
1.5.2 Radar absorbing materials	30
1.6 Objectives of the current work	31
References	32

<b>Chapter 2</b>	<b>Polyaniline coated short Nylon fiber</b>	<b>41</b>
2.1	Introduction	41
2.2	Experimental	44
2.2.1	Materials	44
2.2.2	Preparation of polyaniline	44
2.2.3	Etching treatment	44
2.2.4	<i>In situ</i> polymerization	44
2.2.5	Characterization	45
2.3	Results and discussion	50
2.3.1	Characterization of polyaniline	50
2.3.1.1	Scanning electron microscopy	50
2.3.1.2	Infrared spectroscopy	51
2.3.1.3	X-ray diffraction analysis	52
2.3.1.4	Thermal analysis	53
2.3.2	Etching of Nylon fiber	54
2.3.2.1	Strength of the fiber	54
2.3.2.2	Surface characteristics	55
2.3.2.3	Thermal characteristics	58
2.3.3	PANI coated Nylon fiber	60
2.3.3.1	Strength of the fiber	60
2.3.3.2	DC electrical conductivity	61
2.3.3.3	Scanning electron microscopy	62
2.3.3.4	Infrared spectroscopy	63
2.3.3.5	X-ray diffraction analysis	64
2.3.3.6	Thermal stability	64
2.4	Conclusions	67
	References	67



<b>Chapter 3</b>	<b>PANI coated short fiber reinforced natural rubber conducting composites: Fabrication and characterization</b>	<b>71</b>
3.1	Natural rubber	71
3.2	Conducting natural rubber composites	73
3.2.1	Materials	73
3.2.2	Preparation of conducting polymer composites	74
3.2.3	Cure characteristics and kinetics	75
3.2.4	Filler dispersion	76
3.2.5	Mechanical properties	77
3.2.6	Morphological characterization	78
3.2.7	DC electrical conductivity	78
3.2.8	Thermogravimetric analysis	78
3.3	Results and discussion	82
3.3.1	Cure characteristics of the CPCs	82
3.3.2	Cure kinetics	85
3.3.3	Filler dispersion in the CPCs	87
3.3.4	Mechanical properties of the CPCs	88
3.3.5	Morphology	90
3.3.6	DC electrical conductivity of the CPCs	92
3.3.7	Thermal stability	93
3.3.7.1	Thermal degradation kinetics	96
3.4	Conclusions	98
	References	98

**Chapter 4 PANI coated short fiber reinforced chloroprene  
rubber conducting composites: Preparation and  
characterization 103**

4.1	Chloroprene rubber	103
4.2	Conducting chloroprene rubber composites	105
4.2.1	Composite preparation	105
4.2.2	Characterization	106
4.3	Results and discussion	106
4.3.1	Cure characteristics	106
4.3.2	Cure kinetics	109
4.3.3	Filler dispersion	110
4.3.4	Mechanical properties	112
4.3.5	Morphology	116
4.3.6	DC electrical conductivity	117
4.3.7	Thermal analysis	117
4.3.7.1	Thermal degradation kinetics	121
4.4	Conclusions	124
	References	124

**Chapter 5 Dielectric properties of conducting  
elastomer composites 127**

5.1	Introduction	127
5.2	Dielectric measurements	131
5.2.1	Method of measurements	131
5.2.2	Cell for the measurements	132
5.3	Results and discussion	134
5.3.1	Dielectric permittivity	134
5.3.1.1	Frequency dependence of pristine PANI	134

## *Contents*

---

5.3.1.2	Temperature dependence of pristine PANI	135
5.3.1.3	Frequency dependence of dielectric loss factor of pristine PANI	136
5.3.1.4	Effect of frequency of NR gum vulcanizate	139
5.3.1.5	Effect of temperature of NR gum vulcanizate	140
5.3.1.6	Frequency dependence of NR based CPCs	141
5.3.1.7	Temperature dependence of NR based CPCs	143
5.3.1.8	Effect of loading of NR based CPCs	144
5.3.1.9	Effect of frequency and temperature of CR gum vulcanizates	145
5.3.1.10	Frequency dependence of CR based CPCs	146
5.3.1.11	Temperature dependence of CR based CPCs	147
5.3.1.12	Loading dependence of CR based CPCs	149
5.3.1.13	Tailoring of dielectric permittivity of the CPCs	149
5.3.2	AC conductivity	153
5.3.2.1	Frequency dependence of pristine PANI	154
5.3.2.2	Temperature dependence of pristine PANI	156
5.3.2.3	Effect of frequency of NR based CPCs	157
5.3.2.4	Effect of temperature of NR based CPCs	158
5.3.2.5	Loading dependence of NR based CPCs	159
5.3.2.6	Frequency dependence of CR based CPCs	160
5.3.2.7	Effect of temperature of CR based CPCs	162
5.3.2.8	Loading dependence of CR based CPCs	163
5.4	Conclusions	164
	References	165

<b>Chapter 6</b>	<b>Microwave characteristics of conducting elastomer composites</b>	<b>169</b>
6.1	Introduction	169
6.2	Measurement of microwave properties by cavity perturbation technique	171
6.2.1	Design of rectangular wave-guide cavities	171
6.2.2	Theory of microwave characterization	173
6.3	Results and discussion	175
6.3.1	Permittivity measurements	175
6.3.1.1	Dielectric permittivity of NR based CPCs	175
6.3.1.2	Loss tangent of NR based CPCs	178
6.3.1.3	Heating coefficient of NR based CPCs	180
6.3.1.4	Conductivity, absorption coefficient and skin depth of NR based CPCs	182
6.3.1.5	Dielectric permittivity of CR based CPCs	183
6.3.1.6	Loss tangent of CR based CPCs	184
6.3.1.7	Heating coefficient of CR based CPCs	185
6.3.1.8	Conductivity, absorption coefficient and skin depth of CR based CPCs	187
6.3.2	Electromagnetic interference shielding	187
6.3.2.1	Theory of electromagnetic shielding	188
6.3.2.2	Measurement technique	189
6.3.2.3	The shielding effectiveness	190
6.4	Conclusions	193
	References	194

<b>Chapter 7 Summary and conclusions</b>	<b>197</b>
<b>Index of abbreviations and symbols</b>	<b>201</b>
<b>Author index</b>	<b>205</b>
<b>Subject index</b>	<b>207</b>
<b>Publications and presentations</b>	<b>211</b>

## *Preface*

---

Today, much of our industrial progress is based on the use of organic materials such as polymers as insulators of heat and electricity and on the use of metals as conductors of both. However, our modern lifestyle increasingly demands more from the polymers than their traditional role of insulators. With the rapid development of electronics industry, the demand for electrically conductive materials, such as electromagnetic wave interference shielding materials for personal computers and home electronic devices, flooring and ceiling materials, de-electrifying cloths and radar cross-section reducing protective fabrics for stealth technology has increased. The indiscriminate use of microwave devices has thrown up fresh new challenges to develop efficient microwave absorbers. Such a task has become imminent because of stricter environmental regulations. Development of efficient microwave absorbers in the form of emulsions/coatings can find aerospace applications in the form of stealth coatings for aircrafts and other devices. This has led to the investigation and the subsequent commercial exploitation of organic polymers as conductors of electricity. Conducting polymers have been the subjects of study for many decades as possible synthetic metals.

However, the practical uses of conducting polymers are not very likely because of their poor mechanical properties and processability that rarely meet the industrial requirements. Thus, a unique combination of electronic and mechanical properties of blends/composites of conducting polymers with conventional polymers seems to have great applications. Since the conducting polyblends are stable and retain the mechanical properties of the host polymers, films, fibers and coatings can be fabricated for use in antistatic applications, electromagnetic interference shielding (EMI) and/or absorption. In such applications, conducting polymers or other

materials such as metals are compounded with other insulating polymers. The electrical and mechanical properties of such blends/composites depend on the aspect ratio of the additive. Fibers are characterized by high aspect ratios. Fibrous fillers are the most common forms of reinforcement in reinforced thermoplastics and elastomers. Also, conducting fibers can be more cost effective than metals or other forms of conducting materials in most applications requiring electrical conduction. They have design advantages over other types of conducting materials in superior impact resistance, flexibility, and non-corrosiveness. They can be used as sensors due to very high sensitivity to changes in the environment.

In the present venture, an attempt has been made to prepare conducting composites by incorporating conducting polyaniline coated short Nylon fiber in insulating elastomer matrices and to study its DC electrical conductivity, dielectric properties and electromagnetic shielding characteristics, in addition to evaluating the mechanical properties. Elastomers can provide a lossy dielectric platform, which is the main criterion for a material to be classified as a microwave absorber. Polyaniline coated short Nylon fiber provides necessary reinforcement while imparting conductivity to the elastomeric matrix. Two different elastomers- nonpolar natural rubber and polar chloroprene rubber- were selected due to their industrial importance and attractive properties.

The dissertation consists of seven chapters.

Chapter 1 gives a brief introduction to polyaniline, its structure, charge storage, mechanism of conduction and its synthesis. The state-of-art research on polyaniline/polymer blends and composites are presented. The essentiality of dielectric spectroscopy and an introduction to microwave technology are also given. The specific objectives of the work are mentioned at the end of this chapter.

Chapter 2 describes the preparation and characterization of polyaniline coated conducting short Nylon fibers. The conducting fibers have been prepared by *in situ* polymerization technique after a chemical etching process of the Nylon fibers. The surface characteristics of the fibers have been analyzed using scanning electron

microscopy, X-ray photoelectron spectroscopy, infrared spectroscopy and X-ray diffraction analysis. The thermal stability and electrical conductivity of the fibers have also been examined.

Chapter 3 includes the preparation of conducting elastomer composites of natural rubber, polyaniline and polyaniline coated short Nylon fibers by mechanical mixing. The physicochemical and morphological characteristics of the composites are described. The DC electrical conductivity, thermal stability and thermal degradation kinetics of the conducting elastomer composites are also discussed.

Chapter 4 explains the preparation, processability and mechanical properties of chloroprene rubber/polyaniline/polyaniline coated short Nylon fiber conducting polymer composites. The cure characteristics, cure kinetics, filler dispersion, mechanical properties and morphological features of the composites are investigated. The DC electrical conductivity and thermal analysis of the composites are also included.

Chapter 5 investigates the dielectric behavior of the conducting elastomer composites. The variation in dielectric permittivity and AC conductivity with changes in frequency and temperature is investigated. The observed data has been fitted to some theoretical models.

Chapter 6 examines the dielectric properties of the conducting polymer composites at microwave frequencies. The dielectric permittivity, loss tangent, heating coefficient, conductivity, absorption coefficient and skin depth of the composites is investigated. The electromagnetic interference shielding efficiency of the composites is also presented.

Chapter 7 is the concluding chapter briefing the major findings of the investigation.





*Intrinsically conducting polymers and conducting polymer composites are finding growing acceptance in the academic world and in the electronics industry. Polyaniline is a conducting polymer which has a decent status among the so-called synthetic metals. The dielectric properties of conducting polymers have in store, a handful of extremely useful information on the specific interactions between the molecules and about the structure of the material. Microwave technology has attained new application potentials with the growth of conducting polymers. An introduction to polyaniline and its composites, a peek into the technique of dielectric spectroscopy and the applications concerned with the use of microwave properties of conducting polymers/conducting polymer composites are briefed here.*

---

# Chapter 1

## General introduction

Polymer systems with special properties is a field of increasing scientific and technical interest, offering the opportunity to polymer and synthetic organic chemists to synthesize a broad variety of promising materials, with a wide range of electrical and magnetic properties. This has led to the development of different routes in the discovery of different conducting materials such as conducting films, conducting fibers and conducting polymer composites. Polymers are generally insulators and the low conductivity of polymers has been extensively used in the manufacture of insulators and dielectric substances in electrical industry. However, some polymers have been synthesized with remarkable ability to conduct electricity. An organic polymer that possesses the electronic, magnetic, electrical and optical properties of a metal is called an *intrinsically conducting polymer* (ICP). Among the large variety of conducting polymers, polyaniline (PANI) has emerged as the most promising one because of its diverse properties. During the past two decades, conductive polymers and conductive polymer composites have been the subject of intensive research and

development in the academic world and also in the chemicals and electronics industry world-wide. Their use as new materials in value-added industrial and consumer products is opening up entirely new domains of polymeric applications.

Conducting fibers is a new branch of polymers, which has a very high potential for growth. One major application area is the preparation of conducting composites. The present work aims to investigate the preparation and use of polyaniline coated short Nylon conducting fibers to fabricate conducting polymer composites and to evaluate its mechanical and dielectric properties.

In this chapter, a concise introduction to the subject is presented. Polyaniline, its structure, charge storage, mechanism of conduction and synthesis are briefly discussed. The state-of-art research in polyaniline/polymer blends and composites, the adequacy of dielectric spectroscopy and the application of conducting polymers in microwave technology are presented. An outline of the principal objectives of the work is given at the end of this chapter.

## **1.1 Polyaniline**

Technological uses of polymer systems depend crucially on the reproducible control of the molecular and supramolecular architecture of the macromolecule via a simple methodology of organic synthesis. Polyaniline is one such polymer whose synthesis does not require any special equipment or precaution. Among the ICPs, PANI has become one of the most technologically important one due to its unique processability, together with relatively inexpensive monomer and high yield of polymerization [1]. PANI is fast replacing the conventional materials because of its fascinating electrical properties. This interest is caused by diverse, but also unique, properties of PANI allowing its potential applications in various fields, such as energy storage and transformation (alternative energy sources, erasable information storage, non-linear optics, shielding of electromagnetic interference), as well as catalysts, indicators, sensors, membranes of precisely controllable morphology, etc.

### 1.1.1 The birth and growth

PANI is one of the oldest conductive polymers known. It is the oxidative polymeric product of aniline under acidic conditions and has been known since 1862 as aniline black. It was first prepared by Letheby in 1862 by anodic oxidation of aniline in sulphuric acid [2]. At the beginning of the twentieth century, organic chemists started investigating the constitution of aniline black and its intermediate products. Willstatter and co-workers in 1907 and 1909 regarded aniline black as an eight-nuclei chain compound having an 'indamine' structure [3, 4]. However, in 1910, Green and Woodhead were able to report various constitutional aspects of aniline polymerization [5]. They carried out oxidative polymerization studies using mineral acids and oxidants such as persulfate, dichromate, and chlorate and determined the oxidation state of each constituent by redox titration using  $\text{TiCl}_3$ . During this period, it did not occur to anyone to investigate its electrical and magnetic properties for the obvious reasons that organic compounds are insulators, though in 1911, Mecoy and Moore suggested electrical conduction in organic solids [6]. Almost 50 years later, in 1967, Jozefowicz *et al.* reported that the conductivity of PANI increases by several orders of magnitude when doped with protonic acids with decreasing pH values [7]. They also recognized that polyaniline could serve as an electrode material for rechargeable batteries. Surville *et al.*, in 1968 reported proton exchange and redox properties with the influence of water on the conductivity of polyaniline [8]. Unfortunately, all these early studies were fraught with problems such as uncertain composition and were lost in literature.

A major breakthrough occurred in 1977 when Heeger, MacDiarmid and Shirakawa discovered that polyacetylene could be made conducting almost like a metal [9]. This was seminal to the development of contemporary studies on intrinsically conducting polymers. In 1980, Diaz and Logan reactivated research on polyanilines [10] and several other groups immediately followed up during the following decades [11-13]. Since then, the interest in ICPs, including polyaniline has developed through three stages: (1) an initial interest motivated by their unique properties and practical possibilities; (2) a decline in interest owing to difficulties in processing and poor mechanical properties; (3) renewed interest following the discovery of solution and

melt processability of PANI in the early 1990s [14-19]. Now polyaniline has become the most extensively studied conducting polymer because of its ease of preparation and processing, its richness in chemistry and physics, and its technological applications. It has been commercialized on a relatively large scale owing to its relatively good environmental stability. It is in fact, the first commercially available conducting polymer. Fig. 1.1 shows a conductivity ladder locating the conductivity of polyaniline with that of other conducting polymers and copper metal.

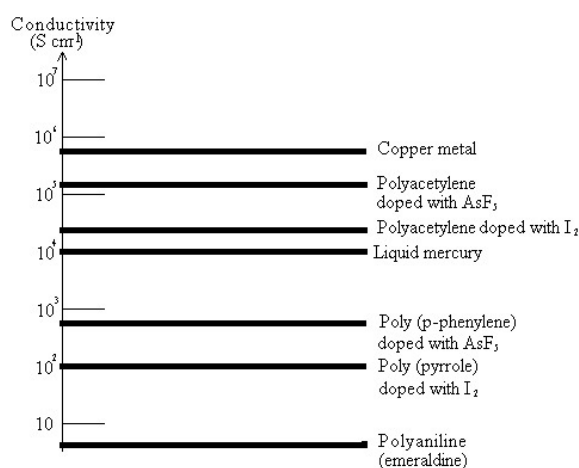
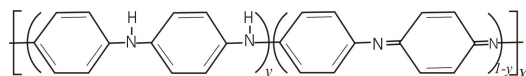


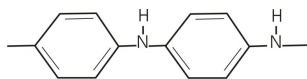
Fig. 1.1 The conductivity ladder

### 1.1.2 The structure

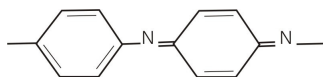
Polyaniline is a typical phenylene-based polymer having a chemically flexible -NH- group flanked on either side by phenylene rings. The protonation and deprotonation and various other physico-chemical properties of polyaniline can be related to the presence of the -NH- group. Polyaniline can be considered as being derived from a polymer, the base form of which has the generalized composition:



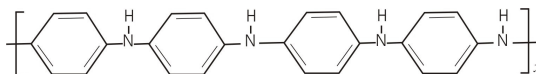
and which consists of alternating reduced:



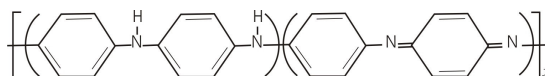
and oxidized:



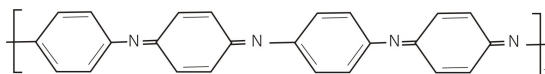
repeat units [20-23]. The average oxidation state ( $1-y$ ) can be varied continuously from zero, to give the completely reduced polymer:



to 0.5, to give the “half-oxidized” polymer:



to one, to give the completely oxidized polymer:



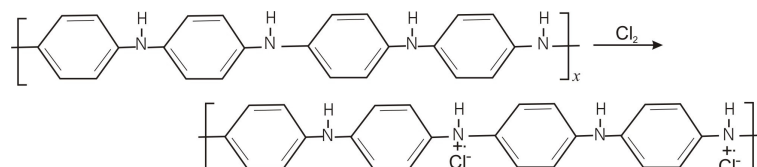
The terms “leuco-emeraldine”, “emeraldine” and “pernigraniline” refer to the different oxidation states of the polymer where  $(1-y) = 0, 0.5$ , and  $1$ , respectively, either in the base form e.g., emeraldine base, or in the protonated salt form, e.g., emeraldine hydrochloride [20-23]. In principle, the imine nitrogen atoms can be protonated in whole or in part to give the corresponding salts, the degree of protonation of the polymeric base depending on its oxidation state and on the pH of the aqueous acid. Complete protonation of the imine nitrogen atoms in emeraldine base by aqueous HCl, for example, results in the formation of a delocalized polysemiquinone radical cation and is accompanied by an increase in conductivity of  $\sim 10^{10}$  [20-24]. The partly protonated emeraldine hydrochloride salt can be synthesized easily by either the chemical or the electrochemical oxidative polymerization of aniline [22, 23, 25]. It can be deprotonated by aqueous ammonium

hydroxide to give emeraldine base powder (a semiconductor). The protonated emeraldine is green in color and conducting, emeraldine base is blue and non-conducting, protonated pernigraniline is blue in color, pernigraniline base is violet and non-conducting. The leuco-emeraldine is colorless and non-conducting. The emeraldine base form of PANI is the most stable of the three states because, leuco-emeraldine is easily oxidized when exposed to air and pernigraniline is easily degraded.

### 1.1.3 Doping

Doping is the process by which polymers that are insulators or semi-conductors as synthesized are exposed to charge transfer agents (dopants) in the gas or solution phase or through appropriate electrochemical oxidation or reduction. This process will increase the polymer's ability to conduct electricity because of the increased concentration of charge carriers [23]. Pure PANI, in the undoped state, is a poor semiconductor with conductivity of about  $10^{-8}$  S/cm. However, once it is doped, its conductivity could increase by a factor of 10 S/cm or more depending on the dopant used. Polyaniline holds a special position amongst conducting polymers in that it's most highly conducting doped form can be reached by two completely different process- protonic acid doping and oxidative doping. Protonic acid doping of emeraldine base units with, for example, 1 M aqueous HCl results in complete protonation of the imine nitrogen atoms to give the fully protonated emeraldine hydrochloride salt [22, 23]. The protonation is accompanied by a 9-10 order of magnitude increase in conductivity reaching a maximum with  $\sim 1$  M aqueous HCl.

The same doped polymer can be obtained by chemical oxidation (*p* doping) of leuco-emeraldine base [25]. This actually involves the oxidation of the  $\sigma/\pi$  system rather than just the  $\pi$  system of the polymer as is usually the case in *p*-type doping. Its reaction with a solution of chlorine in carbon tetrachloride proceeds to give emeraldine hydrochloride:



#### 1.1.4 Charge storage and conduction

One early explanation of conduction in conducting polymers uses band theory as a method of conduction. This says that a half filled valence band would be formed from a continuous delocalized  $\pi$  system. This would be an ideal condition for conduction of electricity. However, it turns out that the polymer can more efficiently lower its energy by bond alteration (alternating short and long bonds), which introduces a band width of 1.5 eV, making it a high energy gap semiconductor. The polymer is transformed into a conductor by doping it with either an electron donor or electron acceptor. This is reminiscent of doping of silicon based semiconductors where silicon is doped with either arsenic or boron. However, while the doping of silicon produces a donor energy level close to the conduction band or an acceptor level close to the valence band, this is not the case with conducting polymers. The evidence for this is that the resulting polymers do not have a high enough concentration of free spins, as determined by electron spin resonance spectroscopy (ESR). Initially, the free spins concentration increases with concentration of dopant. At larger concentrations, however, the concentration of free spins levels off at a maximum [26-30].

The polymer may store charge in two ways. In an oxidation process, it could either lose an electron from one of the bands or it could localize the charge over a small section of the chain. Localizing the charge causes a local distortion due to a change in geometry, which costs the polymer some energy. However, the generation of this local geometry decreases the ionization energy of the polymer chain and increases its electron affinity making it more able to accommodate the newly formed charges. This method increases the energy of the polymer less than it would if the charge was delocalized and hence takes place in preference to charge delocalization. The two Kekule structures derived from PANI structure is not equal in energy and hence they



have a non-degenerate ground state. The oxidative doping of polyaniline proceeds in the following way. Upon oxidation, an electron is removed from the  $\pi$  system of the backbone producing a free radical and a positive charge. The radical and cation are coupled to each other via local resonance of the charge and the radical. This cation radical possesses a spin =  $\frac{1}{2}$  and a unit charge [31]. This combination of a charge site and a radical is called a 'polaron'. Thus, a polaron is either a positively charged hole site (radical cation) or a negatively charged electron site (radical anion). This creates new localized electronic states in the gap with the lower energy states being occupied by single unpaired electrons. Up on further oxidation, the free radical of the polaron is removed creating a new spinless defect called 'bipolaron', which is a dication or a dianion, which accounts for spinless conductivity in polyaniline. Theoretical models demonstrate that two radical ions i.e. polarons on the same chain react exothermically to produce a bipolaron [32]. A bipolaron has a charge =  $2e$  and spin = 0. The polaron and bipolaron structures of polyaniline are shown in fig. 1.2.

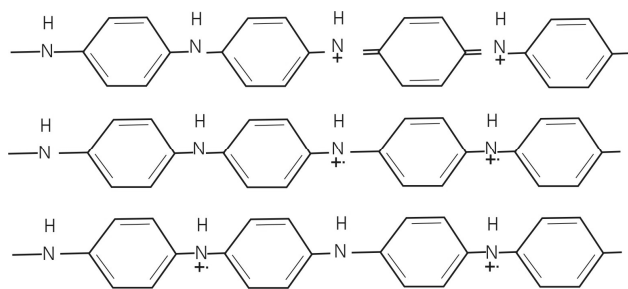


*Fig. 1.2 Polaron and bipolaron lattice (a) Emeraldine salt in bipolar form (b) Dissociation of the bipolaron into two polarons (c) Rearrangement of the charges into a polaron lattice (Adapted from references [33, 34])*

The energy increase due to coulombic repulsion (in the formation of a bipolaron) is more than compensated for by the energy gained when the two charges share the same lattice distortion. Quantum chemical calculations indicate that the formation of a bipolaron requires 0.4 eV less energy than the formation of two polarons [35, 36]. However, bipolarons are not created directly, but must form by the coupling of pre-existing polarons, or possibly by the addition of charge to pre-existing polaron. At

higher doping levels, polarons are replaced by bipolarons. This, eventually with continuing doping, forms into continuous bipolaron bands (fig. 1.3). Their band gap also increases, as newly formed bipolarons are made at the expense of the band edges. For a heavily doped polymer, it is conceivable that the upper and lower bipolaron band will merge with the conduction and the valence bands, respectively, to produce partially filled bands and metal-like conductivity.

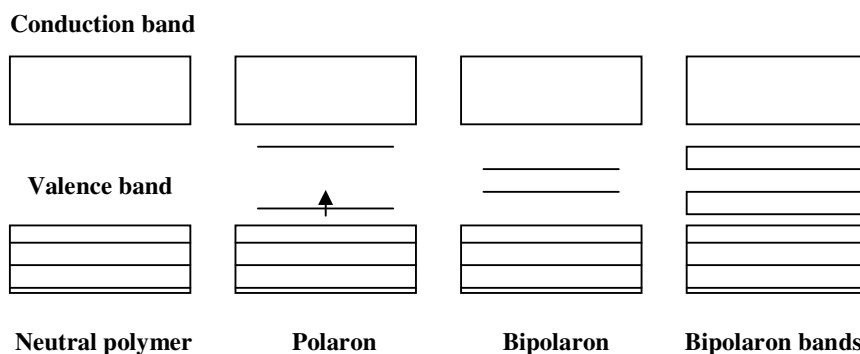


Fig. 1.3 Schematic representation of the bipolaron bands

Although polarons and bipolarons are known to be the charge carriers, the precise conduction mechanism is not fully understood. The problem lies in attempting to trace the path of the charge carriers through the polymer. PANI is highly disordered, containing a mixture of crystalline and amorphous regions. It is necessary to consider the transport along and between the chains and also the complex boundaries established by a number of phases. This has been studied by examining the effect of doping, temperature, magnetism and the frequency of the current used. These show that a variety of conduction mechanisms are present. The main mechanism used is by movement of charge carriers between localized sites or between polaron and bipolaron states. Frequency-dependent conductivity measurements of partly protonated emeraldine were proposed to support the presence of inter-polaron hopping mechanisms [37, 38] such as variable range hopping (VRH) [39-41], the quasi-1D VRH model [42] or the metallic rods model [43]. The effects of protonation on the emeraldine base led to a proposal of the transformation of its electronic structure to that of a granular polaron metal [44]. For intermediate protonation levels,

magnetic and optical experiments supported the phase segregation between highly conducting regions and the insulating background [45]. Where inhomogeneous doping produces metallic islands dispersed in an insulating matrix, conduction is by movement of charge carriers between highly conducting domains. It has been proposed that the charge conduction is via charging energy-limited tunneling among the small granular polymeric grains [46].

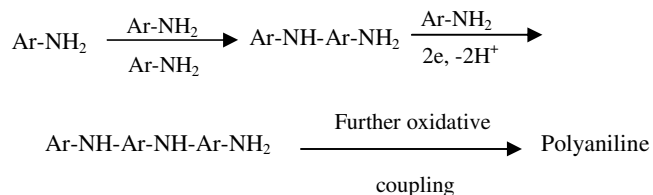
### 1.1.5 Synthesis

Polyaniline is prepared by either chemical or electrochemical oxidation of aniline under acidic conditions. An aqueous medium is preferred. The synthesis of polymer by either chemical or electrochemical methods depends upon the intended application of the polymer. Whenever thin films and better-ordered polymers are required, an electrochemical method is preferred. The acid dissociation constant ( $pK_a$ ) is an important aspect of PANI synthesis, because in PANI, protonation equilibria involves exclusively the quinone diamine segment, having two imine nitrogens with  $pK_{a1} = 1.05$  and  $pK_{a2} = 2.55$  [47]. Therefore, any acid whose  $pK_a$  value falls within this range would be suitable as a dopant whereas the anilinium ion has a  $pK_a$  of 4.60 and the ammonium ion 9.24. Acids having  $pK_a$  values around that of an anilinium ion would be suitable as solvents if they are liquids and can also be used to prevent over-oxidation of PANI.

A variety of oxidants have been used to effect chemical polymerization of aniline under acidic conditions. The most preferred method for synthesis is to use either hydrochloric or sulphuric acid with ammonium persulfate as an oxidant [22, 48-51]. A simple oxidizing agent like ammonium persulfate yields a polymer of better quality than oxidizing agents containing metal ions. The principal function of the oxidant is to withdraw a proton from an aniline molecule, without forming a strong coordination bond with either substrate/intermediate or with the final product. Oxidative polymerization is a two-electron change reaction and hence, the persulfate requirement is one mole per mole of a monomer. However, a smaller quantity of the oxidant is used to avoid oxidative degradation of the polymer formed. It has been

noticed that better polymer formation occurs if the monomer solution in acid and the oxidants are cooled separately before initiating polymerization.

Armes *et al.* studied the polymerization of aniline at 20 °C using ammonium persulfate as oxidant [49]. In their study of the effect of the oxidant/monomer initial mole ratio, they concluded that the conductivity, yield, elemental composition and the degree of oxidation of the resulting PANI are essentially independent of this ratio when its value is below 1.15. Elemental analysis showed that over-oxidation of PANI occurs at higher oxidant/monomer ratios. Cao and co-workers established optimum synthesis conditions for the polymerization of aniline by ammonium persulfate with respect to viscosity, electrical conductivity and the reaction yield [51]. They found that the reaction yield was not strongly sensitive to most synthesis variables, while the viscosity, the molecular weight and the conductivity was found to be markedly affective. It was reported that the polymerization process proceeds as follows [52]:



## 1.2 Polyaniline/polymer blends and composites

One can find analyses of numerous attempts to apply high conductivity, electrochromic, catalytic, sensor, redox and other properties of PANI to different practical needs [53-57]. However, since 1984, efforts have shifted to its use as PANI composites or blends with common polymers [54, 58-60]. This trend has been driven by the need to replace traditional inorganic conducting fillers and to improve the processability of PANI, along with its mechanical properties and stability. These composite materials have introduced PANI to practical applications in different fields, including electromagnetic shielding and microwave absorption [56, 61, 62], static electricity dissipation [63, 64], conducting glues [65], paint coatings for anticorrosion protection [66] and sensor materials [67]. Nevertheless, the choice of

the best method to produce composites with specified characteristics remains an unresolved problem, because the processing method may significantly determine the properties of the manufactured composite materials. Known methods to produce PANI containing composites [60] may be essentially reduced to two distinct groups: (1) synthetic methods based on aniline polymerization in the presence of or inside a matrix polymer, and (2) blending methods to mix a previously prepared PANI with a matrix polymer. The synthetic direction is probably preferable if it is necessary to produce inexpensive conducting composites, due to the use of inexpensive aniline instead of more expensive PANI, or when there is a need to form composites which have conductivity only in a thin surface layer. Conductive fibers are usually prepared by this method. Good homogeneity and a low percolation threshold characterize these composites. On the other hand, blending methods sometimes seem to be more technologically desirable from the standpoint of large-scale production, particularly in the case of melt processing techniques.

### ***1.2.1 Conducting fibers***

The term “intelligent and multifunctional fibrous materials” describes a class of yarns or textiles that have active functions in addition to traditional textile properties. The novel functions and properties are obtained by modifying the textile structures. The textile industry has made considerable advances in the field of high valued textiles, mainly in the sectors of high performance textiles, yarns, and fibers. Electrically insulating nature of the synthetic polymer fibers for general purpose applications brings about inevitable disadvantages such as electrical shock caused by static charge accumulation and electromagnetic interference (EMI) caused by transmission of detrimental electromagnetic waves. Therefore materials scientists all over the world have made several attempts to prepare synthetic fibers with electrical conductivity. The demand for the electrically conductive fibers and textiles is growing rapidly not only in relation to industrial needs such as sensing, electrostatic discharge, corrosion protection, dust- and germ-free clothing, monitoring, data transfer in clothing, but also for military applications such as camouflage and stealth technology [68-74].

Conductive fibers have been mostly obtained either as pure conductive polymers or as composites. The modification of fibers and yarns using conductive polymers seems to be an interesting approach. Since polypyrrole-coated polyester textiles have been developed by Milliken Research Corporation [18, 75, 76], many research groups are active in this field. Clemenson, Furman and Ga. Tech. Laboratories have begun to conduct research in chameleon fibers that change the substrate color upon application of an electrical field. These intelligent textiles based on conductive materials have been prepared by direct surface coating or by *in situ* polymerization on textile substrates [77]. Polyamides, polyesters, carbon fibers and kevlar are commonly used to produce conducting fibers. Commonly used conductive materials are  $\pi$  electron conjugate polymers such as polythiophene, polyaniline or polypyrrole [76, 78-80]. It has been reported that the electrically conducting polypyrrole coated textiles can have excellent mechanical strength and flexibility, coupled with good electrical and microwave properties [79-82]. Among the conducting polymers, PANI is lightweight and a very thin coating is sufficient to give good results for EMI shielding and electrostatic charge dissipation (ESD) [83, 84]. PANI, coated or *in situ* polymerized on nonwoven fabric, Nylon 6, cotton, polyester fabric, and nomex fabric have been reported [85-87].

Conducting polymers can be electrochemically produced in the fiber or film forms. Carbon fibers have been coated electrochemically with PANI, producing a fiber composite. The carbon fibers were used as a working electrode in a three-electrode-one compartment cell [88]. In a more recent study, an electrochemical method was developed to deposit uniform and continuous coatings of PANI on carbon fiber [89]. The authors studied the conduction mechanism by electrochemical impedance spectroscopy and suggested that two types of doping are involved in the redox process of PANI. The electrochemical grafting of PANI onto cotton, wool and silk fibers was reported, provided by subjecting them to electrical treatment in the electropolymerization solution in aqueous *p*-toluene sulfonic acid electrolyte [90]. During electrolysis, the weight of the fibers increased monotonically, and their electrical conductivity decreased [90, 91]. Conductivity of the composite materials

thus prepared was found to vary between 0.2 and 15 S/cm, depending on the nature of the fibers and the coating procedure [92].

The electrochemically coated fibers show weak mechanical properties disabling their application in traditional textile process. Considering this difficulty, thin coating using conducting solutions or polymerizing on the surface of fibers should be a reasonable method to prepare conductive textiles and fibers. Deposition of PANI on glass-fiber fabric provided a method for the production of conductive fabrics [93]. The coating was achieved by several cycles of immersion of the fibers in an acid aniline solution, followed by drying at 60 °C and immersion in an oxidant solution. The mean growth rate of the deposit thickness was reported to be 150 nm per cycle. The conductivity of the coated fabrics reached 0.23 S/cm. According to the authors, the adhesion of polyaniline to the substrate seemed to be sufficient, since the mechanical properties of composites did not change in comparison to those of untreated fabric.

A comprehensive approach for preparing conductive yarns has been developed by Kim *et al.* based on a sol-gel coating process [94]. PANI coating was carried out during the impregnation of poly(ethylene terephthalate) (PET) yarns in a PANI/solvent system. The solvent evaporation at the end led to the formation of PANI-coated PET conductive yarns. The electrical resistance of PANI-coated yarns decreased as the concentration of PANI solution increased. The concentration of PANI solution had an important effect and they reported that the threshold concentration was between 6 and 9 % of PANI. The yarns showed good environmental stability with respect to conductivity.

Fibrils of PANI were prepared by the polymerization of aniline in a gel of poly(acrylic acid) using  $\text{FeCl}_3$  as oxidant [95]. Fibrils with a diameter of approximately 50 nm and 1-5  $\mu\text{m}$  long were observed by scanning electron micrography. Colloidal suspensions of the fibrils in the poly(acrylic acid) solutions could also be obtained by this method. Colloidal suspension showed optical spectrum changes with pH similar to pure polyaniline.

Heegers's research group obtained monofilament conductive fibers from a blend of PANI and poly(*p*-phenylene terephthalamide) (Kevlar from Du-Pont) by wet-spinning [96]. The monofilament fibers, with different concentrations of PANI, were wet-spun from a solution of the component polymers in sulfuric acid, into a 1 N sulfuric acid solution. In the process, an extrusion speed of 0.12-0.30 m min<sup>-1</sup> and a draw ratio of 7:20 enabled the continuous production of bobbins. These were sprayed with deionized water to prevent fiber collapse and to remove the excess of sulfuric acid. The bobbins were immersed in HCl to protonate polyaniline and dried in a vacuum oven. Pure PANI fibers were also wet-spun by the same method. The Kevlar fibers became brittle with increasing concentration of PANI. In general, the mechanical properties of the fibers changed proportionally to the concentration of PANI. Enhancement of the strain at break occurred at the expense of electrical conductivity. The most significant result from this work was the observation that small amounts of polyamide improved the mechanical properties of PANI fibers markedly, while retaining its conductivity.

### ***1.2.2 Conducting elastomer composites***

Elastomers are a class of polymers comprising of rubbers and latexes. Their main characteristic is a glass transition temperature below -20 °C, resilience and the possibility of crosslinking. They are used by the polymer industry in the form of rubber compounds, which are cross-linked rubbers containing in its formulation: reinforcing fillers, vulcanization agents and accelerators, pigments and other additives. In general, these polymers have unsaturated C=C bonds which promote the crosslinking reactions, either with sulfur or with peroxides. Their range of applications is very large and grows continuously. It spans from large-scale uses such as tires to the small scale such as solid-state electrolytes.

Incorporation of conductive additives into a host elastomer matrix constitutes an excellent approach for the development of special materials, which combine electronic conductivity with elasticity and other important mechanical properties imparted by the insulating rubber matrix [60]. The use of blends in rubber industry is important because it allows tailoring of the characteristics of a material by using two



or more polymers with different properties in the composition. Electrically conductive vulcanized rubbers find applications in fuel hoses, spark plug cables and high-voltage cable insulations. Typical metals such as copper or aluminum, which have high conductivity and dielectric constant, have been employed for fabricating such materials. While metals have good mechanical and conducting properties, they have disadvantages such as heavy weight, easy corrosion and poor processability. Several reports deal with the development of such conducting materials by employing conducting carbon black as the conducting additive [97] and their potential applications which include electromagnetic shielding [98], electrostatic charge dissipation [99] and sensors [100-102]. In recent years, conducting polymers with highly extended conjugated electron systems in their backbones have attracted great interest due to their electrical, electrochemical and optical properties [103]. The electrically conducting polymers like polypyrrole (PPy), polythiophene (PTh) and polyaniline have been examined for possible electronic and chemical applications. There are several studies in the literature describing the preparation of blends and composites of elastomers and conducting polymers.

#### **1.2.2.1 State- of- art research**

Zoppi and De Paoli prepared blends of polypyrrole and ethylene-propylene-diene monomer rubber (EPDM) by the sorption of pyrrole in vapor phase in an EPDM matrix containing  $\text{CuCl}_2$  [104]. Elastomeric blends with conductivity of the order of  $10^{-7}$  S/cm were obtained. In another work, the same authors prepared semi-interpenetrating networks (SIPNs) by swelling the vulcanized EPDM rubber with a tetrahydrofuran solution of  $\text{FeCl}_3$ , followed by exposure to pyrrole vapors [105]. The highest conductivity obtained by this method was  $10^{-5}$  S/cm. Yigit *et al.* presented the electrochemical synthesis and characterization of conducting composites of polythiophene with a synthetic rubber (*cis*-1,4-polyisoprene) and natural rubber [106].

Conducting elastomer blends based on polyaniline and unsaturated rubbers have several potential applications, especially as pressure sensors. These blends/composites have been prepared by different techniques such as

electropolymerization, solution mixing, mechanical mixing and *in situ* polymerization. A blend of PANI and nitrile rubber (NBR) has been prepared by coating a platinum working electrode with a thin film of nitrile rubber (29 % acrylonitrile) and polymerizing aniline by the potentiodynamic method. The electrochemical properties of the blend were very similar to pure PANI in cyclic voltammetry measurements [107]. The good miscibility of the components of this blend was demonstrated by differential scanning calorimetry (DSC) and scanning electron microscopy (SEM) [108]. In this work, the feasibility of preparing this blend by galvanostatic or potentiostatic methods was also demonstrated. In a subsequent study, the cyclic voltammetry, complex impedance spectroscopy, electrochromism and mechanical properties of this material have been reported [109]. Stress-strain tests indicated a behavior typical of crosslinked rubbers, with a strain at break of 2700 %. These results contrasted with those obtained by other authors [110], who observed a toughening of poly(vinyl chloride) and poly(ethylene acetate-co-vinyl chloride) upon electrochemical blending with polypyrrole. The optical properties of this blend enabled its use in a device as an anodic electrochromic material in combination with  $\text{WO}_3$ , a cathodic electrochromic material [111]. Due to its mechanical properties, this material could be used as an antistatic coating in industrial installations.

Nitrile rubber and polyaniline were also blended by cold mixing in a type of roll mill called 'calender'. Calendaring is routinely used in the rubber industry to produce rubber compounds prior to vulcanization. PANI was synthesized by chemical polymerization using ammonium persulfate as oxidizing agent and with different acids as dopant: dodecylbenzenesulfonic acid (ADBS), tetrapropylbenzenesulfonic acid (ATBS), *p*-toluenesulfonic acid (APTS) and hydrochloric acid. All samples were electroactive and presented similar conductivities [112]. The blends were characterized by stress-strain measurements, dynamic mechanical analysis, conductivity measurements and scanning electron microscopy. The NBR composition affected the mechanical properties of the blends. The tenacity decreased with increasing PANI concentration for all dopants studied. The increase in PANI concentration caused phase segregation, as indicated by two glass transition

temperatures for the blend containing PANI/ADBS and for that containing PANI/ATBS. From these results, it was concluded that two parameters determine the phase behavior of these blends: NBR composition and PANI dopant. The surface and volume conductivities of the blend exhibited the same dependence on the concentration of the conductive polymer component, and were directly proportional to the concentration of PANI. Blends based on PANI/ATBS showed higher conductivity (volume conductivity for the blend containing 100 phr was  $6.0 \times 10^{-9}$  S/cm) in comparison with other blends [113, 114].

Leyya *et al.* demonstrated an interesting and surprising difference between rubbery blends of styrene-butadiene-styrene (SBS) triblock copolymer and PANI doped with dodecyl benzene sulfonic acid (PANI-DBSA) produced by solution blending under magnetic stirring and ultrasonic vibration [115]. Specifically, they found that blends prepared in solution by magnetic stirring displayed a higher conductivity than those obtained by sonication. Basing on optical microscopy data, the authors deduced that the difference is connected with the fact that sonication led to the formation of very small, conducting particles well distributed inside the matrix, while the magnetic stirring method gave larger PANI-DBSA particles. As a result, the sonicated system gave blends with higher percolation threshold (3.8 wt %) than that for the magnetic stirred system (2.2 wt %). This explanation contradicts the usual guideline that at the same loadings, the higher the dispersion of the conducting particles, the better the formation of conducting pathways. However, we may consider the results as an important indication on the necessity to control stirring conditions to obtain reproducible results for PANI blends obtained by solution blending.

Koul *et al.* have shown enhanced electrical and optical properties, along with higher solubility in all common organic solvents, for PANI doped with a mixture of DBSA/TSA (toluene sulfonic acid) (1:1) [67]. Using this double doped PANI, they prepared composite films with acrylonitrile-butadiene-styrene (ABS) by casting from the chloroform solution. The surface resistance of these composites changed from 300 M $\Omega$ /cm to 1.3 M $\Omega$ /cm dependent on the doped PANI content and the method of mixing the system components.

Melt mixing has been used to disperse conductive polymers in SBS matrix. A strong dependence of conductivity of PANI blend properties on the composition and processing conditions has been demonstrated for melt mixed PANI-DBSA complex with SBS rubber. PANI-DBSA was mixed with SBS rubber in a Brabender mixer [116]. A conductivity of 2 S/cm was achieved with a loading of 50 % of the conductive polymer. According to the authors, this blend could be extruded. However, no supplementary data supporting this conclusion were provided. Leyya *et al.* showed that the conductivity was enhanced for blending at a higher temperature, 130 °C in a Haake internal mixer compared to the blend compression-molded at 100 °C [117]. However, a highly cross-linked material was obtained at higher temperature. It should be emphasized that the mechanical performance of the PANI-DBSA/SBS blends was not good in comparison with pure SBS. Thus, the ultimate tensile strength and elongation at break of the compression-molded samples decreased from 21.0 MPa and 5200 % to 9.5 MPa and 3900 % for pure SBS and its blend with 17 wt % PANI-DBSA loading, respectively.

A thermoplastic elastomer, poly(styrene-ethylene/butylene-styrene) was melt blended with PANI-DBSA at 160 °C and subsequently injection-molded to test bars or compression-molded into films [19]. Stress-strain curves revealed an elastomeric behavior. A very low threshold for the electrical conductivity in relation to pure PANI content was observed (0.1 S/cm for 2 %). An interesting effect was observed on the conductivity upon stretching of the films: at 100 % elongation, the conductivity reached a maximum; between 100 and 400, it decreased; and at 400 %, it remained almost at the original value. This suggests that low elongations align the conductive pathways and a long elongation disrupts the conductive network. The authors do not comment on the possible hysteresis of this effect.

Koul, Chandra and Dhawan reported blends of conventional thermoplastic ABS copolymer with PANI doped with a specific ratio of mixed dopants, consisting of DBSA and TSA [118]. Specifically, conductivities for PANI-DBSA-TSA (1:1)/ABS composites were  $7.6 \times 10^{-8}$ ,  $8.0 \times 10^{-7}$ ,  $1.3 \times 10^{-5}$  and 0.1 S/cm for 20, 30, 40 and 50 wt % of PANI-DBSA-TSA, respectively. Styrene-butadiene rubber (SBR) with PANI doped with DBSA [119], and NBR with PANI doped with different acids were

prepared by mechanical mixing [119, 120]. Pinho and co-workers prepared composites of polychloroprene with PANI doped with chloridric acid by mechanical mixing [121]. The preparation of EPDM rubber composites by mechanical mixing with PANI doped with different sulfonic acids has been reported [119, 122-126].

Chemical polymerization of aniline-swollen vulcanized polychloroprene sheets was reported [127]. Electrically conductive elastomeric blends based on NBR/PANI-DBSA prepared by polymerization of aniline in the presence of NBR, using a direct, one step *in situ* emulsion polymerization method in which DBSA played both the roles of surfactant and dopant was prepared by Soares *et al.* [128]. They also prepared NBR/PANI-DBSA blends by mechanical mixing and found that the *in situ* polymerized blends showed higher conductivity values. Moreover, it has been reported that polyanilines showed high efficiency as an antioxidant and antirad material for SBR vulcanizates [129].

### 1.3 Conduction processes

Electrical conduction in a conducting polymer or conducting polymer composite can take place by several mechanisms such as tunneling conduction, impurity level conduction including hopping of charge carriers from one impurity level to another in the impurity band, space charge limited process due to the impediment of carriers at the interfaces under an external electric field and ionic conduction under high electric fields by the migration of cations and anions in opposite directions. However, all the processes may not be present in all cases and even when present, one of these may be significant under certain conditions while the others may not be so.

#### ***Tunneling***

Tunneling is a quantum mechanical phenomenon in which an electron passes through a potential energy barrier without acquiring enough energy to pass over the top of the barrier. The penetration probability of an electron from one electrode to the other through the insulator is much dependent on the applied electric field. The effects of image forces, temperature, dielectric constant, shape of the potential barrier and effective mass of electron in the conduction band must be taken into account in

determining the tunnel currents. If the barrier is thin enough, electrons can flow through the barrier between the conducting regions by quantum mechanical tunneling. Direct tunneling involves the transfer of electrons directly from one metallic island to the other through their Fermi surface levels. For a thin film under a high applied electric field, tunneling can be direct and according to Fowler-Nordheim expression, the current density;  $J$ , is given by

$$J = F^2 \exp\left(-0.689\phi^{3/2}F\right) \quad (1.1)$$

where  $F=V/d$  is the applied field,  $V$  is the applied voltage,  $d$  is the thickness of the film and  $\phi$  is the metal-insulator work function. These equations predict that the current density;  $J$ , should be independent of temperature.

#### ***Space charge limited conduction***

Carriers can be injected from the metal electrode into the conduction band of the polymer under an applied electric field. If the amount of injected carriers is more than that which can be transported across the film, a space charge will be built up at the interface. Electrons flowing through the system under an electric field will be impeded and controlled by the space charge collected at the interface and this gives rise to the phenomenon known as space charge limited conduction (SCLC). SCLC currents are important because the injected current is independent of the mechanism of carrier generation and depends only on the transport and trapping of the carriers within the sample. SCLC shows three to four distinct regions in the current-voltage plots. The first region corresponds to the low field conduction region where the variation of current density with voltage is ohmic. As the voltage is increased, the injected carriers outnumber the thermally generated ones and SCLC starts. The current density under SCLC conduction;  $J$ , is directly proportional to  $V^2$  and inversely to  $d^3$ . The region close to the ohmic one is the square law region where  $J$  varies as  $V^2$ . The transition from ohmic to square law shows the onset of SCLC conduction. The presence of traps in the material will reduce the SCLC current considerably because the empty traps remove the injected carriers. If the voltage is further increased, at some higher voltage, all the traps become filled and then the current increases rapidly

to the trap free case. Beyond this, any slight change in voltage will increase the current sharply.

### ***Hopping conduction***

Conduction via localized electrons implies discrete jumps across an energy barrier from one site to the next. In other words, if two molecules are separated by a potential barrier, a carrier on one side can move to the other side either by tunneling through the barrier or by moving over the barrier via an activated state. The latter process is called hopping. The relative importance of these two mechanisms depends on the shape of the barrier and on the availability of thermal energy. This thermally activated type of mobility will increase with temperature, of course, in contrast to that in band conduction. It is apparent that we learn a lot about the conduction process by determination of carrier mobility e.g., its temperature dependence provides a good criterion by which we can distinguish band and hopping types of mechanisms. Though polymers are amorphous materials, a short-range order prevails in most of these materials. Hence the theory that is used to explain the electronic band structure in crystalline phase can also be applied in amorphous polymers. If the spatial fluctuations in the interatomic distances are large, the correspondingly large and random fluctuations in the height or depth of the potential wells may lead to the localization of states below a certain critical and well-defined energy. When the carrier mobility is low and the mean free path is comparable with interatomic distance, the conduction can be expected to take place by a hopping process in the localized states. In a hopping mechanism, only those carriers with an energy  $kT$ , where  $k$  is the Boltzman constant and  $T$  is the temperature, below the Fermi level have a significant probability of hopping. Mott showed that for strongly localized states, the conductivity at low temperatures must follow a relationship of the form,

$$\sigma \approx \exp\left(\frac{-B}{T^{1/4}}\right) \quad (1.2)$$

where  $\sigma$  is the conductivity and  $B$  is a constant related to the hopping mechanism. At high temperatures, deviations from  $T^{1/4}$  occur which can be understood in terms of interchain hopping [130]. A carrier trapped in a chain, after detrapping may drift along the same chain or may hop into an adjacent chain. In amorphous polymers, the conduction occurs due to two distinct processes; a temperature dependent trap hopping and a comparatively less dependent interchain hopping.

#### **1.4 Dielectric spectroscopy**

Dielectric spectroscopy is an informative technique to determine the molecular motions and structural relaxations present in polymeric materials possessing permanent dipole moments [131, 132]. The measurements can be used to find dielectric relaxation times and distribution parameters. The relaxation time depends on the molecular size, shape, intramolecular and intermolecular forces, and can be used to investigate molecular and intramolecular motions and their relation to molecular structure. These studies can be used to evaluate the barrier height hindering internal rotation, problems of complex formation, dipole-dipole interactions and other short-range intermolecular forces. Dielectric relaxation measurements have great potential for studying weak molecular interactions. An extensive study of dielectric behavior of polar solutes at low concentration in non-polar solvents has led to valuable information regarding hydrogen bonding and solute-solvent interactions. A systematic study on the dielectric properties provides valuable information on the behavior of localized electric charge carriers within the system. The dielectric properties of a substance can be used as a source for deriving information about specific interactions between the molecules and about the structure of the material. Hence, a thorough and in-depth study of the dielectric behavior of the composites is inevitable. Dielectric spectroscopy has proven highly useful for studying the structure and dynamics of polymeric materials. Studies of various polar polymers [131, 133-136], polymer blends [137, 138], copolymers [139] and composite materials [140-142] by means of dielectric analysis have shown that it is one of the most efficient techniques for defining characteristic structural features. More recently, dielectric test methods were used to study polymer crystallization due to their high sensitivity to morphological changes [133, 143-146].



In dielectric measurements, the material is exposed to an alternating electric field, which is generated by applying a sinusoidal voltage; this process causes alignment of dipoles in the material, which results in polarization. The polarization will cause the output current to lag behind the applied electric field by a phase shift angle,  $\theta$ . The magnitude of the phase shift angle is determined via measuring the resulting current. The capacitance and conductance of the material over a range of temperature and frequency are then calculated from the relationship between the applied voltage, measured current and phase shift angle and are related to dielectric permittivity;  $\epsilon'$ , and the dielectric loss factor;  $\epsilon''$ , respectively [131, 132, 147]. The dielectric permittivity;  $\epsilon'$ , represent the amount of dipole alignment (both induced and permanent) and the loss factor;  $\epsilon''$ , measures the energy required to align the dipoles or move ions. The ability of an insulator to resist the passage of alternating current or serve as a capacitor is determined by the permittivity or dielectric constant and the dissipation factor. These properties are measured using low voltage so that bound charges are displaced but not ruptured. Dielectric permittivity is a measure of the energy stored in a material subjected to electrical stress. It is defined as the ratio of the field strength in vacuum to that in the material for the same distribution of charges. A number of parameters like temperature, grain size and orientation, molecular structure of the material and frequency of the applied field affect the dielectric permittivity of the materials. The dielectric permittivity and loss factor are the real and imaginary components of the complex permittivity;  $\epsilon^*$ , given by  $\epsilon^* = \epsilon' - j\epsilon''$ .

#### 1.4.1 Polarization

The difference between the dielectric constant of a polymer and that of free space is due to the restricted movements of charges within the polymer. Under the influence of the applied field, positive charges move with the electric field and an equal number of negative charges move against it, resulting in no net charge anywhere within the polymer. However, there is a net positive charge at the surface where the positive direction of the field emerges and a negative charge at the surface where the field enters. Thus the field within the polymer is produced by a larger field outside it, and the normal components have the ratio given by the dielectric constant. This general process is called polarization. The charges are bound in the dielectric. They

cannot move throughout it; otherwise they would produce conduction, not polarization. In a dielectric material, several types of polarization mechanisms can occur under the influence of an applied AC field. The dielectric permittivity is a consequence of these polarization mechanisms such as electronic, ionic, dipole and interfacial polarizations.

### ***Electronic polarization***

An electric field will cause a slight displacement of the electron cloud of any atom in the polymer molecule relative to its positive nucleus. As a result of this relative movement, the nuclei are no longer at the centers of the electron “orbits”. This condition is called electronic polarization. However, the displacement resulting from this polarization is quite small, because the applied electric field is usually very weak compared with the intra-atomic field at an electron, which is caused by the nucleus. Electronic polarization is observed in all materials irrespective of whether other types of polarization mechanisms are present or not, and is responsible for the refraction of light [148]. This is a very rapid process. Typically, the time required for the process is around  $10^{-15}$  s and is predominant at optical frequencies. At these frequencies, dielectrics possessing electronic polarization satisfy the relation  $\varepsilon = n^2$ , where  $n$  is the high frequency refractive index of the material and  $\varepsilon$ , the relative permittivity of the material.

### ***Ionic or atomic polarization***

An electric field can also distort the arrangement of atomic nuclei in a polymer molecule, a process called atomic polarization. This is due to the displacement of negative ions and positive ions in opposite directions under the action of the external applied field. It generally arises in ionic solids. The movement of heavy nuclei is more sluggish than that of electrons, so atomic polarization cannot occur at as high frequencies as electronic polarization, and occurs in the infrared region and in such cases,  $\varepsilon > n^2$ . The time required for atomic polarization is around  $10^{-13}$  s. A major contribution of atomic polarization comes from bending and twisting motions.

Usually, the magnitude of atomic polarization for ordinary polymers is only one-tenth that of electronic polarization.

Both electronic and atomic polarizations are displacements of positive and negative charge centers within the molecule, or alternatively, molecular deformation or molecular distortion. Thus, these processes may also be called displacement deformation or distortion polarization, and the dipole moment so produced is called an induced dipole moment.

### ***Dipolar or orientation polarization***

If the polymer molecules already possess a permanent dipole moment, such as polar molecules, the moment will tend to be aligned by the applied field to give a net polarization in that direction. This orientation polarization typically requires  $10^{-9}$  s. In visualizing this process, we think of dipoles pointing in all directions and continually jumping from one orientation to another as a result of thermal agitation. When the field is applied, the polarization that develops is a relatively small average of orientations favoring the direction of the applied field. The tendency to revert to random orientation opposes the tendency of the field to align the dipoles and thus allows for polarization to vary in proportion to the applied field. The orientation polarization produced by a field as high as  $10^5$  V/mm, nearly the highest used in engineering practice, results only in less than one-hundredth of the calculated polarization if all the dipoles were aligned.

### ***Interfacial polarization***

Interfacial polarization is due to the space charge accumulation at the structural interfaces of an inhomogeneous dielectric material. Electronic, atomic and orientation polarization are all due to charges that are locally bound in atoms, molecules, or the structures of solids and liquids. But in addition, charge carriers usually exist that can migrate for some distance through the dielectric. When the charge carriers are impeded in their motion, either because they become trapped in the material or at an interface or because they cannot be freely discharged or replaced at the electrodes, space charges and a macroscopic field distortion result. Grain/phase

boundaries and free surfaces are common barriers. The effect of this will be the creation of a localized accumulation of charge that will induce its image charge on an electrode and give rise to a dipole moment. This type of polarization occurs particularly in heterogeneous systems where a relatively conductive component is mixed in an insulator. This phenomenon has been first recognized by Maxwell in 1892. He examined the effect of a field applied across a specimen consisting of layers of two different materials with dielectric constants;  $\epsilon_1', \epsilon_2'$  and conductivities;  $\sigma_1, \sigma_2$ , respectively. His results showed that charges will accumulate in time at the interfaces between the layers, whenever  $\epsilon_1' \sigma_2 \neq \epsilon_2' \sigma_1$ . Wagner, in 1914 gave an approximate treatment of the important practical case where a very highly insulating dielectric suffers from inclusions of conductive impurities. Taking the model where the impurity exists as a sparse distribution of small spheres in the dielectric matrix of negligible conductivity, he derived equations for the components of the complex dielectric constant of the composite. Sillars, in 1937 developed the subject further and demonstrated the importance of the shape of the conductive inclusions.

Generally, interfacial polarization may be detected in polymers having structural inhomogeneities even when there is no orientation polarization of the polar inclusions, or even if the inclusions are non-polar. In any case, when structural inhomogeneities between materials of different dielectric constants and conductivities are present, interfacial polarization is expected to occur. This principally influences the low-frequency ( $10^{-5}$  to  $10^2$  Hz) dielectric properties, because the interfacial polarization usually decreases with increasing frequency. Since even pure polymers are never homogeneous, the very low-frequency dielectric constants are expected, and found to be much higher than the dielectric constants obtained from extrapolation of values measured at intermediate and high frequencies.

### **1.5 Microwave technology**

The microwave constitutes only a small portion of the electromagnetic spectrum (300 MHz to 300 GHz), but their uses have become increasingly important in investigations of material properties. Material characterization is essential for the proper selection and implementation of a substance when used in industrial, scientific

and medical applications. The dielectric parameters over a wide range of temperature are needed to assess their suitability for use in telecommunications, dielectric waveguides, lenses, radomes, dielectric resonators and microwave-integrated circuits (MICs), and on lossy materials for estimating their heating response in microwave heating applications. Microwave heating is a very efficient method of heating dielectric materials and is extensively used in industrial as well as household heating applications. For design of microwave absorbers and food packages, dielectric data for lossy materials are required. The knowledge of the dielectric parameters of biological tissues is essential for the proper application of microwave diathermy. The measurement of dielectric parameters will serve as a tool for investigating the intermolecular and intramolecular mechanisms of compounds. Hence, an in-depth study of the microwave characteristics of a material assumes significance.

Determination of dielectric properties and the use of dielectric heating for polymer synthesis attribute microwaves an important status in polymer chemistry. Polar starting materials and very often products, allow rapid and controllable synthesis, the dielectric properties themselves being an excellent indicator of reaction progress. The ability to control synthesis with high accuracy and with direct heating of the reactants has the advantage of large potential savings in energy. Economic analyses suggest that the costs of curing polymers may be reduced from 4-11 MJ/Kg to 0.3-0.5 MJ/kg by switching to the use of microwaves [149]. The synthesis of polyamides and polyurethane films suggests that energy transfer is more efficient with the use of pulsed microwaves than by continuous power [150, 151]. Conductive polymers are causing a great interest due to their wide variety of properties. In particular, from the evolution of their conductivity with frequency, many ideas have been attempted to adapt these phenomena to microwave applications. Inherently conducting polymers are excellent microwave absorbers and make ideal materials for effecting welding of plastics [103]. The two important applications concerned with the use of microwave properties are EMI shielding and radar absorbing materials.

### ***1.5.1 Electromagnetic shielding***

Electromagnetic interference (EMI) is one of the unfortunate byproducts of the rapid proliferation of electronic devices such as cell phones, wireless internet, LAN system or Bluetooth devices [152, 153]. Electromagnetic interference of radio frequency radiation is a serious concern in society. EMI can be defined as spurious voltages and currents induced in electronic circuitry by external sources. In simple words, EMI is unwanted electrical and magnetic energy that causes a disturbance in a receiving device. Such interferences have been considered as a form of pollution. EMI has become a major problem, as it reduces the lifetime and efficiency of the instrument. Cardiac pacemakers have been known to stop working, classical computer information has been lost and vital air traffic control instructions have been misinterpreted due to this invisible form of pollution.

Lightweight EMI shielding is needed to protect the workspace and environment from radiation emanating from computers and telecommunication equipments as well as for protection of sensitive circuits. Radiation shielding materials are essential for high operational reliability and long life of electronic equipment since they reduce or suppress the electromagnetic noise [152, 153]. The term “shield” usually refers to a metallic enclosure that completely encloses an electronic product or a portion of a product. There are, in general, two purposes of a shield *viz.*, to prevent the emissions of the electronics of the product from radiating outside the boundaries of the product, and to prevent radiated emissions external to the product’s electronics, which may cause EMI in the product. This latter purpose is particularly important in military applications, where vital equipment may be exposed to very high-power external sources of electromagnetic radiation such as from radars and possibly even nuclear explosions. A shield is, conceptually, a barrier to the transmission of electromagnetic fields. In order to achieve large values of shielding effectiveness, the shield must completely enclose the electronics and must have no penetrations such as holes, seams, slots or cables. Any penetration in a shield, unless properly treated, may drastically reduce the effectiveness of the shield. The main motivation behind the proper design of shield is to make a product that can comply to National/International Electromagnetic Interference Regulatory Standards. Owing to

their aesthetic appeal, plastics have replaced metal cabinets of electronic housings. However, plastics are transparent to electromagnetic radiations and cannot be earthed to provide electrostatic control. Investigation of new effective materials applicable as microwave absorbers for EMI shielding of various electronic devices ranks among important present-day activities [154-157]. Extensive studies have been carried out to develop new microwave absorbing materials with high magnetic and electric loss [158-161]. Conducting polymers and composites are excellent candidates as shielding materials [162, 163].

### ***1.5.2 Radar absorbing materials***

Dissimulation and camouflage has ever been present in the human mind. Since the beginnings of aeronautics, many attempts have been made to build less visible aircraft. Until 1940, the observation telescope was the only way to observe the enemy's movements. Since then, the entry of radar and the use of different wavelengths have upset the observation techniques. The change in wavelength from visible to microwaves obliged observers to take into account the object shape as well as the physical and chemical nature of the coating materials. The echo, that is to say, the reflected wave indicates the presence of an object in the radar field observation. The military aircraft industry has really taken into account the necessity of reducing the echo (called Radar Cross Section, RCS) of their engines since the sixties [164]. The absorption or dispersion of the electromagnetic energy in the medium between the radar and a protected target by the use of radar absorbing materials to cover the metallic surface of ships/aircrafts is one method of reducing the radar signature of targets. In order to reduce the vulnerability of their aircraft, they looked for a more discrete shape, and used materials intended to absorb radar emitted energy, for example, the 'ironball paint' - a magnetic coating - was the first radar absorbing material described in literature and applied to Lockheed U 2 and SR 71 planes [165, 166]. The metallic aircraft surface is a reflector from the electromagnetic waves point of view. That is why much work has been devoted in France and all over the world, particularly in the USA and in ex-USSR, to the conception of radar absorbing materials (RAM) associated with the former optimized shape.

A number of materials have been developed as RAMs. Conducting polymers present very promising properties because of the chemical nature of the macromolecular chains in which electronic conduction occurs at long range. They have some specific characteristics that make them far more interesting than traditional dielectric materials [167-169]. The insertion of conductivity into various materials such as insulating polymer matrices, reinforcing fabrics, honey-comb structure is now possible and leads to complex structures. They absorb radar waves and can match new environmental constraints, mechanical properties for example. The driving idea is based on the growing process at molecular scale of the conducting entity leading to a uniform macroscopic network in the material. Polyaniline, polypyrrole and polythiophene possess this property.

### **1.6 Objectives of the current work**

The current research has been undertaken to explore the potential of polyaniline coated short Nylon fiber as conductive filler and a reinforcement material in a regionally important elastomer, natural rubber and a polar elastomer, chloroprene rubber. The specific objectives of the present work are:

- ✓ Preparation of polyaniline coated conducting short Nylon fibers
- ✓ Exploration of chromic acid etching treatment as a means to improve the conductivity of the fibers
- ✓ Investigation of the surface characteristics, thermal stability and mechanical strength of the conducting fibers
- ✓ Fabrication of conducting polymer composites of polyaniline/polyaniline coated short Nylon fiber and the elastomers- natural rubber and chloroprene rubber
- ✓ Evaluation of the physico-mechanical properties of the conducting polymer composites
- ✓ Dielectric studies of the conducting polymer composites in the frequency range 0.1-8 MHz at different temperatures



- ✓ Study of the microwave characteristics of the conducting polymer composites in the X and S band frequencies
- ✓ Estimation of the electromagnetic shielding effectiveness of the composites

## References

1. Phillips Y. *Sci Am* 1995;273:75.
2. Letheby H. *J Am Chem Soc* 1862;15:161.
3. Willstatter, Moore. *Ber* 1907;40:2665.
4. Willstatter, Dorogi. *Ber* 1909;42:2147,4118.
5. Green AG, Woodhead AE. *J Chem Soc* 1910;97:2388.
6. Mecoy HN, Moore WC. *J Amer Chem Soc* 2911;33:273.
7. Jozefowicz M, Yu LT, Belorgey G, Buvet R. *J Polym Sci Polym Symp* 1967;16:2934-2954.
8. Surville R, Jozefowicz M, Yu LT, Perichon J, Buvet R. *Electrochim Acta* 1968;13:1451.
9. Shirakawa H, Louis EJ, MacDiarmid AG, Chiang CK, Heeger AJ. *J Chem Soc Chem Commun* 1977;16:578-579.
10. Diaz AF, Logan JA. *J Electroanal Chem* 1980;111:111-114.
11. MacManus PM, Yang SC, Cushman RJ. *J Chem Soc Chem Commun* 1985;1556-1557.
12. Mermilliod N, Tanguy J, Hoclet M, Syed AA. *Synth Met* 1987;18:359-364.
13. MacDiarmid AG, Epstein AJ. *Faraday Discuss Chem Soc* 1989;88:317-332.
14. Cao Y, Smith P, Heeger AJ. *Synth Met* 1992;48(1):91-97.
15. Heeger AJ. *Synth Met* 1993;57(1):3471-3482.
16. Pron A, Osterholm J-E, Smith P, Heeger AJ, Laska J, Zagorska M. *Synth Met* 1993;57(1):3520-3525.
17. Cao Y, Smith P, Heeger AJ. *Synth Met* 1993;57(1):3514-3519.
18. Shacklette LW, Han CC, Luly MH. *Synth Met* 1993;57(1):3532-3537.
19. Ikkala OT, Laakso J, Vakiparta K, Virtanen E, Ruohonen H, Jarvienen H, Taka T, Passiniemi P, Osterholm J-E, Cao Y, Andreatta A, Smith P, Heeger AJ. *Synth Met* 1995;69(1-3):97-100.

20. Chiang CK, Jr. Fincher CR, Park YW, Heeger AJ, Shirakawa H, Louis EJ, MacDiarmid AG. *Phys Rev Lett* 1977;39:1098.
21. Chiang CK, Druy MA, Gau SC, Heeger AJ, Louis EJ, MacDiarmid AG. *J Am Chem Soc* 1978;100:1013.
22. Chiang JC, MacDiarmid AG. *Synth Met* 1986;13:193.
23. MacDiarmid AG, Chiang JC, Richter AG, Epstein AJ. *Synth Met* 1987;18:285.
24. MacDiarmid AG, Chiang JC, Richter AF, Somasiri NLD, Epstein AJ. In: Alcacer L, editor. *Conducting polymers*. Reidel, Dordrecht, 1987, p. 105.
25. MacDiarmid AG, Epstein AJ, *Faraday Discuss Chem Soc* 1989;88:317.
26. Rubner MF. *Molecular electronics*. Research Studies Press, 1992, chapter 2.
27. Alcacer L. *Conducting polymers*. Reidel Publishing Company, 1987.
28. Naarmann H. *Polymers to the year 2000 and beyond*. John Wiley and Sons, 1993, chapter 4.
29. Ian M. *Introduction to synthetic polymers*. Oxford Science Publications, 1994, chapter 10.
30. Salaneck WR, Clark DT, Samuelsen EJ. *Science and application of conducting polymers*, IOP Publishing, 1991.
31. Bredas JL, Chance RR, Silbey R. *Phys Rev* 1982;B26:58431.
32. Bredas JL, Scott JC, Yakushi K, Street GB. *Phys Rev* 1984;B30:1023.
33. Javedi HHS, Angelopolous M, MacDiamid AG, Epstein AJ. *Synth Met* 1988;26:1.
34. Litzelman A, Scheerer B, Fink J, Meerholz K, Heinze J, Sariciftci NS, Kuzmany H. *Synth Met* 1989;29:E313.
35. Campbell DK, Degrand TA, Mazumdar S. *Phys Rev Lett* 1984;52:1717.
36. Bredas JL, Thomas B, Fripiat JG, Andre JM, Chance RR. *Phys Rev B* 1984;29:6761.
37. Kivelson S. *Phys Rev* 1982;B25:3798.
38. Campos M, Braz Bello Jr. *J Phys D Appl Phys* 1997;30:1531-1535.
39. Mott NF. *J Non-Cryst Solids* 1968;1:1
40. Efros AL, Shlovskii BI. *J Phys C* 1975;C8:L49.
41. Sheng P, Abeles B, Arie Y, *Phys Rev Lett* 1973;31:44.

42. Nakhgmedov EP, Progodin VN, Smukhin AN, Sov Phys Sol Stat 1989;31:368.
43. Li Q, Cruz L, Philips P. Phys Rev B 1993;47:323.
44. Wang ZH, Scherr EM, MacDiarmid AG, Epstein AJ. Phys Rev 1992;B45:4190.
45. Choi HY, Mele EJ. Phys Rev Lett 1987;59:2188.
46. Abeles B, Sheng P, Coutts MD, Arie Y. Adv Phys 1975;24:407.
47. Huang WS, MacDiarmid AG, Epstein AJ. J Chem Soc Chem Commun 1987;1784.
48. MacDiarmid AG, Chiang JC, Halpern M, Huang WS, Mu SL, Somasiri NL, Wu W, Yaniger SI. Mol Crys Liq Cryst 1985;121:173.
49. Armes SP, Miller JF. Synth Met 1988;22:385.
50. Asturias GE, MacDiarmid AG, Epstein AJ. Synth Met 1989;29:E157.
51. Cao Y, Andreatta A, Heeger AJ, Smith P. Polymer 1989;30:2305.
52. Nalwa HS. Conductive polymers: Synthesis and electrical properties. Vol 2, John Wiley and Sons, 1977.
53. MacDiarmid AG. Synth Met 1997;84(1-3):27-34.
54. Malinauskas A. Polymer 2001;42(9):3957-3972.
55. Gospondinova N, Terlemezyan L. Prog Polym Sci 1998;23(8):1443-1484.
56. Bhattacharya A, De A. Prog Solid State Chem 1996;24(3):141-181.
57. Negi S, Adhyapak PV. J Chem Soc Chem Commun 1984;13:817-818.
58. Han MG, Im SS. Polymer 2001;42(17):7449-7454.
59. Jeevananda T, Siddaramaiah. Eur Polym J 2003;39(3):569-578.
60. Anand J, Palaniappan S, Sathyanarayanan DN. Prog Polym Sci 1998;23(6):993-1018.
61. Cottevieille D, Le Mehaute A, Challioui C, Mirebeau P, Demay JN. Synth Met 1999;101(1-3):703-704.
62. Makela T, Sten J, Hujanen A, Isotalo H. Synth Met 1999;101(1-3):707.
63. Jonas F, Heywang G. Electrochim Acta 1994;39(8-9):1345-1347.
64. Stenger-Smith JD. Prog Polym Sci 1998;23(1):57-79.
65. Hanhi K, Lonnberg V, Pyorala K, Loennberg V, Pyoeraelae K. WO Patent 9,706,213;1997.

66. Wessling B, Posdorfer J. *Electrochim Acta* 1999;44(12):2139-2147.
67. Koul S, Chandra R, Dhawan SK. *Sens Actuator B* 2001;75(3):151-159.
68. Farrington J, Moore AJ, Tilbury N, Church J, Biemond PD. In: *Proceedings of the 3<sup>rd</sup> IEEE International symposium on wearable computers*, San Francisco, 18-19 Oct 1999.
69. Han MG, Im SS. *J Appl Polym Sci* 2001;82:2760.
70. Kralijic M, Mandic Z, Duic L. *Corros Sci* 2003;45:181.
71. Tan ST, Zhang MQ, Rong MZ, Zeng HM, Zhao FM. *Polym Polym Compos* 2001;30:257.
72. Park ID, Chang DH. *J Kor Fiber Soc* 1996;33:17.
73. Vital Signs Monitor, Fitsens, <http://www.fitsense.com/> Fit-Sense Technology, 21 Boston Road, PO Box 730, Southborough, MA 01772.
74. Gragory YC. *Handbook of conductive polymer*. 2<sup>nd</sup> edition, Marcel Dekker, New York, 1998, chapter 3.
75. Kuhn HH, Kimbrell WC. US Patent 4 803 096, 1989.
76. Gregory RV, Kimbrell WC, Kuhn HH. *Synth Met* 1989;28(1-2):823.
77. Gregory RV, Samuels RJ, Hanks T. National Textile Center annual report. <http://www.furman.edu/~hanks/ntc/>.
78. Wei Y, Hsueh KF. *J Polym Sci Part A Polym Chem* 1989;27:4351.
79. Heisey CL, Wightman JP, Pittman EH, Kuhn HH. *Text Res J* 1993;63:247.
80. Byun SW, Im SS. *Synth Met* 1993;55:3501.
81. Park YH, Cheung JS. *J Kor Soc Tex Eng Chem* 1989;26:65.
82. Kuhn HH. Kluwer Academic Publishers: Spartanburg, 1993:25.
83. Anbarasan R, Jayaseharan, Sudha M, Devi JL, Nirmala PV, Gopalan A. *J Appl Polym Sci* 2001;81(2):468-478.
84. Anbarasan R, Vasudevan T, Gopalan A. *J Mater Sci* 2000;35(3):617-25.
85. Kuhn HH, Child AD. *Handbook of conductive polymer*, 2<sup>nd</sup> edition, Marcel Dekker: New York, 1998, chapter 35.
86. Oh KW, Hong KW. *Textile Res J* 2001;71(8):726.
87. Kim SH, Seong JH, Oh KW. *J Appl Polym Sci* 2002;83:2245.
88. Zinger B, Shkolnik, Hocker H. *Polymer* 1989;30:628.
89. Jannakoudakis PD, Pagalos N. *Synth Met* 1995;68:17.

90. Bhadani SN, Sen Gupta SK, Sahu GC, Kumari M. *J Polym Mater* 1996;13:61-67.
91. Bhadani SN, Sen Gupta SK, Sahu GC, Kumari M. *J Appl Polym Sci* 1996;61:207-212.
92. Bhadani SN, Kumari M, Sen Gupta SK, Sahu GC. *J Appl Polym Sci* 1997;64:1073-1077.
93. Forveille JL, Olmedo L. *Synth Met* 1995;65:5.
94. Kim B, Koncar V, Dufour C. *J Appl Polym Sci* 2006;101:1252-1256.
95. Liu, Yang SC. *J Chem Soc Chem Commun* 1991;49:9.
96. Andreatta A, Heeger AJ, Smith P. *Polym Commun* 1990;31:275.
97. Wan Y, Xiong C, Yu J, Wen D. *Compos Sci Technol* 2005;65:1769-1779.
98. Das NC, Chaki TK, Khastgir D, Chakraborty A. *Adv Polym Technol* 2001;20:226.
99. Ghosh P, Chakraborty A *Eur Polym J* 2000;36:1043-1054.
100. Sau KP, Chaki TK, Khastgir D. *Composites Part A* 1998;29:363.
101. Volf J, Holy S, Vleek J. *Sens Actuators A* 1997;62:556.
102. Knite M, Tetenis V, Kiploka A, Kaupuzs J. *Sens Actuators A* 2004;110:142.
103. Ellis JR. In: Skotheim TA, editor. *Handbook of conducting polymers*. Vol. 1, New York; Marcel Dekker Inc, 1986, p. 489.
104. Zoppi R, De Paoli M-A. *J Polym Sci Part A: Polym Chem* 1994;32:1001.
105. Zoppi R, De Paoli M-A. *Polymer* 1995;37:1999.
106. Yigit S, Hacaloglu J, Akbulut U, Toppare L. *Synth Met* 1996;79:11-16.
107. Tassi EL, De Paoli M-A. *J Chem Soc Chem Commun* 1990:155.
108. Tassi EL, De Paoli M-A. *Polymer* 1992;33:2427.
109. Tassi EL, De Paoli M-A, Panero S, Scrosati B. *Polymer* 1994;35:565.
110. Niwa O, Kakuchi M, Tamamura T. *Macromolecules* 1987;20:749.
111. Tassi EL, De Paoli M-A. *Electrochim Acta* 1994;39:2481.
112. Vallim MR, Felisberti MI, De Paoli M-A. *Proceedings 16<sup>th</sup> Reuniao Anual da SBQ, Caxambu, 1993, p. QM-22.*
113. Vallim MR, Felisberti MI, De Paoli M-A. *Proceedings 2<sup>nd</sup> Congresso Brasileiro de Polimeros, Sao Paulo, 1993, p. 574-577.*

114. Vallim MR, Felisberti MI, De Paoli M-A. Proceedings 2<sup>nd</sup> Simposio Iberoamericano de Polimeros, 4<sup>th</sup> Simposio Latinoamericano de Polimeros, 6<sup>th</sup> International Macromolecular Colloquium, Gramado 1994, p. 215-217.
115. Leyya ME, Bara GMO, Soares BG. Synth Met 2001;123(3):443-449.
116. Davies SJ, Ryan TG, Wilde CJ, Beyer G. Synth Met 1995;69(1-3):209-210.
117. Leyya ME, Bara GMO, Gorelova MM, Soares BG, Sens M. J Appl Polym Sci 2001;80(4):626-633.
118. Koul S, Chandra R, Dhawan SK. Polymer 2000;41(26):9305-9310.
119. Tsanov T, Ditchewa-Kortchakova M, Terlmezian L. Polym Polym Comp 2000;8:115.
120. Vallim MR, Felisberti MI, De Paoli M-A. J Appl Polym Sci 2000;75:677.
121. Pinho MS, Gorelova MM, Dezzotti M, Soares BG, Pertsin AJ. J Appl Polym Sci 1998;70:1543.
122. Faez R, De Paoli M-A. J Appl Polym Sci 2001;82:1768.
123. Faez R, De Paoli M-A. Eur Polym J 2001;37:1139-1143.
124. Faez R, Gazotti WA, De Paoli M-A. Polymer 1999;40:5497-5503.
125. Faez R, Schuster RH, De Paoli M-A. Eur Polym J 2002;38:2459-2463.
126. Schmidt V, Domenech SC, Soldi MS, Pinheiro EA, Soldi V. Polym Degrad Stab 2004;83:519.
127. Pinho MS, Gorelova MM, Dezzotti M, Soares BG, Pertsin AJ. J Appl Polym Sci 1999;71:2329.
128. Soares BG, Amorim GS, Souza Jr FG, Oliveira MG, Pereira da Silva JE. Synth Met 2006;156:91-98.
129. Ismail MN, Ibrahim MS, Abd El-Ghaffar MA. Polym Degrad and Stab 1998;62(2):33.
130. Mott NF. Phil Mag 1969;19:835.
131. Mc Crum NG, Read BE, Williams G. Anelastic and dielectric effects in polymeric solids. New York: Dover; 1967.

132. Avakian P, Starkweather Jr. HW, Kampert WG. In: Cheng SZG, editor. Dielectric analysis of polymers. Handbook of thermal analysis and calorimetry, Vol 3, New York: Elsevier; 2002, p. 147-64.
133. Ezquerra TA, Liu F, Boyd RH, Hsiao BS. Polymer 1997;38:5793.
134. Negau E, Pissis P, Apecis L, Ribelles G. J Phys D Appl Phys 1997;30:1551.
135. Coburn JC, Boyd RH. Macromolecules 1986;19:2238.
136. Iannace S, Nicolais L. J Polym Sci B Polym Phys Ed 1997;64:911.
137. Algeria A, Colmenero J, Ngai KL, Roland CM. Macromolecules 1994;27:4486.
138. Bristow JF, Kalika DS. Polymer 1997;38:287.
139. Cook M, Williams G, Tyssul T Jones. Polymer 1975;16:835.
140. Jayamol G, Bhagawan SS, Sabu T. J Polym Eng 1997;17:383.
141. Perrier G, Bergert A. J Polym Sci B Polym Phys 1997;35:1349.
142. Brosseau C, Boulic F, Queffelec P, Bourbigot C, Le Mest Y, Loaec J, Beroual A. J Appl Phys 1997;81:882.
143. Ezquerra TA, Balta-Calleja FJ, Zachmann HG. Polymer 1994;35:2600.
144. Dendizik Z, Gburski Z. J Molec Struct 1997;410/411:238.
145. D'Amore A, Kenny JM, Nicolais L. Polym Eng Sci 1990;30:314.
146. Saad GR, Manssour AA, Hamed AH. Polymer 1997;38:4091.
147. TA Instruments, DEA 2970 Dielectric Analyzer, TA-057, TA instruments applications library: [www.tainst.com](http://www.tainst.com).
148. Blythe AR. Electrical properties of polymers. University of Cambridge, Cambridge, 1979.
149. Finzel M, Hawley M, Jon J. Polym Eng Sci 1991;31:1240-1244.
150. Jullien H, Valot H. Polymer 1985;26:506-510.
151. Phillips G. J Appl Phys 1991;69:899.
152. Maeda T, Sugimoto S, Kagotani T, Tezuka N, Inomata K. J Magn Magn Mater 2004;281:195.
153. Dhawan SK, Singh N, Venkatachalam S. Synth Met 2002;129:261.
154. Ricca A, Bjorlin R, Peacock D, Gochman M, Shawhan G. ITEM 2000, Int J EMC USA 2000;139.

155. Thompson LS, Quinn RK, ITEM 2000, Int J EMC USA 1999;60.
156. Klein CA. IEEE Trans Microwave Theory Tech 1990;38:321.
157. Clupper T. ITEM 2000, Int J EMC USA 1999;59.
158. Ruan S, Xu B, Suo H, Wu F, Xiang S, Zhao M. J Magn Magn Mater 2000;212:175.
159. Babbar VK, Razdan A, Puri RA, Goel TC. J Appl Phys 2000;87:4362.
160. Cho SB, Kang DH, Oh JH. J Mater Sci 1996;31:4719.
161. Chandrasekhar P, Naishadhan K. Synth Met 1999;105:115.
162. Dhawan SK, Trivedi DC. J Electromagnet Compat 1991;1:1-4.
163. Barnes A, Despotakis A, Wright PV, Wong TCP, Chambers B, Anderson AP. Electron Lett 1996;32:358.
164. Richardson D. Stealth. Salamander Books Ltd. 1989.
165. Sweetman B. International Defense Review, 1992;2:159.
166. Brown AS. Aerospace America March 1990:16.
167. Sherman RD, Middleman LM, Jacobs SM. Polym Eng Sci 1988;23:36.
168. Mobius KH. Kunststoffe 1988;78:53.
169. Taka T. Synth Met 1991;41:1177.



*Conducting Nylon fibers were prepared by in situ polymerization of aniline on to the fiber surface, after providing a chemical etching treatment to the fibers using chromic acid. The properties of the etched and polyaniline coated fibers were evaluated using scanning electron microscopy, X-ray photoelectron spectroscopy, infrared spectroscopy, X-ray diffraction, thermogravimetry and differential scanning calorimetry. Though the etching process caused a marginal decline in the mechanical properties of the fiber, it provided a reasonably rough surface for PANI adhesion and enhanced the conductivity of the fiber. The conductivity increased from  $4.22 \times 10^{-2}$  S/cm to  $3.72 \times 10^{-1}$  S/cm at an etching time of 4 h.*

---

## Chapter 2

### Polyaniline coated short Nylon fiber\*

#### 2.1 Introduction

Conductive polyaniline (PANI)/polymer fibers can be produced either by inclusion of PANI or by *in situ* oxidative polymerization of aniline monomer. Owing to low thermal stability and insolubility of PANI, the former method is hardly acceptable for producing conductive composite fabrics. Therefore, most studies have focused on *in situ* polymerization route to produce conductive fabrics. This method does not require destruction of the substrate and provides reasonably good conductivity and

---

\* A part of the work described in this chapter has been presented at:

- ✓ *International Conference **POLYCHAR-16**, World Forum of Advanced Materials, Feb 17-21, 2008, World Unity Convention Center, Lucknow, India*
- ✓ *17<sup>th</sup> AGM of Materials Research Society of India, **AGM-MRSI**, Feb 13-15, 2006, University of Lucknow, India*
- ✓ *National Conference on Frontiers in Polymer Science and Technology, **POLYMER 2006**, Feb 10-12, 2006, Indian Association for the Cultivation of Science, Kolkata, India*

produces modified polymer matrices with a PANI layer at their surface. The thickness and conductivity of the layers depend on the method of modification and on the time of contact of the solid matrix with the reaction medium. The surface conductivity obtained may range, from semiconductor level up to the conductivity of pure PANI. Even a simple dipping method resulted in conductivity of 1-5 S/cm and transmittance of 80 % at 450-650 nm for a 0.5  $\mu\text{m}$  PANI layer [1]. Apparently, this method is not technically suitable for sheet materials, because it requires the use of polymer matrixes with a good adhesion to PANI. Moreover, it produces pure PANI deposits having poor mechanical properties. At the same time, for fibers and textile materials with a well-developed reactive surface, it may lead to the production of conducting fibers and fabrics with PANI grafted on the surface and inside the pores.

Genies *et al.* have reported the impregnation of PANI onto glass textiles [2]. Chemical polymerization of polypyrrole on poly(ethylene terephthalate) fabric was reported by Kim *et al.* [3]. Aniline can be polymerised on the fabrics from the aqueous solution [4-6] or the vapor phase [7] using appropriate oxidizing agents. The use of peroxosalts as oxidants causes a graft copolymerization of aniline and its derivatives onto a polymer matrix [8]. Anbarasan and co-workers investigated the kinetics of this grafting onto rayon [9], wool [10] and PET [11] fibers and proposed a possible mechanism of graft and homo polymerization of aniline. Specifically, they carried out oxidative chemical polymerization of aniline using peroxydisulfate and peroxomonosulfate as the sole initiator in an aqueous acidic medium in the presence of the fibers. This resulted in the chemical grafting of PANI onto the fibers, confirmed by Fourier Transform Infrared spectroscopy (FTIR), cyclic voltammetry, weight loss study, and conductivity measurements. The authors proposed a probable mechanism involving graft polymerization of aniline through interaction of the oxidant with the fiber surface, inducing the formation of radical sites at the fiber surface, followed by grafting aniline with its subsequent participation in a typical aniline oxidative polymerization. The conductivity of such fabrics depended on deposition of conductive polymer on the surface or in the interstices of the fabric [4, 12]. A PANI layer bonded strongly to the fiber surface is required for better conductivity

and durability. This can be achieved by improving the adhesion of PANI on the fiber surface.

Two methods to obtain electrically conductive fabrics by *in situ* polymerization of aniline were compared by Oh and coworkers [13]. These materials were prepared by immersing the Nylon fabrics in pure aniline or an aqueous hydrochloride solution of aniline followed by initiating the successive direct polymerization in a separate bath (DPSB) or in a mixed bath (DPMB) of oxidant and dopant solution with aniline. They showed that the DPMB process produced higher conductivity in the composite fabrics, reaching  $0.6 \times 10^{-1}$  S/cm. Moreover, this process induced a smaller decrease in the degree of crystallinity than the DPSB process. The PANI/Nylon composite fabrics displayed a good serviceability. Thus, no important changes in the conductivity were observed after abrasion of the composite fabrics over 50 cycles and multiple acid and alkali treatment. The stability of the conductivity decreased by less than one order after exposure to light for 100 h, but it was significantly decreased after washing with a detergent.

In another work, the same authors attempted plasma treatment of the fabrics to improve the surface adhesion between PANI and Nylon fabric and hence the serviceability, conductivity and durability [14]. But this is an expensive method. An alternate, less expensive method is chemical etching of the fiber surface. The monomer and the oxidant are adsorbed on the surface of the fiber instead of diffusing into the fiber. Therefore, it is expected that the fabric conductivity and adhesion of the polymer on the fiber surface can be improved with an increase in the surface energy and surface area. This can be achieved by the chemical etching process. In this work, we have explored the possibility of using chromic acid for improving the adhesion properties and conductivity of Nylon fibers. Optimization of chromic acid concentration and etching time and the electrical properties of the PANI deposited etched Nylon fiber are presented. Surface characteristics of the etched fibers were analyzed using scanning electron microscopy, X-ray photoelectron spectroscopy, infrared spectroscopy and X-ray diffraction analysis. The thermal characterization of the coated fibers is also presented.

## **2.2 Experimental**

### **2.2.1 Materials**

Nylon-6 fibers (1680/2D) were obtained from Sri Ram Fibers Ltd., Chennai, India. Aniline, ammonium peroxydisulfate, hydrochloric acid and chromium trioxide were supplied by S. D. Fine Chemicals Ltd., Mumbai, India.

### **2.2.2 Preparation of polyaniline**

An aqueous solution of ammonium peroxydisulfate (1.62 M) was added drop wise to a solution of 0.0219 M aniline in 50 ml, 1 N hydrochloric acid at ambient temperature. After complete addition, the reaction was left to proceed for 4 h. The precipitate formed was then filtered, washed with acetone till the filtrate became colorless, followed by a wash with dilute hydrochloric acid and finally with water. The PANI formed was then dried in an air oven at 60 °C.

### **2.2.3 Etching treatment**

1 g of the chopped Nylon fibers (5 mm) were immersed in 250 ml of aqueous chromic acid solution of a specified concentration at 60-65 °C with continuous stirring for a specified time. The etched fibers were subsequently filtered and washed with distilled water till the washings were free from coloration and then dried at 60 °C in an air oven.

### **2.2.4 In situ polymerization**

0.5 g of the etched fiber was soaked in 10 ml of aniline for 24 h at room temperature. The excess aniline was then drained off and the fibers were blotted with tissue paper. The weight of the fiber before and after soaking was noted. The percentage of aniline absorption was determined to be 23.8 %. The soaked fibers were then added to a solution of 0.0219 moles of aniline in 50 ml, 1 N hydrochloric acid. The polymerization was carried out for 4 h at room temperature using an aqueous solution of ammonium peroxydisulfate (1.62 M). These were then filtered, washed with water till the washings became colorless and further dried.

### **2.2.5 Characterization**

#### **2.2.5.1 Tensile strength**

The mechanical properties of the fibers were studied using a Shimadzu Universal Testing Machine (UTM model AG I) with a load cell capacity of 10 kN. The gauge length between the grips at the start of each test was adjusted to 50 mm. The fibers of 254 mm length were held between the two grips and a uniform rate of grip separation (cross-head speed) of 20 mm/min was applied. The strength was evaluated after each measurement automatically by the microprocessor and presented on a visual display. Average of atleast six sample measurements were taken to represent each data point.

#### **2.2.5.2 Scanning electron microscopy (SEM)**

Scanning electron microscopy is a very useful tool to gather information about topography, morphology, composition and micro structural information of materials. In a typical SEM, electrons are thermionically emitted from a tungsten or lanthanum hexaboride (LaB<sub>6</sub>) cathode and are accelerated towards an anode; alternatively, electrons can be emitted via field emission. The electron beam, which typically has an energy ranging from a few hundred eV to 100 keV, is focused by one or two condenser lenses into a beam. Characteristic X-rays are emitted when the primary beam causes the ejection of inner shell electrons from the sample and are used to tell the elemental composition of the sample. The back-scattered electrons emitted from the sample may be used alone to form an image or in conjunction with the characteristic X-rays. These signals are monitored by detectors (photo multiplier tubes) and magnified. An image of the investigated microscopic region of the specimen is thus observed in cathode ray tube and is photographed.

The SEM images of the short fibers were obtained using a Cambridge Instruments S 360 stereo scanner (version V02-01). The fibers were mounted on a metallic stub and an ultrathin coating of electrically conducting material (gold) is deposited by low vacuum sputter coating. This is done to prevent the accumulation of static electric fields at the specimen due to the electron irradiation during imaging. Another reason

for coating, is to improve contrast. The SEM is capable of producing high-resolution images of a sample surface.

#### **2.2.5.3 X-ray photoelectron spectroscopy (XPS)**

For each and every element, there will be a characteristic binding energy associated with each core atomic orbital i.e. each element will give rise to a characteristic set of peaks in the photoelectron spectrum at kinetic energies determined by the photon energy and the respective binding energies. The presence of peaks at particular energies therefore indicates the presence of a specific element in the sample under study. Furthermore, the intensity of the peaks is related to the concentration of the element within the sampled region. The shape of each peak and the binding energy can be slightly altered by the chemical state of the emitting atom. Hence XPS can provide chemical bonding information as well. XPS is not sensitive to hydrogen or helium, but can detect all other elements. Thus, X-ray photoelectron spectroscopy is a quantitative spectroscopic technique that measures the elemental composition, empirical formula, chemical state and electronic state of the elements that exist within a material. XPS is also known as ESCA, an abbreviation for Electron Spectroscopy for Chemical Analysis.

The phenomenon is based on the photoelectric effect. XPS spectra are obtained by irradiating a material with a beam of aluminum or magnesium X-rays while simultaneously measuring the kinetic energy and number of electrons that escape from the top 1 to 10 nm of the material being analyzed. XPS requires ultra-high vacuum conditions. Commercial XPS instruments use either a highly focused 20 to 200  $\mu\text{m}$  beam of monochromatic aluminum K-alpha X-rays or a broad 10-30 mm beam of non-monochromatic Mg X-rays.

The surface of the fibers was analyzed using an X-ray induced photoelectron VG Scientific ESCA-3000 spectrometer using a non-monochromatic Mg  $K_{\alpha}$  radiation (1253.6 eV). First a general scan was recorded from 0-1000 eV at steps of 1 eV to confirm the presence of C, N and O in the sample. Then, narrow scans were done for  $C_{1s}$ ,  $N_{1s}$  and  $O_{1s}$  at steps of 0.1 eV. To correct for possible deviations caused

by electric charge of the samples, the  $C_{1s}$  line at 285 eV was taken as internal standard.

#### **2.2.5.4 Infrared spectroscopy (IR)**

Infrared spectroscopy is the absorption measurement of different IR frequencies ( $400\text{--}4000\text{ cm}^{-1}$ ) by a sample positioned in the path of an IR beam. Infrared spectroscopy exploits the fact that molecules have specific frequencies at which they rotate or vibrate corresponding to discrete energy levels. These resonant frequencies are determined by the shape of the molecular potential energy surfaces, the masses of the atoms and, by the associated vibronic coupling. In order for a vibrational mode in a molecule to be IR active, it must be associated with changes in the permanent dipole. The frequency of the vibrations can be associated with a particular bond type.

The infrared spectrum of a sample is collected by passing a beam of infrared light through the sample. Examination of the transmitted light reveals how much energy was absorbed at each wavelength. This can be done with a monochromatic beam, which changes in wavelength over time, or by using a Fourier Transform instrument to measure all wavelengths at once. From this, a transmittance or absorbance spectrum can be produced, showing at which IR wavelengths the sample absorbs. Analysis of these absorption characteristics reveals details about the molecular structure of the sample. This technique works almost exclusively on samples with covalent bonds.

Infrared spectra of the fibers were recorded on a Bruker FTIR spectrophotometer model Tensor 27 (spectral range of  $7500\text{ cm}^{-1}$  to  $370\text{ cm}^{-1}$  with standard KBr beamsplitter) in attenuated total reflectance (ATR) mode. It uses zinc selenide as the crystal material with high sensitivity DLATGS detector with KBr window.

#### **2.2.5.5 X-ray diffraction (XRD)**

X-rays are electromagnetic radiation of wavelength about  $1\text{ \AA}$ , which is about the same size as an atom. X-ray diffraction has been in use in two main areas, for the fingerprint characterization of crystalline materials and the determination of their

structure. Each crystalline solid has its unique characteristic X-ray powder pattern which may be used as a "fingerprint" for its identification. Once the material has been identified, X-ray crystallography may be used to determine its structure, i.e. how the atoms pack together in the crystalline state and what the interatomic distance and angle are, etc. X-ray diffraction is one of the most powerful characterization tools used in solid state chemistry and materials science. We can determine the size and the shape of the unit cell for any compound most easily using the diffraction of X-rays.

X-ray diffractograms of the fibers were recorded using a Bruker AXS D8 Advance Diffractometer using  $\text{CuK}_\alpha$  radiation ( $\lambda = 1.54 \text{ \AA}$ ) at 35 kV and 25 mA with a smallest addressable increment of  $0.001^\circ$ . XRD results were obtained in the range  $2\theta = 3^\circ$  to  $80^\circ$  at a scan rate of  $4^\circ/\text{min}$ .

#### **2.2.5.6 Thermogravimetric analysis (TGA)**

Thermogravimetric analysis is a type of testing that is performed on samples to determine changes in weight in relation to change in temperature. Such analysis relies on a high degree of precision in three measurements: weight, temperature, and temperature change. TGA is commonly employed in research and testing to determine characteristics of polymers, to determine degradation temperatures, absorbed moisture content of materials, the level of inorganic and organic components in materials, decomposition points of explosives, solvent residues and composition of blends and composites. The analyzer usually consists of a high-precision balance with a pan loaded with the sample. The sample is placed in a small electrically heated oven with a thermocouple to accurately measure the temperature. The atmosphere may be purged with an inert gas to prevent oxidation or other undesired reactions. A computer is used to control the instrument. Analysis is carried out by raising the temperature gradually and plotting weight against temperature.

Thermogravimetric studies lend a hand in determining the thermal stability of the fibers. The TGA instrument produces a continuous record of weight as a function of temperature. TGA studies were carried out on a Q-50, TA Instruments



thermogravimetric analyzer (TGA) with a programmed heating of 20 °C/min from ambient to 800 °C. The chamber was continuously swept with nitrogen at a rate of 90 ml/min. The onset temperature of degradation was recorded and temperature at maximum degradation was taken as the peak degradation temperature. The weight percentage of the samples remaining at 800 °C was recorded as the residue.

#### **2.2.5.7 Differential scanning calorimetry (DSC)**

Differential scanning calorimetry is a technique for measuring the energy necessary to establish a nearly zero temperature difference between a substance and an inert reference material, as the two specimens are subjected to identical temperature regimes in an environment heated or cooled at a controlled rate. Both the sample and reference are maintained at nearly the same temperature throughout the experiment. The basic principle underlying this technique is that, when the sample undergoes a physical transformation such as phase transitions, more (or less) heat will need to flow to it than the reference to maintain both at the same temperature. Whether more or less heat must flow to the sample depends on whether the process is exothermic or endothermic. By observing the difference in heat flow between the sample and reference, differential scanning calorimeters are able to measure the amount of heat absorbed or released during such transitions.

Differential scanning calorimetry was employed to determine the degree of crystallinity, heat of fusion and melting temperature of the fibers. The measurements were conducted using a DSC Q-100, TA Instruments calorimeter having a temperature accuracy of  $\pm 0.1$  °C. Analyses were done in nitrogen atmosphere using standard aluminum pans. The samples were exposed to a heating rate of 10 °C/min from ambient to 300 °C. The peak temperature of the melting endotherm was taken as the melting temperature;  $T_m$ , and the heat of fusion;  $\Delta H_f$ , was determined from the area of the melting endotherm. The degree of crystallinity;  $\chi_c$ , was determined by normalizing the observed heat of fusion of the sample to that of a 100 % crystalline sample of Nylon, which is available from literature [15, 16].

#### **2.2.5.8 DC electrical conductivity**

The DC electrical conductivity of the fibers was measured by a two-probe method using a Keithley 2400 source-measure unit, which is a fully programmable instrument capable of sourcing and measuring voltage or current simultaneously with accuracy. A constant current source was used to pass a steady current through one of the probes and the voltage across the other was measured. The measurements were done at room temperature. The conductivity of the sample was calculated by the following formula:

$$\sigma(S/cm) = (I/V) \times (l/A) \quad (2.1)$$

where,  $\sigma$  is the electrical conductivity,  $I$  is the current through the probe in amperes,  $V$  is the voltage across the probe in volts,  $l$  is the spacing between the probes in centimeters and  $A$  is the area of contact of the probes with the sample in centimeter square.

### **2.3 Results and discussion**

#### **2.3.1 Characterization of polyaniline**

##### **2.3.1.1 Scanning electron microscopy**

The SEM micrograph of pristine PANI can be seen in fig. 2.1. It shows aggregated granular form and lacks macroscopic molecular orientation. Several reports on such a granular morphology of PANI are available in the literature [17]. Especially, such morphology is obtained in the absence of a surfactant [18]. The shape of the chemically polymerized polyaniline particles is generally difficult to be controlled in a bulk polymerization process. PANI aggregates are made of small grains comprised of a collection of small spheres, which in turn, is comprised of smaller spheres built from still smaller primary particles. These primary particles have a metallic core surrounded by an amorphous non-metallic shell. Haba and coworkers calculated the average size of the DBSA doped primary PANI particles to be 18.7 nm using Small angle X-ray scattering (SAXS) [19]. These primary particles generate aggregates,

which further cluster into agglomerates. These agglomerates, about 50  $\mu\text{m}$  in size, are located within gel-like units, which are structured due to the formation of hydrogen bonds between free DBSA molecules. The granular morphology obtained for PANI is presumed to be due to the characteristic feature of the hydrochloric acid dopant used in the preparation. There are reports which state that the dopant size and its nature affect the surface morphology of the composite. Oh *et al.* synthesized PANI with various acidic dopants with an electrochemical method and found that the dopants had a great influence on the morphology of PANI [20].

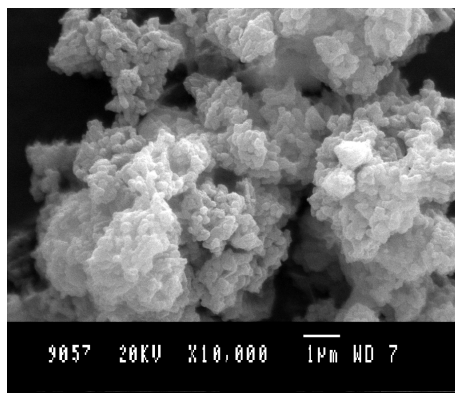


Fig. 2.1 Scanning electron micrograph of pristine PANI

#### 2.3.1.2 Infrared spectroscopy

Fig. 2.2 presents the IR spectrum of pristine PANI. The absorption at  $3235\text{ cm}^{-1}$  is assigned to the  $\text{NH}^+$  group and indicates the protonated PANI salt. There were no features in the spectra between  $2800\text{ cm}^{-1}$  and  $1650\text{ cm}^{-1}$ , because no functional groups of PANI showed vibration absorption peaks in this region. The peaks at  $1569\text{ cm}^{-1}$  and  $1492\text{ cm}^{-1}$  are due to the  $\text{C}=\text{C}$  stretching in the quinoid ring and benzenoid ring, respectively [21-23]. The peak at  $1299\text{ cm}^{-1}$  is due to the  $\text{C}-\text{N}$  stretching of the secondary amine of the PANI backbone. A strong band characteristically appears at  $1146\text{ cm}^{-1}$  which has been explained as an electronic band or a vibrational band of nitrogen quinone, an in-plane bending vibration of imino-1,4-phenylene, and has been reported to be associated with the electrical conductivity of PANI [22-25].

The -C-H aromatic out of plane bending mode is a key to identify the type of substituted benzene. For PANI, this mode is observed as a single band at  $817\text{ cm}^{-1}$ , which falls in the range  $800\text{--}860\text{ cm}^{-1}$  and is reported for 1, 4 disubstituted benzene [26-28].

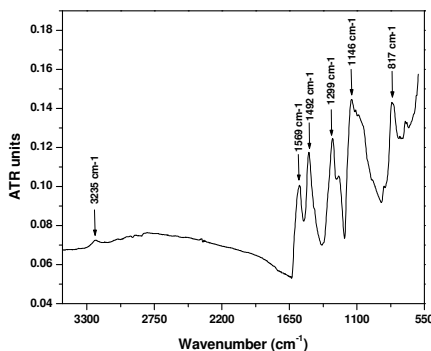


Fig. 2.2 IR spectrum of pristine PANI

### 2.3.1.3 X-ray diffraction analysis

The XRD pattern of pristine PANI was obtained as shown in fig. 2.3.

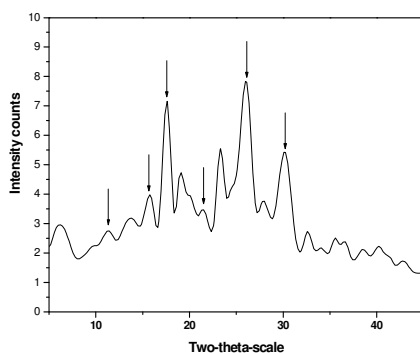


Fig. 2.3 XRD spectrum of pristine PANI

Pristine PANI gives diffraction peaks at  $2\theta \approx 11^\circ, 15^\circ, 17.5^\circ, 21^\circ, 26^\circ$  and  $30^\circ$ . Poughet *et al.* also have reported similar diffraction peaks for PANI [29]. Ram and

coworkers reported sharp peaks at  $2\theta \approx 9^\circ$ ,  $20^\circ$ ,  $25^\circ$ ,  $30^\circ$  and  $35^\circ$  [26]. Moon *et al.* reported that the peak at  $2\theta \approx 10^\circ$  arises from scattering with momentum transfer approximately parallel to the polyaniline chains [30].

#### 2.3.1.4 Thermal analysis

The TGA trace of pristine PANI is presented in fig. 2.4. PANI shows three degradations. The first one is due to the loss of moisture, which ends at  $139^\circ\text{C}$ . The second degradation, which starts at  $153^\circ\text{C}$ , ends at  $295^\circ\text{C}$  and corresponds to a weight loss of 7.4 % is due to the dopant evolution. The final one in the range  $342\text{--}689^\circ\text{C}$  is due to degradation of the PANI chain [31]. About 70 % weight loss occurs during this degradation. This is the general thermal behavior of PANI [32]. PANI doped with DBSA too exhibited similar degradations [33]. The possibility of stable carbonaceous char formation is greater in the case of aromatic compounds and hence PANI leaves a residue of 5.19 %.

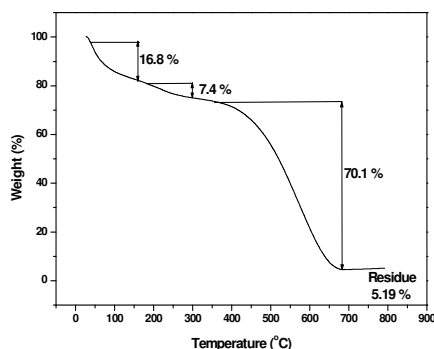
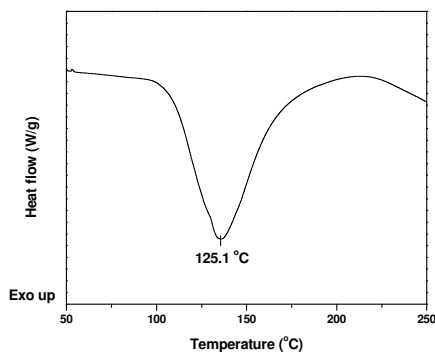


Fig. 2.4 TGA trace of pristine PANI

The DSC curve of PANI is shown in fig. 2.5. The PANI powder shows two endotherms; the first one between  $100^\circ\text{C}$  and  $190^\circ\text{C}$  due to deprotonation and the second one due to the PANI backbone degradation starting at about  $200^\circ\text{C}$ .



*Fig. 2.5 DSC curve of PANI*

### **2.3.2 Etching of Nylon fiber**

Chemical etching treatment using chromic acid can be an effective method to increase aniline deposition and polymerization on Nylon fiber. The etching conditions were optimized with reference to concentration of chromic acid and time of etching. Nylon fibers were treated with chromic acid of differing concentrations and to different time durations.

#### **2.3.2.1 Strength of the fiber**

Effect of etching conditions on the strength of the fiber was determined as a function of acid concentration and time of etching. Fig. 2.6 shows the strength of the fiber etched with different concentrations of chromic acid for a period of 6 h. There is a regular decrease in the strength of the fiber on etching. This may be attributed to the possible degradation of the Nylon fibers. Higher concentrations drastically reduce the strength of the fiber. Hence the concentration of chromic acid was optimized at 0.012 N for further studies.

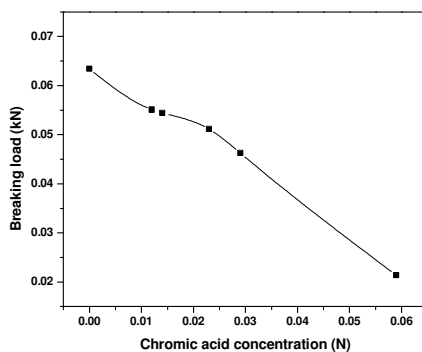


*Fig. 2.6 Variation of the strength of Nylon fiber with chromic acid concentration*

The strengths of the fiber etched to different extents of time are depicted in fig. 2.7. There is a major drop in the strength of the fiber during the initial one hour, after which the fall slows down and, stabilizes at 4 h. Beyond this, the strength further drops. Hence the optimum time of etching is found to be 4 h.

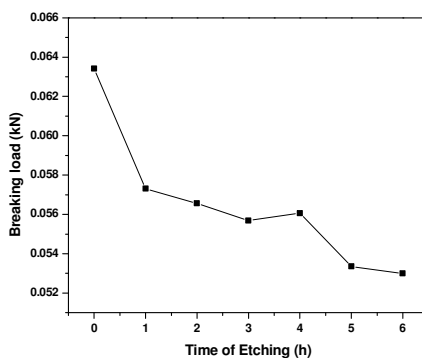


*Fig. 2.7 Variation of strength of Nylon fiber with etching time*

### 2.3.2.2 Surface characteristics

The morphology changes in the Nylon fiber surface on etching with chromic acid were observed with SEM. Fig. 2.8 shows the scanning electron micrographs of virgin fiber and fiber etched with 0.012 N chromic acid for 4 h. Clean and smooth surface is

observed for virgin Nylon fiber. The etched fiber shows an irregular surface with minor cracks, probably arising from the hydrolysis of the fiber surfaces in the acidic medium. Such irregularity in the fiber surface is expected to help in the physical anchoring and to improve adhesion of PANI on the fiber.

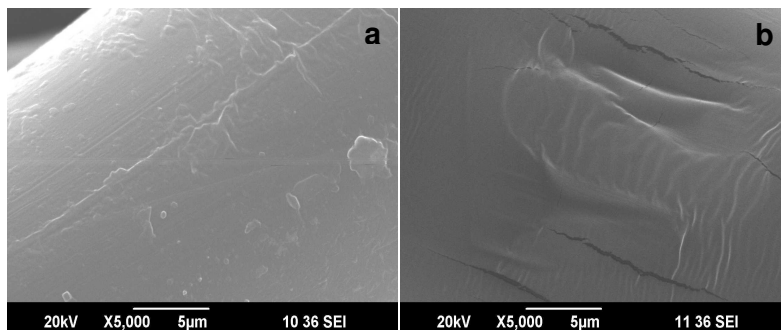


*Fig. 2.8 Scanning electron micrographs of (a) virgin fiber and (b) etched fiber*

The general scan in the XPS spectra of the virgin and etched fibers show the presence of C, N and O. Individual scans were done for C, N and O. The peak in the XPS spectrum of the virgin fiber is at 406.2 eV and that of the etched fiber is at 399.4 eV (fig. 2.9). This change in the peak position might be due to the difference in the environment of the N-H bonds. The peak at 406.2 eV in the virgin fiber may be due to that of N-H bond and the peak at 399.4 eV is due to the H-N-H bond. This means that as a result of etching, hydrolysis of the amide linkage has taken place changing the amide NH to primary amine. The intensity of the N-H peak is decreased in the case of etched fibers as the amide group hydrolyses to yield  $\text{NH}_2$  groups.



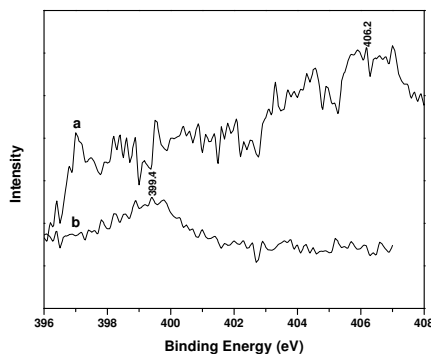


Fig. 2.9 XPS spectra of (a) virgin fiber and (b) etched fiber

The infrared spectra of the virgin and etched fibers are presented in fig. 2.10.

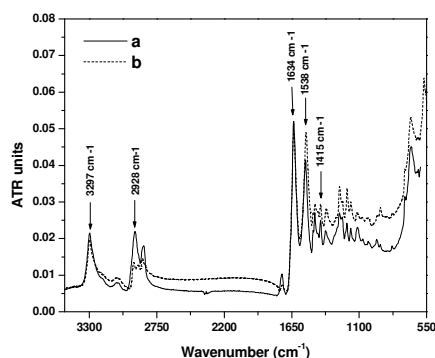


Fig. 2.10 IR spectra of (a) virgin fiber and (b) etched fiber

The absorption at  $3297\text{ cm}^{-1}$  is due to the N-H stretching; peak at  $2928\text{ cm}^{-1}$  is due to the C-H stretching; peaks at  $1634\text{ cm}^{-1}$  and  $1538\text{ cm}^{-1}$  can be assigned to C=O stretching in the amide and N-H bending in secondary amide (-N-H), respectively, and the peak at  $1415\text{ cm}^{-1}$  is assigned to the C-N stretching of amide group in Nylon [32, 34]. The ratio of intensities of absorption corresponding to N-H and C-H vibrations (N-H/C-H intensity ratio) of the etched fiber increased to 1.625 from 1.109 of the virgin fiber, indicating that hydrolysis of the amide linkage has taken place during etching. The N-H bonds change to  $\text{NH}_2$  during hydrolysis. Since there are

more number of H atoms per N atom in the  $\text{NH}_2$  bonds, the intensity of the N-H peaks will be higher. This indicates that the etching process induces hydrolysis of the amide linkages in the Nylon fiber.

Fig. 2.11 presents the XRD patterns of the virgin and etched fibers. The virgin fiber shows maxima at  $2\theta \approx 20.2^\circ$  and  $23.5^\circ$ , which are reasonably close to the values assigned by previous researchers for the  $\alpha_1$  and  $\alpha_2$  peaks, respectively [13, 35]. The etched fibers showed maxima at  $2\theta \approx 20.3^\circ$  and  $23.6^\circ$ . Upon etching, the intensity of the  $\alpha_1$  peak reduces slightly due to the slight decrement in the percentage crystallinity as confirmed by the DSC measurements. Oh *et al.* have also reported such a decrement in intensity owing to a decrease in the percentage crystallinity [13].

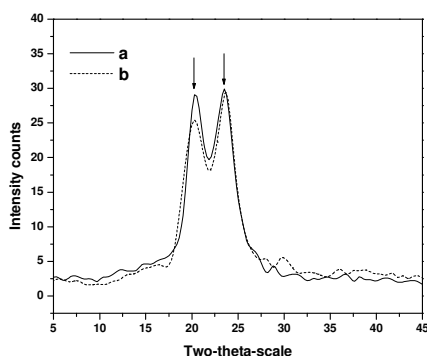


Fig. 2.11 X-ray diffraction patterns of (a) virgin fiber and (b) etched fiber

### 2.3.2.3 Thermal characteristics

The TGA traces of the virgin and etched fibers are given in fig. 2.12 and the thermal degradation characteristics are presented in table 2.1. The thermograms show only one major weight loss attributed to the structural decomposition [25] starting at  $\sim 340^\circ\text{C}$  for the virgin fiber and  $\sim 330^\circ\text{C}$  for the etched fiber. The onset temperature of degradation, the peak degradation temperature and the temperature at 50 % weight loss decrease on etching pointing to the decreased thermal stability of the etched fiber. But the etched fiber gives a lesser weight loss during the degradation and higher amount remains at the peak degradation temperature.

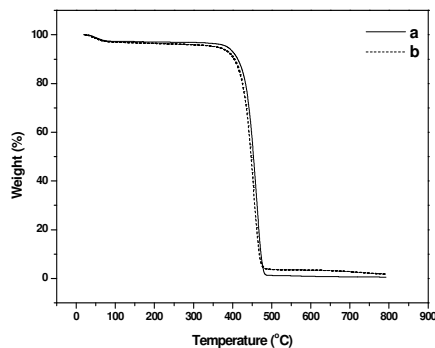


Fig. 2.12 TGA traces of (a) virgin fiber and (b) etched fiber

Table 2.1 Thermal decomposition data of the virgin and etched fibers

	Virgin fiber	Etched fiber
Onset temperature (°C)	342.9	331.9
Peak degradation temperature (°C)	461.1	452.9
Weight loss (%)	94.9	92.4
Weight remaining at Peak degradation temperature (%)	33.4	37.7
Temperature at 50 % weight loss (°C)	453.5	447.1

The melting temperature, heat of fusion and degree of crystallinity of the fibers were determined by differential scanning calorimetry and are presented in table 2.2. Fig. 2.13 shows the DSC curves of the virgin and etched fibers. All these parameters decrease upon etching, as expected. This decrease may be attributed to the degradation of the fiber surface during the etching process.

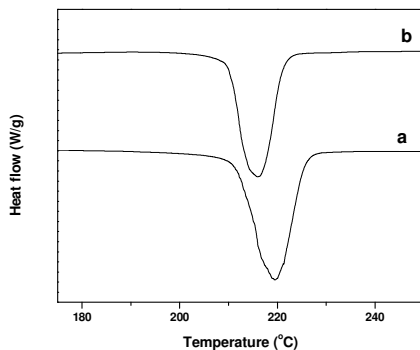


Fig. 2.13 DSC curves of (a) virgin fiber and (b) etched fiber

Table 2.2 Melting temperature, heat of fusion and degree of crystallinity of the virgin and etched fibers

Fiber	Melting temperature,	Heat of fusion,	Degree of crystallinity,
	$T_m$ (°C)	$\Delta H_f$ (J/g)	$\chi_c$ (%)
Virgin	219.4	64.5	28.0
Etched	215.8	57.8	25.1

### 2.3.3 PANI coated Nylon fiber

#### 2.3.3.1 Strength of the fiber

The effect of etching time on the strength of PANI coated fiber was evaluated by etching the fiber to different time durations at 60-65 °C with 0.012 N chromic acid, and subsequently effecting *in situ* polymerization as explained in section 2.2.4. The breaking load of the PANI coated fibers was plotted against the time of etching as shown in fig. 2.14. Generally, PANI is known as a very rigid material, and the tensile strength of most PANI blends or composites has a decreasing tendency as the concentration of PANI increase [36, 37]. This trend is seen in our case also. An increase in etching time leads to better surface etching, enhancing the physical adsorption of aniline molecules on the fiber surface. This result in the formation of

more amount of PANI on the fiber surface leading to a better coating of PANI layer strongly bonded to the surface. There is a sudden fall in the strength of the fiber during the first hour, after which there is a gradual decrease and it stabilizes at an etching time of 4 h. Beyond 4 h, again, the strength shows a drastic decrease. Comprehending fig. 2.7 and fig. 2.14, it can be inferred that the PANI coating does not affect the fiber strength significantly up to an etching time of 4 h, beyond which there is a rapid fall.

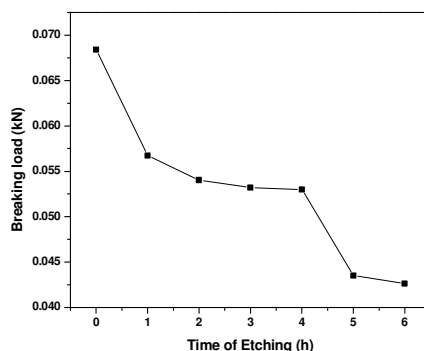


Fig. 2.14 Variation of breaking load of PANI coated fiber with etching time

### 2.3.3.2 DC electrical conductivity

Fig. 2.15 presents the variation of conductivity of PANI coated fibers with time of etching. The conductivity of the PANI coated virgin Nylon fiber is  $4.22 \times 10^{-2}$  S/cm (log conductivity of -1.37 S/cm). An etching time of 1 h itself increases the conductivity to  $1.73 \times 10^{-1}$  S/cm. i.e. A four-times increase in conductivity is observed for the fibers that have been given etching treatment for 1 h compared to the unetched ones. The conductivity increases almost steadily to  $3.72 \times 10^{-1}$  S/cm at 4 h. As the etching time is again increased, there is a further increase in conductivity. Obviously, the conductivity should increase on increasing the etching time as the amount of PANI formed on the surface increases. Since the strength of the fiber decreases beyond 4 h, and a reasonable conductivity is obtained at 4 h, the optimum time of etching is deduced to be 4 h. At an etching time of 4 h, the fiber conductivity

is  $3.72 \times 10^{-1}$  S/cm (log conductivity of -0.42 S/cm), approximately 8 times than that of the unetched fibers. Genies and co-workers prepared conducting materials made with polyaniline and glass textiles [2]. The glass textiles were given a chemical treatment with 20 % sulphuric acid solution for 6 h before giving the PANI coating, to wash off the glass of any surface agents. They could achieve only a conductivity in the range of  $1.5 \times 10^{-3}$  to  $5.2 \times 10^{-2}$  S/cm. By plasma treatment, Oh *et al.* reports only a fabric log conductivity of -2.2 to -1.6 S/cm [14]. Thus, chemical etching is effective in giving improved surface adhesion and better coating of PANI, resulting in improved conductivity than the expensive plasma treatment method.

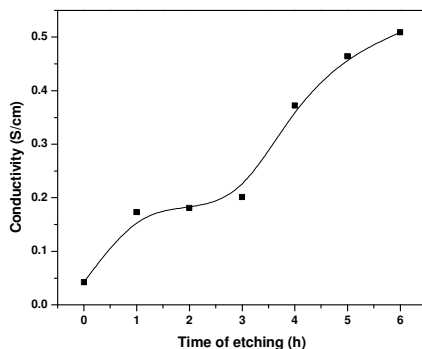


Fig. 2.15 Variation of conductivity of the PANI coated fibers with time of etching

### 2.3.3.3 Scanning electron microscopy

Figs. 2.16(a) and (b) show the micrographs of PANI coated etched fibers and PANI coated virgin fibers, respectively. PANI particles grown on the fiber surface are visible. Such globular deposits have been observed in several reports on PANI and polypyrrole films produced on fibers or micro particles [14, 38-41]. Pud *et al.* also reported the morphology of PET/PANI composites with atomic force microscopy (AFM), and they observed that PET and the undoped form of the PET/PANI composite exhibited comparatively flat surfaces, whereas doping led to the emergence of mountainous features [42]. With etched fibers, better deposition of PANI on the fiber surface is obtained. Thus, etching is effective in increasing the deposition of PANI.

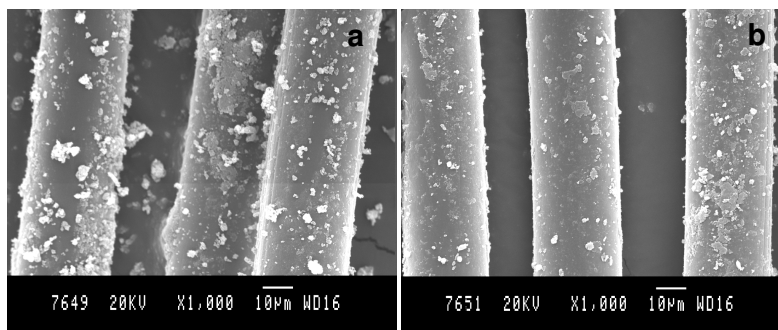


Fig. 2.16 Scanning electron micrographs of (a) PANI coated etched fibers and (b) PANI coated virgin fibers

#### 2.3.3.4 Infrared spectroscopy

The spectra of PANI coated etched fiber and PANI coated virgin fiber are presented in figs. 2.17(a) and (b), respectively.

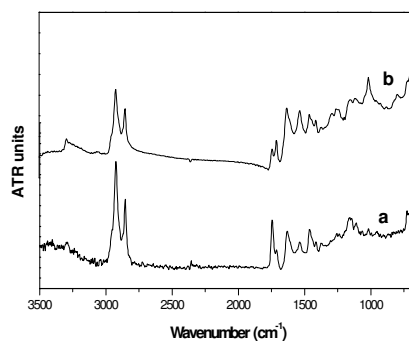


Fig. 2.17 Infrared spectra of (a) PANI coated etched fiber and (b) PANI coated virgin fiber

The N-H/C-H intensity ratio reduced from 1.63 to 0.388 for PANI coated etched fiber, which can be attributed to the shielding of the Nylon fibers as a result of the PANI coating on the fiber surface. We expect the ratio to be higher for PANI coated etched fiber since more N-H bonds are formed during etching. On the contrary, the PANI coated virgin fiber gives a value of 0.802, which is higher than that of the

PANI coated etched fiber. The increase is due to the lesser shielding of the Nylon fibers as compared to the latter, as there is a lesser amount of PANI coating on the unetched fibers.

### 2.3.3.5 X-ray diffraction analysis

The X-ray diffraction patterns of the PANI coated fibers (fig. 2.18) differ from the uncoated Nylon fibers (fig. 2.11) suggesting that PANI coating affects the crystal structure of Nylon fiber. In the XRD spectrum of the PANI coated fibers, in addition to the peaks of the fiber, diffraction peaks of PANI at  $2\theta \approx 17.5^\circ$ ,  $27^\circ$  and  $30^\circ$  can be seen. The intensity of the  $\alpha_1$  and  $\alpha_2$  peaks of the uncoated Nylon fibers (fig. 2.11) reduces upon PANI coating (fig. 2.18) due to a decrease in the percentage crystallinity of the fiber. Oh *et al.* too have reported such a decrease in the intensity of the peaks after PANI coating [13]. The  $\alpha_1$  and  $\alpha_2$  peaks can be seen at  $2\theta \approx 20.1^\circ$  and  $23.6^\circ$  for the PANI coated etched fiber. These are seen at  $2\theta \approx 20.5^\circ$  and  $24.1^\circ$  for the PANI coated virgin fiber. The  $\alpha_2$  values slightly shifted to higher side after PANI coating, in comparison to the virgin and etched fibers.

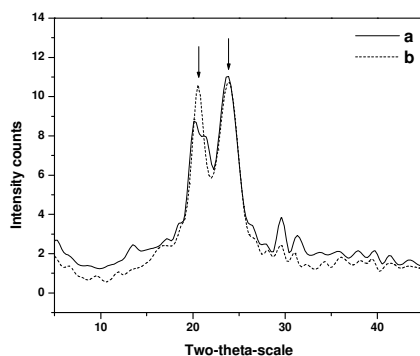


Fig. 2.18 X-ray diffraction patterns of (a) PANI coated etched and (b) PANI coated virgin fiber

### 2.3.3.6 Thermal stability

The thermal degradation characteristics of PANI and PANI coated fibers as extracted from TGA data is given in table 2.3. The TG curves are presented in fig. 2.19. The



PANI coated fibers exhibit a lower onset decomposition temperature than the virgin fiber, but the slope of the decomposition curve is more gentle [25]. The peak degradation temperatures of the etched and PANI coated etched fibers are 453.4 °C and 452.5 °C, respectively, and that of the virgin fiber and PANI coated virgin fiber are 460.9 °C and 460.5 °C, respectively (tables 2.1 and 2.3). This indicates that the PANI deposition does not affect the thermal stability of the fiber. The onset temperature, weight loss during degradation, weight remaining at peak degradation temperature and the temperature at 50 % weight loss of the PANI coated, etched and virgin fibers does not show variation. Even though etching causes a reduction in the thermal stability of the fibers, PANI coated fibers does not show much variation in the thermal characteristics. The thermal characteristics of the PANI coated fibers do not show the significant improvement in thermal stability that has been reported for other conductive polymer composite systems [43, 44]. Similar results in the case of PANI/Nylon composite systems have been reported elsewhere [32]. Abraham and coworkers reported poor thermal stability of PANI/Nylon composite films when compared to pristine Nylon film [45]. PANI coated etched fibers leave slightly more residue than the PANI coated virgin fibers showing that PANI deposition is higher on the former.

Table 2.3 Thermal decomposition data of the PANI coated fibers

Fiber	PANI coated etched	PANI coated virgin
Onset temperature (°C)	293.5	291.5
Peak degradation temperature (°C)	452.9	460.0
Weight loss (%)	92.3	93.2
Weight remaining at Peak degradation temperature (%)	33.4	33.9
Temperature at 50 % weight loss (°C)	444.8	452.2
Residue (%)	2.57	2.43

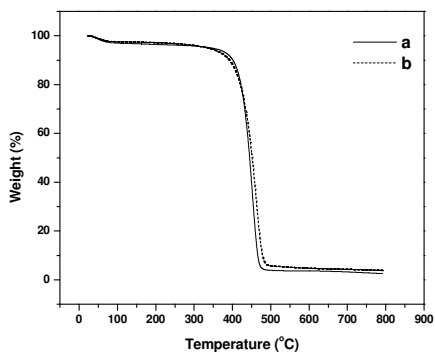


Fig. 2.19 TG curves of (a) PANI coated etched fiber and (b) PANI coated virgin fiber

Fig. 2.20 presents the DSC curves of the PANI coated fibers.

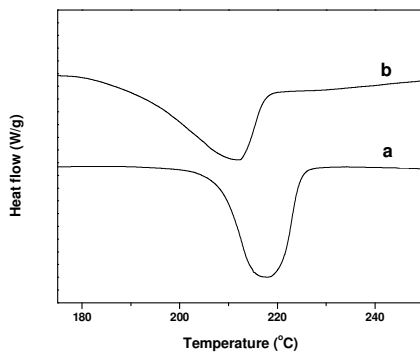


Fig. 2.20 DSC curves of (a) PANI coated etched fiber and (b) PANI coated virgin fiber

The melting temperature, heat of fusion and degree of crystallinity are presented in table 2.4. PANI coating on the Nylon fiber reduces the degree of crystallinity and heat of fusion. The melting temperature also shifts to a slightly lower value. This can be visualized in the DSC curves too. This means that the crystalline regions are partly destroyed by the formation of PANI on the fiber surface. Similar observations have been reported by Oh *et al.* [13, 14] and Byun *et al.* [25]. Diffusion of aniline

into the Nylon fiber presumably disturbs the crystalline regions and decreases its thermal properties. The aniline diffused into the Nylon fibers localizes in the amorphous regions and acts a plasticizer, disturbing the orientation and arrangement of Nylon macromolecular segments [46].

Table 2.4 Melting temperature, heat of fusion and degree of crystallinity of PANI coated fibers

Fiber	Melting temperature, $T_m$ (°C)	Heat of fusion, $\Delta H_f$ (J/g)	Degree of crystallinity, $\chi_c$ (%)
PANI coated etched	218.0	61.5	26.7
PANI coated virgin	211.8	58.7	25.5

## 2.4 Conclusions

Electrically conducting fibers were prepared by *in situ* polymerization of aniline on Nylon fibers. Chemical etching of Nylon fibers using chromic acid prior to *in situ* polymerization is found to be effective in improving the adhesion of PANI to the fiber surface and conductivity. The etching process involves hydrolysis of the amide linkages. The crystallinity and thermal stability of the fiber reduces upon etching. The etching process roughens the fiber surface and slightly reduces the strength of the fiber. PANI deposition on the etched fibers does not further lower its strength and thermal stability. Better deposition of PANI on the fiber and improved conductivity is attained by the etching treatment of the fibers. By giving an etching treatment for 4 h, 8 times increase in conductivity is attained. The crystallinity of the fiber reduces on PANI coating.

## References

1. Malinauskas A. Polymer 2001;42(9):3957-3972.
2. Genies EM, Petrescu C, Olmedo L. Synth Met 1991;41:665-668.

3. Kim SK, Kim MS, Chun SY, Park YH, Jeon BS, Lee JY, Hong YK, Joo J, Kim SH. *Mol Cryst Liq Cryst* 2003;405:161.
4. Gregory RV, Kimbrell WC, Kuhn HH. *Synth Met* 1989;28(1-2):823.
5. Forveille JL, Olmedo L. *Synth Met* 1994;65:5.
6. Byun SW, Im SS. *J Appl Poly Sci* 1994;51:1221.
7. Park YH, Choi SH, Miyata S. *J Appl Poly Sci* 1992;45:843.
8. Tzou K, Gregory V. *Synth Met* 1992;47(3):267.
9. Anbarasan R, Jayaseharan J, Sudha M, Devi JL, Nirmala PV, Gopalan A. *J Appl Polym Sci* 2000;81(2):468-478.
10. Anbarasan R, Vasudevan T, Gopalan A. *J Mater Sci* 2000;35(3):617-625.
11. Anbarasan R, Vasudevan T, Kalaignan GP, Gopalan A. *J Appl Polym Sci* 1999;73(1):121-128.
12. Kuhn HH. *Text Chem Color* 1997;29:17.
13. Oh KW, Hong KH, Kim SH. *J Appl Poly Sci* 1999;74:2094-2101.
14. Oh KW, Kim SH, Kim EA. *J Appl Poly Sci* 2001;81:684-694.
15. Wunderlich B. *Thermal Analysis*. Academic Press, 1990:417.
16. Blaine RL. TN48, *Polymer Heats of fusion*. TA Instruments, New Castle, DE 19720, USA.
17. Stejskal J, Riede A, Hlavata D, Prokes J, Helmstedt M, Holler P. *Synth Met* 1998;96:55-61.
18. Hong KH, Kang TJ. *J Appl Polym Sci* 2006;99:1277-1286.
19. Haba Y, Segal E, Narkis M, Titelman GI, Siegmman A. *Synth Met* 2000;110:189-193.
20. Oh KW, Park HJ, Kim SH. *J Appl Polym Sci* 2003;188:1225.
21. Kim SH, Oh KW, Kim TK. *J Appl Polym Sci* 2005;96:1035-1042.
22. Tang J, Jing X, Wang B, Wang F. *Synth Met* 1988;24:231.
23. Kim YH, Foster C, Chiang J, Heeger AJ. *Synth Met* 1988;25:49.
24. Cao Y, Li S, Xue Z, Guo D. *Synth Met* 1986;16:305.
25. Byun SW, Im SS. *Polymer* 1998;39:485-489.
26. Ram MS, Palaniappan S. *J Mater Sci* 2004;39:3069-3077.

27. Raghavendra SC, Khasim S, Revanasiddappa M, Prasad MVNA, Kulkarni AB. Bull Mater Sci 2003;26(7):733-739.
28. Xu JC, Liu WM, Li HL. Mater Sci Eng 2005;C25:444-447.
29. Poughet JP, Jozefowicz ME, Epstein AJ, Tang X, MacDiarmid AG. Macromolecules 1991;24:779.
30. Moon YB, Cao Y, Smith P, Heeger AJ. Polym Commun 1989;30:196.
31. Wei Y, Hsueh KF. J Polym Sci Part A Polym Chem 1989;27:4351.
32. Hong KH, Oh KW, Kang TJ, 2005;97:1326-1332.
33. Chen CH. J Polym Research 2002;9:195-200.
34. Hong KH, Oh KW, Kang TJ, 2005;96:983-991.
35. Muellerleile JT, Freeman JJ. J Appl Poly Sci 1994;54:135.
36. Chipara M, Hui D, Notingher PV, Chipara MD, Lau KT, Sankar J, Panaitescu D. Composites Part B 2003;34:637.
37. Choda'kI, Omastova' M, Pionteck J. J Appl Polym Sci 2001;82:1903.
38. Armes SP, Aldissi M, Hawley M, Beery JG, Gottesfeld S. Langmuir 1991;7:1447.
39. Armes SP, Gottesfeld S, Beery JG, Garzon F, Mombourquette C, Hawley M, Kuhn HH. J Mater Chem 1991;1:525.
40. Beadle P, Armes SP, Gottesfeld S, Mombourquette C, Houlton R, Andrews WD, Agnew SF. Macromolecules 1992;25:2526.
41. Lascelles SF, Armes SP. J Mater Chem 1997;7:1339.
42. Pud AA, Tabellout M, Kassiba A, Korzhenko AA, Rogalsky SP, Shapoval GS, Houze' F, Schneegans O, Emery JR. J Mater Sci 2001;36:355.
43. Wang HL, Toppare L, Fernandez JE. Macromolecules 1990;23:1053.
44. Wang HL, Fernandez JE. Macromolecules 1992;25:6179.
45. Abraham D, Bharathi A, Subramanyam SV. Polymer 1996;37:5295-5299.
46. Pud A, Ogurtsov N, Korzhenko A, Shapoval G. Prog Polym Sci 2003;28:1701-1753.



*Natural rubber/polyaniline (PANI)/polyaniline coated short Nylon fiber (PANI-N) conducting polymer composites (CPCs) were prepared by mechanical mixing and its cure characteristics, filler dispersion, mechanical properties, conductivity and thermal stability were evaluated. The amount of fiber was varied from 40 to 120 phr and the amount of PANI used was in the range 40-140 phr. PANI and PANI-N increased the rate of cure reaction. The PANI-N CPCs showed higher tensile strength, tear strength and modulus values and lower elongation at break. Characterization of the CPCs using scanning electron microscopy showed that there were changes in the morphology of the fracture surface with filler loading. The DC electrical conductivity and the thermal stability of the CPCs increased with PANI and PANI-N concentration. The highest conductivity obtained was  $1.99 \times 10^{-6}$  S/cm. The kinetic parameters of thermal degradation of the composites were estimated by different methods.*

---

## Chapter 3

### PANI coated short fiber reinforced natural rubber conducting composites

#### Fabrication and characterization

##### 3.1 Natural Rubber

Natural rubber (NR) is an elastic hydrocarbon polymer that naturally occurs as a milky colloidal suspension, or *latex*, in the sap of some plants and is the oldest known rubber and the most versatile one for fabrication into rubber products [1]. The major commercial source of natural rubber latex is the Para rubber tree, *Hevea Brasiliensis*. Natural rubber is a high molecular weight polymer of isoprene (2-methyl 1,3-butadiene) with a molecular weight of 1,00,000 to 10,00,000 (fig. 3.1). Typically, a few percent of other materials, such as proteins, fatty acids, resins and inorganic materials are found in high quality natural rubber. Of the several isomeric

forms that polyisoprene can adopt, NR consists almost exclusively of the *cis*-1,4 polymer, the structure of which is shown below:

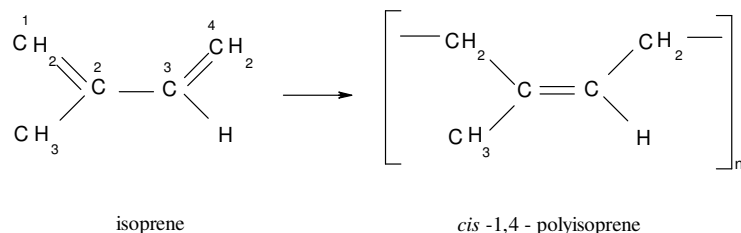


Fig. 3.1 Structure of natural rubber (molecular weight of repeat unit: 68.12 g/mol)

Despite the availability of petroleum-based synthetics, natural rubber is highly valued because no synthetic substitute has comparable elasticity, resilience and resistance to high temperature [2]. The uniqueness of NR lies in its remarkable extensibility and toughness, as evidenced by its ability to be stretched repeatedly to seven or eight times its original length. Natural rubber is a unique biopolymer of strategic importance that, in many of its most significant applications, cannot be replaced by synthetic alternatives.

The high and reversible deformability of natural rubber is of great industrial importance. However, its initial modulus and durability are low and an additional reinforcing phase is required for practical use [3-7]. Carbon black and silica particles have been extensively used for this purpose [8-12]. In addition,  $\text{CaCO}_3$ ,  $\text{ZnO}$ ,  $\text{MgO}$ , talc, mica etc. have also been used [13-19]. Influence of these particulate fillers on the deformability of the polymer was earlier considered to be purely hydrodynamic. However, later it was proven that specific interactions between the filler and matrix are very important in imparting the reinforcement [20-22]. Fibrous fillers are yet another type of reinforcement.

As described in chapter 1 (section 1.2.2), composites of PANI with many elastomers have been reported. Even though all these PANI/elastomer composites exhibit excellent conducting and shielding properties, the main concern with them is the lack of good mechanical properties. In order to couple these two properties, special



materials have to be developed. The electrical and mechanical properties of the elastomer composites depend on the aspect ratio of the filler. Fibers are characterized by high aspect ratios. It is well established that the mechanical properties of rubber composites can be greatly improved by adding short fibers [23]. The development of fiber reinforced composites has made available materials lighter than aluminum and stiffer than steel. Generally, short fiber reinforced rubber composites are popular in industrial fields because of their processing advantages, low cost and their greatly improved technical properties such as strength, stiffness, modulus and damping [23-25]. Normally a rubber-fiber composite can offer a set of properties that may give it the potential of entering application areas not possible with either of the components in the composite [26]. These composites combine the elastic behavior of rubber with the strength and stiffness of fiber. Hence, the drawback of poor mechanical properties of the PANI/rubber conducting composites can be overcome by using short fibers grafted/coated with PANI. This will impart the elastomer, the high conductivity of PANI and good reinforcement of short fibers.

Works on PANI composites based on many synthetic rubbers have been reported, however, reports on natural rubber in this field are quite rare [27]. This part of the work describes the preparation of conducting polymer composites (CPCs) of NR, PANI and PANI coated short Nylon fiber. PANI coated short Nylon fiber is expected to enhance the mechanical properties, simultaneously providing sufficient conductivity. The cure characteristics and cure kinetics, filler dispersion, mechanical properties and morphological characterization of the composites are described. The DC electrical conductivity and thermal analysis of the composites are presented. The thermal degradation kinetics is also discussed.

### **3.2 Conducting natural rubber composites**

#### **3.2.1 Materials**

Natural rubber was obtained from Rubber Research Institute of India, Kottayam, Kerala, India. The sample had a Mooney viscosity ML1+4 (@100 °C) of 85.3.

Dicumyl peroxide (DCP) was supplied by S. D. Fine Chemicals Ltd., Mumbai, India. Rest of the chemicals used were of commercial grade.

### 3.2.2 Preparation of conducting polymer composites

PANI was prepared by the chemical oxidative polymerization of aniline in presence of hydrochloric acid (*section 2.2.2 of the thesis*). PANI coated Nylon fiber was prepared after giving an etching treatment to the fibers using chromic acid (*see section 2.2.3 and 2.2.4*). The PANI coated etched fiber thus obtained is hereafter referred to as PANI-N. The formulation for the preparation of the CPCs is given in table 3.1.

Table 3.1 Formulation for the preparation of CPCs

Ingredients (phr <sup>*</sup> )	P series				F series		
	NP <sub>0</sub>	NP <sub>1</sub>	NP <sub>2</sub>	NP <sub>3</sub>	NF <sub>1</sub>	NF <sub>2</sub>	NF <sub>3</sub>
NR	100	100	100	100	100	100	100
PANI	0	40	90	140	90	90	90
PANI-N <sup>#</sup>	0	0	0	0	40	80	120

\* parts per hundred rubber

<sup>#</sup> PANI coated etched fiber

All the mixes contain Stearic acid- 1 phr and DCP- 3 phr

Two series of CPCs were prepared- first series with varying amounts of PANI (P series) and the second with 90 phr PANI and varying amounts of PANI-N (F series). The CPCs were prepared in a laboratory size (15 × 33 cm) two-roll mill (Santosh, SMX lab 613) at a friction ratio of 1:1.25 as per ASTM D 3184 (1980). During the final sheeting at low nip gap, the fibers were oriented along the mill direction. The mixes were kept for 24 h for maturation. The optimum cure time at 150 °C was determined using a Rubber Process Analyzer (RPA 2000, Alpha Technologies). The compounds were compression molded at 150 °C in an electrically heated hydraulic press (Santosh, SMP-50) having 30 × 30 cm platens at a pressure of 200 kg/cm<sup>2</sup> into sheets using standard mould (15 × 15 × 2 cm). The samples were cured to their

respective optimum cure times. After curing, the pressure was released and the sheets were suddenly cooled in water. These sheets were used for subsequent tests.

### 3.2.3 Cure characteristics and kinetics

The processing characteristics of the vulcanizates were monitored using a Rubber Process Analyzer. The die type used was biconical and the die gap was 0.487 mm. The cure time;  $T_{90}$ , scorch time;  $T_{10}$ , maximum torque;  $D_{max}$  and minimum torque;  $D_{min}$  values were determined at 150 °C at a frequency of 50.0 cpm and a strain of 0.20 deg.

The cure rate index (CRI) [28, 29], which is a direct measure of the quickness of the curing reaction and the kinetic rate constant of cure reaction, were determined from the rheometric data.

$$CRI = 100 / (T_{90} - T_{10}) \quad (3.1)$$

The vulcanization kinetics was studied by the method given below [30-32]. The general equation for the kinetics of a first order chemical reaction is

$$\ln(a - x) = -kt + \ln a \quad (3.2)$$

where,  $a$  is the initial reactant concentration,  $x$  is the reacted quantity of reactant at time  $t$  and  $k$  is the first order rate constant. The kinetic principle of rubber crosslinking is based on the kinetic theory of elasticity. It assumes a direct relation between the calculated shearing modulus and the crosslinking density. In the rheometer, the shearing strain is constant, the shear stress or torque value is proportional to the crosslinking density. Thus, for the vulcanization of rubber, measuring the torque developed during vulcanization monitors the rate of crosslinking formation. The torque obtained is proportional to the modulus of rubber. If one assumes that the crosslinking reaction follows a first order kinetics, the following substitutions can be made.

$$(a - x) = D_{max} - D_t \quad (3.3)$$

$$a = D_{\max} - D_{\min} \quad (3.4)$$

where  $D_t$  is the torque at time;  $t$ . Therefore, the equation can be written as

$$\ln(D_{\max} - D_t) = -kt + \ln(D_{\max} - D_{\min}) \quad (3.5)$$

Therefore, if a plot of  $\ln(D_{\max} - D_t)$  against time  $t$  is a straight line, then the cure reaction follows first order kinetics. The cure reaction rate constant ( $k$ ) can be obtained from the slope of the corresponding straight lines [33].

### 3.2.4 Filler dispersion

Lee has studied the filler dispersion and formation of filler agglomerates in polymer matrices in detail [34]. According to his report, even well dispersed filler-rubber systems show differences in degree of filler agglomeration in the cured and uncured state. Lee assumed that  $\eta_r > M_r$  where  $\eta_r$  and  $M_r$  are the relative viscosity (ratio of the viscosities due to loaded and unloaded elastomer) and the relative modulus (ratio of the modulus for loaded and unloaded elastomer), respectively. The paper also proposed that  $\eta_r$  and  $M_r$  could be determined from rheometric data by using the expressions:

$$n_r = D^f_{\min} / D^0_{\min} \text{ and } M_r = D^f_{\max} / D^0_{\max} \quad (3.6)$$

where  $D$  denotes the torque and the superscripts  $f$  and  $0$  are related to the loaded and unloaded polymer, respectively. Lee introduced a new parameter  $L$  defined as:

$$L = n_r - M_r \quad (3.7)$$

For ideal dispersions,  $\eta_r = M_r$ . This happens when the individual particles are well dispersed in the matrix. In the case of non-ideal dispersions, the value of  $L$  changes slowly at low filler loadings, but above a certain limit, it increases sharply. The abrupt rise of the index  $L$  at high filler loadings may be ascribed to the predominance of agglomerates remaining relatively undispersed in the rubber. In such a situation, it

is assumed that the filler concentration has now reached the point where there is not enough rubber to fill the available voids in the filler.

Another mathematical expression has been proposed by Wolf in terms of rheometric data to characterize the filler structure present in rubber vulcanizates [35, 36]. When a filler is incorporated into a compound, the maximum torque variation,  $\Delta D^f = D_{max}^f - D_{min}^f$  observed during vulcanization increases. The ratio between  $\Delta D^f$  and  $\Delta D^0$  i.e. the torque variations for the loaded and unloaded compounds, respectively, is directly proportional to filler loading. By plotting the relative torque as a function of filler loading, a straight line is obtained whose slope was defined by Wolf as  $\alpha_f$  [37-40].

$$(D_{max}^f - D_{min}^f) / (D_{max}^0 - D_{min}^0) - 1 = \alpha_f (m_f / m_p) \quad (3.8)$$

where  $m_p$  is the mass of polymer in the compound and  $m_f$  is the mass of filler in the compound and  $\alpha_f$  is a specific constant for the filler, which is independent of the cure system and closely related to the morphology of the filler. The parameter  $\alpha_f$  represents the final structure of the filler as it exists in the vulcanizates after all possible structure breakdowns that occurred during mixing and vulcanization. The reinforcement build-up and crosslinking reaction both take place during curing without affecting each other. The application of equation (3.8) allows the definition of a filler specific constant, related to the filler structure, and also predicts whether or not crosslink density is unaffected by the presence of the filler, in which case, a straight line is obtained. The equation also shows that based on a single test,  $\alpha_f$  can be calculated from the changes in the torque which occur during vulcanization of two compounds, the unloaded and loaded composition.

### 3.2.5 Mechanical properties

The mechanical properties of the CPCs were determined using a Shimadzu Universal Testing Machine (model AG1) with a load cell of 10 kN capacity at a cross-head speed of 500 mm/min at a gauge length of 40 mm. The measurements were carried out as per ASTM D 412-98a (2002). Dumbbell shaped samples were punched out

from the compression-molded sheets along the mill grain direction using a standard die (Type D). Tear strength of the samples were measured as per ASTM D 624-2000 using standard test specimens with 90° angle on one side and tab ends (Type C die). Average of at least six sample measurements were taken to represent each data point.

### **3.2.6 Morphological characterization**

Scanning electron microscopic images (SEM) of tensile fracture surface of the CPCs were obtained using a Cambridge Instruments S 360 Stereo scanner (version V02-01). The fractured surfaces have been sputtered with gold before they were observed in SEM.

### **3.2.7 DC electrical conductivity**

The DC electrical conductivity of the CPCs (rectangular strips of dimensions  $4 \times 2 \times 2$  mm) was measured by a standard two-probe electrode configuration using a Keithley Nanovoltmeter (model 2182) in dry air at ambient temperature. The sample was placed between two electrodes through which current was passed and the resistance was measured directly from the instrument. The conductivity of the samples was calculated using the formula:

$$\sigma (S / cm) = (I / V) \times l / A \quad (3.9)$$

where  $\sigma$  is the electrical conductivity,  $I$  is the current through the electrode in amperes,  $V$  is the voltage in volts,  $l$  is the thickness of the sample in centimeters and  $A$  is the area of contact of the electrodes with the sample in centimeter square.

### **3.2.8 Thermogravimetric analysis (TGA)**

Thermogravimetric analysis of the CPCs were performed as described in *chapter 2, section 2.2.5.6* on a TGA Q-50, TA Instruments thermogravimetric analyzer (TGA) with a programmed heating of 20 °C/min from ambient to 800 °C.

### 3.2.8.1 Evaluation of kinetic parameters

The TGA data can also be used in studying the kinetics of decomposition, which provide an insight into the thermal stability of polymeric materials. There are many proposed methods to calculate the kinetic parameters of decomposition and the reported values depend not only on the experimental conditions, but also on the mathematical treatment of data.

#### *Formulation of the rate equation*

For many kinetic processes, rate of reaction may be expressed as a product of a temperature dependent function;  $k(T)$ , and a composition- or conversion-dependent term;  $f(X)$ :

$$r = dX / dt = k(T) f(X) \quad (3.10)$$

where  $T$  is absolute temperature in Kelvins;  $X$  is conversion i.e. weight of polymer volatilized/initial weight of polymer and  $r$  is the rate of change of conversion or composition per unit time;  $t$ . The temperature dependent term in equation (3.10) is the reaction rate constant, which is assumed to obey the usual Arrhenius relationship:

$$k(T) = A \exp(-E_a / RT) \quad (3.11)$$

where  $E_a$  is the activation energy of the kinetic process,  $A$  is the pre-exponential factor and  $R$  is the universal gas constant. The conversion-dependent function;  $f(X)$ , is generally very complicated. A particular term is usually valid only for a limited range of experimental conditions. If it is assumed that a simple  $n^{th}$  order kinetic relationship holds for the conversion-dependent term such that:

$$f(X) = (1-x)^n \quad (3.12)$$

and that the quantity  $(1-x)$  can be replaced by  $W$ , the weight fraction remaining in a TGA run, then:

$$r = dW / dt = AW^n \exp(-E_a / RT) \quad (3.13)$$

$$\ln r = \ln(-dW / dt) = \ln A + n \ln W - E_a / RT \quad (3.14)$$

Published methods of deriving the kinetic parameters from TGA data center about equation (3.14). They may be either differential i.e. involving the derivative term;  $-dW/dt$  or integral i.e. based upon an integration of equation (3.14). The emphasis in these methods is on finding a way of plotting the data to provide a rapid visual assessment of the order of the reaction and its activation energy.

***Differential methods for determining rate equation parameters***

The difference form of equation (3.14) at different temperatures is:

$$\Delta \ln r = \Delta \ln(-dW / dt) = n \Delta \ln W - (E_a / R) \Delta(1/T) \quad (3.15)$$

Dividing (3.15) by  $\Delta(1/T)$  gives

$$[\Delta \ln r / \Delta(1/T)] = n[\Delta \ln W / \Delta(1/T)] - (E_a / R) \quad (3.16)$$

A plot of  $[\Delta \ln r / \Delta(1/T)]$  against  $[\Delta \ln W / \Delta(1/T)]$  should be a straight line with slope equal to the order of reaction;  $n$ , and an intercept of  $-E_a/R$ .

Dividing (3.15) by  $\Delta \ln W$  gives

$$\Delta \ln r / \Delta \ln W = n + E_a \left[ -\Delta(1/T) / R \Delta \ln W \right] \quad (3.17)$$

A plot of  $[\Delta \ln r / \Delta \ln W]$  versus  $[-\Delta(1/T)/R \Delta \ln W]$  should also be a straight line of slope  $E_a$  and an intercept  $n$ . These two methods are generally attributed to Freeman and Carroll [41]. In spite of its limited precision, it is quite convenient for processing the acquired TGA data. This method may be used to obtain a rapid but rough estimate of the kinetic parameters when a limited number of data points are available.



Chan and Balke [42] have proposed a kinetic treatment assuming that the order of reaction;  $n$  is constant. Then the equation (3.14) may be rearranged as follows:

$$[\ln r - n \ln W] = E_a (-1/RT) + \ln A \quad (3.18)$$

If  $n=1$ , then equation (3.18) becomes:

$$\ln(r/W) = E_a (-1/RT) + \ln A \quad (3.19)$$

If it is assumed that the activation energy  $E_a$  is constant over a specific temperature range, then the slope over this range of a plot of  $\ln(r/W)$  against  $(-1/RT)$  should be equal to the activation energy;  $E_a$ . Non-linearity in this plot caused by a change in mechanism may be accommodated by retaining the pseudo first order hypothesis and attributing the non-linearity to a change in the activation energy.

### ***Integral methods***

The integral methods involve the integration of equation (3.10) by separation of variables. By substituting equation (3.11) into this expression and defining  $\beta = (dT/dt)$  as the heating rate, the following is obtained:

$$F(X) = \int_0^X dX / f(X) = \int_{T_0}^T (A / \beta) \exp(-E_a / RT) dT \quad (3.20)$$

where  $T_0$  is the initial temperature in the TGA analysis and  $T$  is the final temperature. For a constant heating rate  $\beta$  and if  $T_0 \approx 0$ , equation (3.20) becomes:

$$F(X) = (A / \beta) \int_0^T \exp(-E_a / RT) dT \quad (3.21)$$

The different integral methods involve an approximation to the right-hand integral term in equation (3.21).

Among the integral methods, the Coats and Redfern approach [43] seems to be the most suitable from a practical point of view and is preferred over others and is applied here. The activation energy and the order of reaction were evaluated utilizing this equation for reaction order  $n \neq 1$ , which when linearized for a correctly chosen  $n$  yields the activation energy from the slope.

$$\log \left[ 1 - (1 - \alpha)^{1-n} / T^2 (1 - n) \right] = \log [AR / \beta E] - E / 2.303 RT \quad (3.22)$$

where  $\alpha$  is the fraction decomposed,  $T$  is the temperature (K),  $n$  is the order of reaction,  $A$  is the Arrhenius constant,  $R$  is the universal gas constant,  $E_a$  is the activation energy and  $\beta$  is the heating rate. The plot of the left hand side of the equation (Y) against  $1/T$  should be a straight line with slope =  $-E_a/(2.303R)$  for the correct value of  $n$ .

### 3.3 Results and discussion

#### 3.3.1 Cure characteristics of the CPCs

The use of rubber products always involves vulcanized materials because crosslinked elastomers present better mechanical properties. Thus, to prepare NR/PANI CPCs, it is necessary to study the effect of the conducting polymer on the crosslinking process of the rubber. Figures 3.1 and 3.2 show the rheographs which characterize the crosslinking process of P series (CPCs with PANI) and F series (CPCs with PANI and PANI-N), respectively. Addition of PANI decreases the torque initially. Higher loadings increase the torque. For the F series, the torque values increase steadily with fiber loading. The observed increase in torque at a given time is directly related to the stiffness of the material.

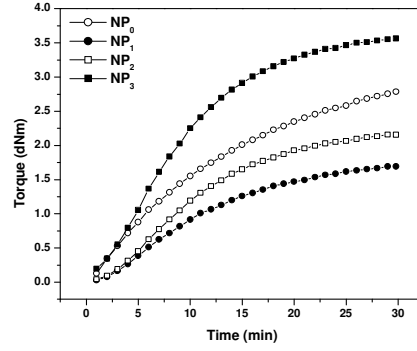


Fig. 3.1 Cure curves of the CPCs of P series

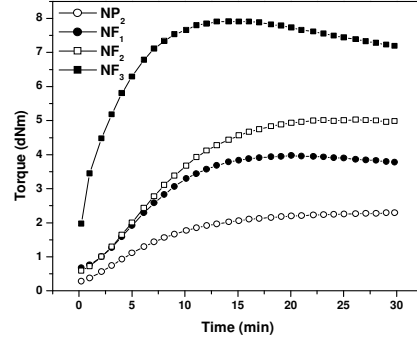


Fig. 3.2 Cure curves of the CPCs of F series

Table 3.2 presents the cure time;  $T_{90}$ , and scorch time;  $T_{10}$ , values for the P series and F series CPCs.

Table 3.2 Cure time and scorch time values of the CPCs

CPC	$T_{90}$ (dNm)	$T_{10}$ (dNm)
NP <sub>0</sub>	23.4	2.0
NP <sub>1</sub>	21.8	2.6
NP <sub>2</sub>	15.7	1.7
NP <sub>3</sub>	19.1	2.7
NF <sub>1</sub>	12.8	2.2
NF <sub>2</sub>	15.2	2.2
NF <sub>3</sub>	7.9	0.4

Cure time represents the time corresponding to the development of 90 % of the maximum torque which is given as

$$T_{90} = (D_{\max} - D_{\min}) \times 0.9 + D_{\min} \quad (3.23)$$

where  $D_{\max}$  is the maximum torque and  $D_{\min}$  is the minimum torque. For the P series, cure time reduces with loading up to 90 phr, which then shows an increase. This

means that PANI accelerates the cure reaction up to 90 phr loading. Addition of PANI-N to the CPC with 90 phr PANI (NP<sub>2</sub>) further reduces the cure time. This indicates that the PANI-N can accelerate the peroxide cure reaction of the natural rubber matrix. This is supported by the cure kinetic studies and cure rate index values, which will be discussed in the following sections. Among the P and F series, F series show lower cure time values; this means that the PANI-N has a much stronger influence on the cure reaction than PANI and that the CPCs of F series is very fast curing than that of P series. Similar results in the case of NR/Nylon fiber elastomer composites have been reported [44, 45].

Scorch time is the time required for the torque value to reach 10 % of maximum torque. It is a measure of the processing safety- the time available for safe processing before the onset of vulcanization reaction. Scorch time shows an increasing trend with loading for P series indicating better processing safety. For the F series, it increases on PANI-N loading, stabilizes and then decreases drastically at higher loadings. Such a decrease at higher PANI-N content is attributable to the premature cure that might happen due to the high heat generated during mill mixing of highly fiber-loaded samples.

The variation of maximum torque;  $D_{max}$ , with filler loading is presented in fig. 3.3. The maximum torque is an index of the extent of crosslinking reactions and represents the elastic modulus of the fully vulcanized rubber. It is also a measure of the filler-polymer interaction. PANI has an intrinsic acid content and increasing the mass fraction of PANI in the composite induces degradation processes of the crosslinking agent by heterolytic decomposition, inhibiting the formation of the free radicals necessary for the vulcanization reaction [46, 47]. Thus, PANI inhibits the crosslinking process of the elastomer; hence we expect a decrease in the  $D_{max}$  values. But this effect can be partially counterbalanced by using a higher concentration of the crosslinking agent [48]. Introduction of PANI causes a slight decrease in the  $D_{max}$  value initially, after which, there is a steady increase. The  $D_{max}$  is increased by 27.7 % at 140 phr PANI loading. The F series CPCs show a steady increase in the maximum torque values with PANI-N loading, as expected. This means that with the addition

of PANI and PANI-N, some sort of interaction between them and the matrix develops. This effect is higher for the PANI-N-loaded samples.

The minimum torque;  $D_{min}$ , represents the effective viscosity of the mixtures before vulcanization. It is found to increase with filler loading for both the series (fig. 3.4). In the case of polymer composites filled with various particulate fillers [49], the minimum torque in rheographs is considered to be a direct measure of the filler content.  $D_{min}$  can be considered as a measure of stiffness of the unvulcanized compound. The increase in viscosity with the addition of filler suggests a reduced mobility of the rubber chains caused by the incorporation of these fillers.

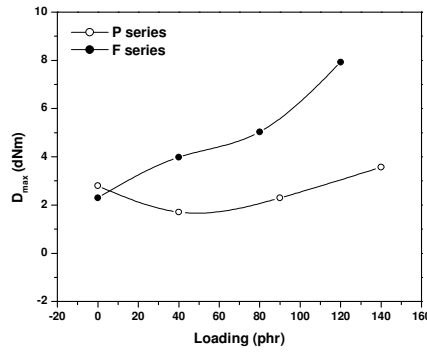


Fig. 3.3 Variation of maximum torque with loading

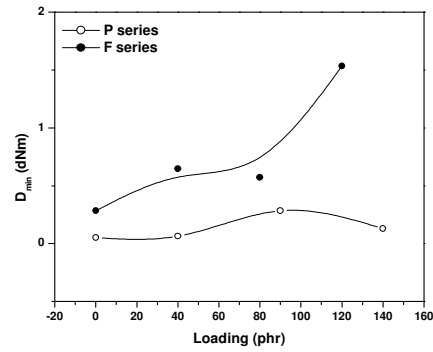


Fig. 3.4 Variation of minimum torque with loading

### 3.3.2 Cure kinetics

The plot of  $\ln (D_{max} - D_t)$  against time  $t$  of the P series and F series CPCs at  $150^\circ\text{C}$  is presented in figures 3.5 and 3.6. The plots are found to be linear which proves that the cure reactions proceed according to first order kinetics.

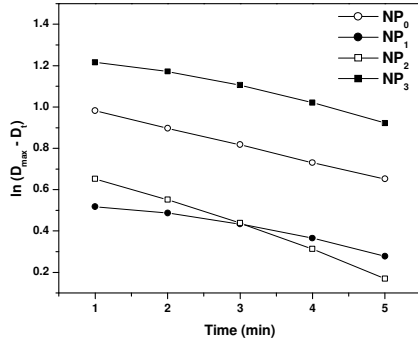


Fig. 3.5 Plot of  $\ln(D_{max} - D_t)$  vs. time for the P series CPCs

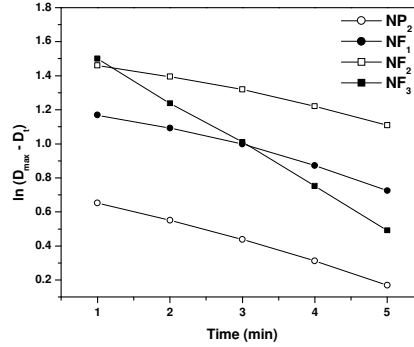


Fig. 3.6 Plot of  $\ln(D_{max} - D_t)$  vs. time for the F series CPCs

The cure rate constants ( $k$ ) were computed from their slope and the cure rate index (CRI) values were determined according to equation (3.1) for both series. The variation of these with filler loading for the P and F series is presented in figs. 3.7 and 3.8, respectively. For the P series, both CRI and the kinetic rate constants increase with loading up to 90 phr, after which, both decreases. In the case of F series, both parameters increase with loading. The increase in CRI and cure reaction constant with loading indicates the activation of cure reaction [50-52]. These results are in perfect accordance with the results of rheometric data (section 3.3.1).

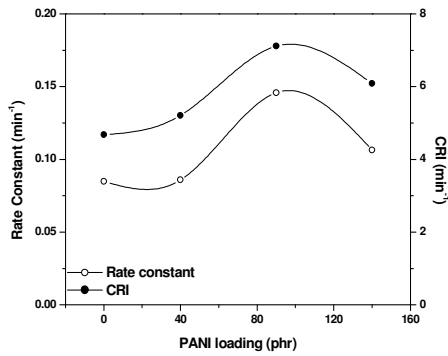


Fig. 3.7 Plot of rate constant and CRI vs. loading for the P series CPCs

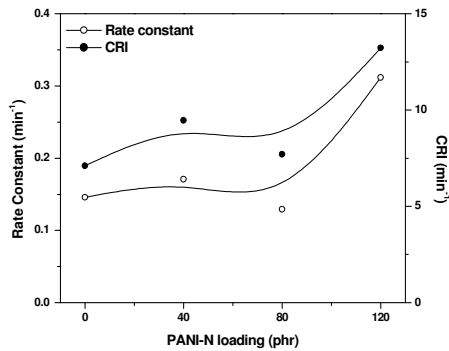


Fig. 3.8 Plot of rate constant and CRI vs. loading for the F series CPCs

### 3.3.3 Filler dispersion in the CPCs

Table 3.3 presents the computed  $\eta_r$ ,  $M_r$  and  $L$  values.  $\eta_r > M_r$  for both series indicating that the filler is not well dispersed in the matrix. Both  $\eta_r$  and  $M_r$  values increase with loading indicating an increase in the relative viscosity and relative modulus of the elastomer. The index  $L$  increases with filler loading pointing to the agglomeration of the filler in the elastomer. The value of  $L$  is found to be higher for PANI loaded samples compared to PANI-N loaded ones. This indicates poor dispersion of PANI particles compared to PANI-N in the NR matrix.

Table 3.3  $\eta_r$  and  $M_r$  values of the CPCs

CPCs	$\eta_r$	$M_r$	$L$
NP <sub>1</sub>	1.25	0.63	0.62
NP <sub>2</sub>	5.46	0.82	4.64
NP <sub>3</sub>	2.50	1.27	1.23
NF <sub>1</sub>	2.27	1.73	0.54
NF <sub>2</sub>	2.01	2.19	-0.18
NF <sub>3</sub>	5.39	3.45	1.94

In fig. 3.9, Wolf equation is applied for the PANI loaded and PANI-N-loaded CPCs. The linear correlations shown in fig. 3.9 imply that  $\alpha_f$  is independent of filler loading and that the PANI and PANI-N structures remain constant over the loading range investigated. The absolute value of  $\alpha_f$  for each composite was calculated using equation (3.8) and is plotted in fig. 3.10. The value of  $\alpha_f$  increases with filler loading for PANI-loaded compounds indicating that PANI particles form agglomerates in the elastomer. But for the PANI-N-loaded compounds,  $\alpha_f$  does not show much variation. These observations are in agreement with those obtained from Lee's approach.

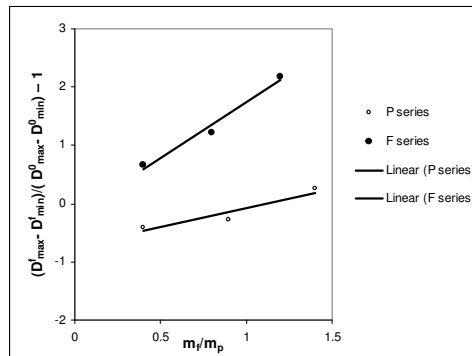


Fig. 3.9 Plot of relative torque as a function of loading

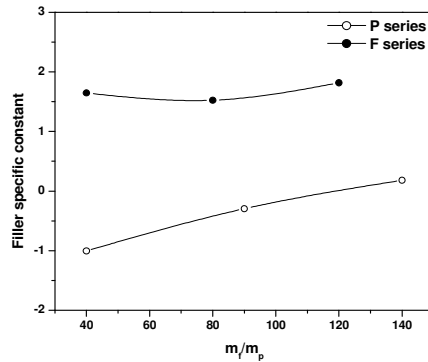


Fig. 3.10 Variation of the filler specific constant with loading

### 3.3.4 Mechanical properties of the CPCs

The variation of tensile strength of the CPCs with loading is shown in fig. 3.11 and fig. 3.12 presents the variation of tear strength with loading. The tensile strength shows a sharp decrease (55 % reduction) on addition of 40 phr of PANI. Further additions do not have much effect on the tensile strength. PANI is not effective in improving the tensile strength due to dilution effect at these high loading levels. Generally, PANI is known as a very rigid material and the tensile strength of most PANI blends or composites has a decreasing tendency as the concentration of PANI increases [53, 54]. At loadings less than 30 % (w/w), however, there have been reports of improvement in tensile strength [46, 55]. The tensile strength of F series



increases with loading due to the reinforcement effect of the fiber. The presence of fiber in the matrix along the longitudinal direction of the application of force requires that greater force be applied to pull out the fiber from the fiber/rubber interface. On incorporation of 120 phr PANI-N, the tensile strength of the CPC with 90 phr PANI (NP<sub>2</sub>) increases by ~ 100 %. The decrease in tensile strength of the composites due to PANI incorporation is thus counter-balanced by the addition of PANI-N.

In the case of CPCs of the P series, tear strength decreases slightly on 40 phr PANI loading (NP<sub>1</sub>), beyond which it shows a slight increase. For the F series, it sharply increases with PANI-N loading and reaches saturation at 80 phr PANI-N loading (NF<sub>2</sub>). PANI-N oriented perpendicular to the direction of propagation of crack front deviates or arrests the crack more effectively. Hence the PANI-N CPCs show higher tear strength than the PANI CPCs.

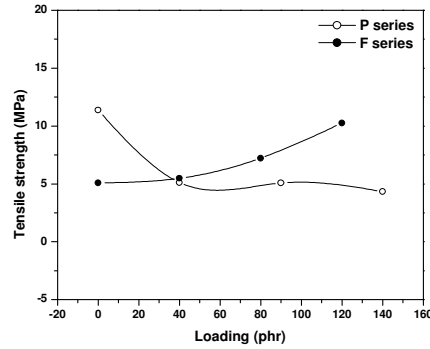


Fig. 3.11 Variation of tensile strength with loading

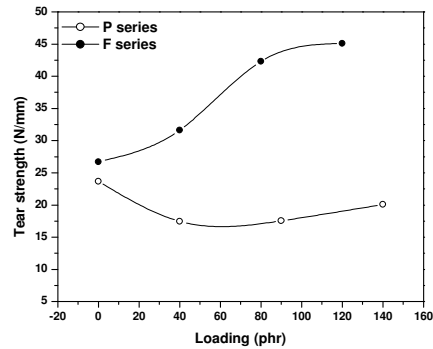


Fig. 3.12 Variation of tear strength with loading

Figs. 3.13 and 3.14 present the elongation at break and modulus at 25 % elongation of the CPCs, respectively. Both the series give an initial sharp decrease in elongation at break. This means that both PANI and PANI-N lack the ability to elongate to high strains. The decrease in elongation at break with filler loading is due to the lower molecular mobility arising from the formation of physical bonds between the filler particles and the polymer chains, apart from the dilution effect.

P series does not show any variation in the modulus whereas F series shows a sharp increase with increasing loading. This effect is assigned to the reinforcing nature of the PANI-N, changing the viscoelastic behavior of the rubber to a rigid material. The increase is less pronounced for the P series. This is assigned to the low viscosity of these composites, as seen in the torque curves (*section 3.3.1*) and *fig. 3.4*. As the fibers restrain the rubber matrix more effectively, the modulus of the PANI-N composites is higher.

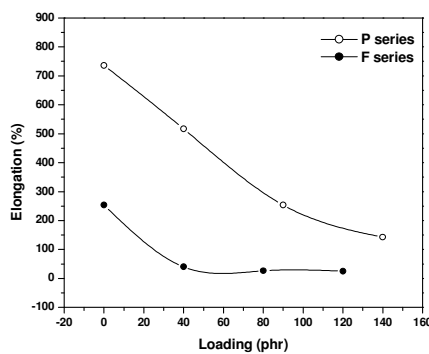


Fig. 3.13 Effect of loading on elongation at break of the CPCs

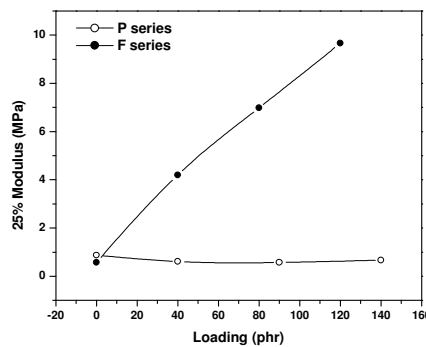


Fig. 3.14 Effect of loading on modulus of the CPCs

### 3.3.5 Morphology

Fig. 3.15 presents the SEM micrographs of the CPCs. There is no change in the lamellar structure of the rubber at low loadings of PANI. By increasing the PANI concentration, there is a change in the morphology of the fracture surface. Formation of microductile type of fracture or slip lines with formation of small microcraters or pits are observed in the CPC NP<sub>1</sub>. Detachment of PANI agglomerates and formation of grooves are clearly visible. Crevices are seen from where PANI particles were peeled off. These justify the poor tensile and tear strength of this CPC. As discussed in chapter 2 (*section 2.3.1.1*), pure PANI exist as agglomerates. At 40 phr loading (CPC NP<sub>1</sub>), the PANI particles with different size and shape are discreetly distributed in the rubber matrix with little interaction between them (*fig. 3.15b*). Such a composite is insulating. For higher concentration, i.e. for 90 phr PANI-loaded sample, (NP<sub>2</sub>) (*fig. 3.15c*), an even distribution is observed. Faez *et al.* observed by

SEM that the morphology of PANI-DBSA/EPDM blends prepared by reactive processing undergoes significant changes during mixing [55, 56]. Initially very compact and hard agglomerates of PANI-DBSA decrease in size and acquire a sponge structure with increasing mixing time. For higher concentration (fig. 3.15c), an even distribution is observed suggesting a better compatibilization of the blend components. The PANI-N loaded CPCs (fig. 3.15d and 3.15e) show good orientation of fiber in one direction, resulting in improved mechanical properties. The uniform distribution of PANI and PANI-N in the matrix results in the formation of a close-knit network enhancing the conductivity.

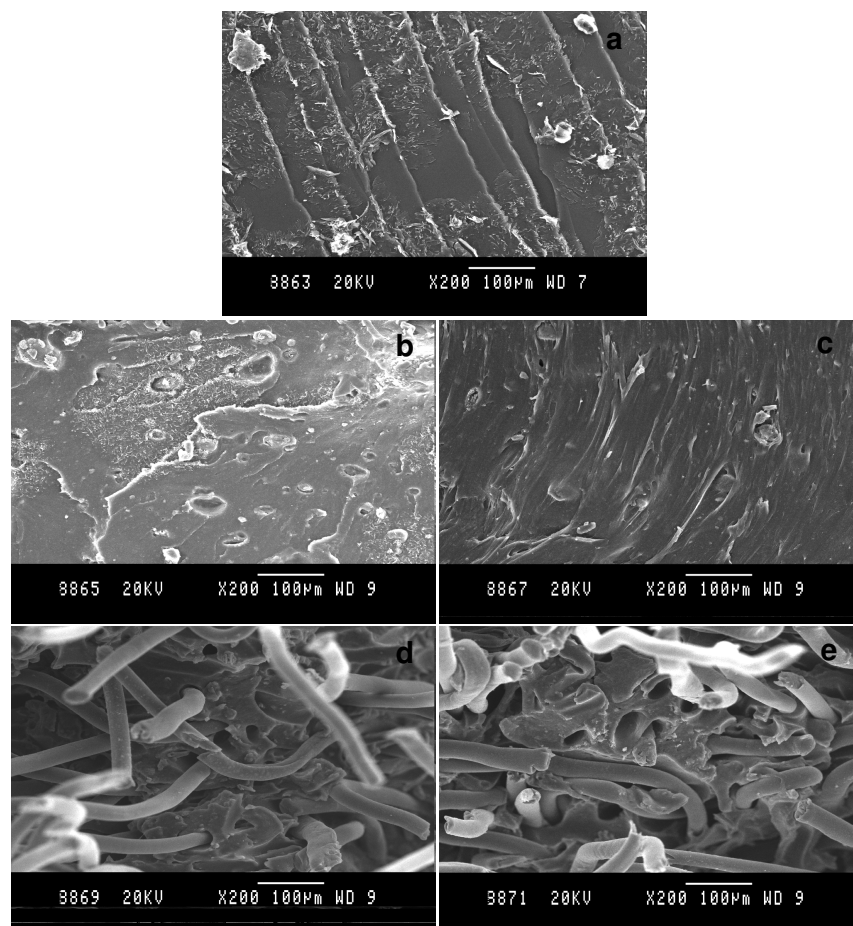


Fig. 3.15 SEM micrographs of (a)  $NP_0$ , (b)  $NP_1$ , (c)  $NP_2$ , (d)  $NF_2$  and (e)  $NF_3$  CPCs

### 3.3.6 DC electrical conductivity of the CPCs

The variation of DC electrical conductivity of the composites with loading is given in fig. 3.16. Even a concentration of 40 phr PANI could not exert much influence on the conductivity of the composite. This might be due to the lesser interaction between the components in the composite, which causes agglomeration of the PANI particles in the matrix, resulting in a non-uniform distribution and hence poor conductivity. It was established by Zilberman *et al.* that the blend morphology and the level of interaction between components of the blends strongly affect the electrical conductivity of the blend [57, 58]. High fracturing level of the PANI particles occurs due to their high interaction with a compatible matrix. Interaction of the matrix polymer with the conducting polymer effects dispersion of the conducting phase in the matrix, and higher PANI fracturing is observed for matrices interacting more strongly with PANI due to better interphase shear stress transfer [57, 59]. Smaller PANI particles thus formed, lead to an increase in the conductivity by dispersing themselves uniformly in the matrix. The dispersed PANI particles partially reaggregate during processing and molding due to PANI incompatibility with the matrix polymer.

It is necessary to recall here that PANI aggregates are made of small grains comprised of a collection of small spheres, which in turn, is comprised of smaller spheres built from still smaller primary particles (*section 2.3.1.1*). These primary particles have a metallic core surrounded by an amorphous non-metallic shell. Lennartz *et al.* showed that these primary particles agglomerate to around 50 nm aggregates in a poly(methyl methacrylate) (PMMA) matrix [60]. These particles are considered to be the hyperstructure, which formed secondary particles of ~ 100 nm in the polymer matrices [60, 61]. Hence the poor conductivity exhibited by the 40 phr PANI-loaded CPC can be attributed to the lesser interaction of the conducting polymer with the NR matrix and its higher extent of agglomeration. Higher concentrations of PANI increase the conductivity. Percolation is observed at 90 phr PANI loading. Introduction of 40 phr PANI-N decreases the conductivity, but higher loadings give conductivity higher than that of the P series. A conductivity of  $\sim 2 \times 10^{-6}$  S/cm is obtained for 120 phr PANI-N loading (CPC NF<sub>3</sub>).

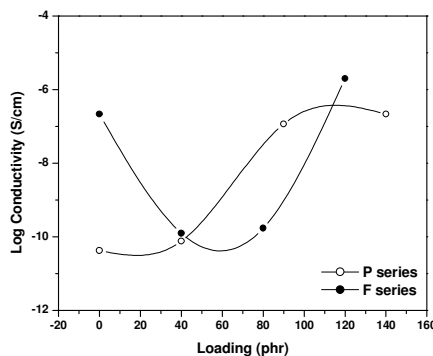


Fig. 3.16 DC electrical conductivity of the CPCs

### 3.3.7 Thermal stability

The TG curves of the P series CPCs are shown in fig. 3.17. The thermal characteristics as estimated by TGA are presented in table 3.4. The degradation behavior can be better understood by the Differential thermogravimetry (DTG) curves in fig. 3.18. Pure NR ( $NP_0$ ) gives a single degradation between 296 and 491 °C and peak maximum at 388.2 °C. The NR-PANI CPC,  $NP_1$  shows an additional degradation starting at 225 °C. This degradation can be seen for all NR-PANI composites and its intensity increases with PANI concentration. This can be assigned to the evolution of PANI dopant. Pure PANI gives a weight loss between 153 °C and 295 °C (section 2.3.1.4 of this thesis). In the composites, this weight loss occurs at a slightly higher temperature range, 201-320 °C. The onset of degradation slightly shifts to lower temperature with increasing PANI concentration, but the temperature of maximum degradation remains unaffected.

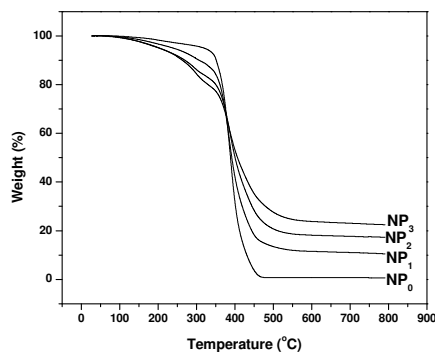


Fig. 3.17 TGA traces of the CPCs  
of P series

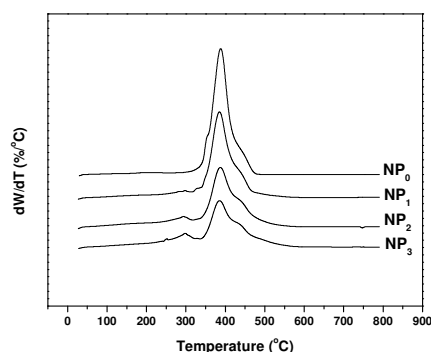


Fig. 3.18 DTG curves of CPCs  
of P series

Table 3.4 Thermal characteristics of P series CPCs

		Degradation	NP <sub>0</sub>	NP <sub>1</sub>	NP <sub>2</sub>	NP <sub>3</sub>
Onset temperature (°C)	First	-	-	225.9	201.7	216.9
	Second		296.5	315.7	319.7	335.9
Peak degradation temperature (°C)	First	-	-	297.9	297.0	298.5
	Second		388.2	385.1	387.2	385.3
Weight loss (%)	First	-	-	5.58	11.03	14.88
	Second		50.8	58.1	60.3	62.1
Temperature at 50 % weight loss (°C)			388.7	392.1	400.6	406.9

With increasing PANI concentration, weight loss due to the NR degradation is still observed, but the relative intensity decreases. The onset of this degradation shows a slight shift to higher temperatures with increasing PANI concentration, though the temperature of maximum degradation remains the same. With increasing PANI concentration, another degradation starting at  $\sim 415^{\circ}\text{C}$  and ending at  $581^{\circ}\text{C}$  can be discerned overlapping with the NR degradation. NR degrades completely by around  $491^{\circ}\text{C}$ . Hence, this weight loss is not connected with NR degradation. This process can be assigned to the dedoped PANI degradation. Pure PANI gives this degradation

at 342-689 °C (see section 2.3.1.4). It is to be noted that this degradation does not manifest itself as a separate process; it is seen as a continuation of the NR degradation. This probably means that there is no phase separation between the components [62]. As can be understood from table 3.4, the thermal stability increases with PANI concentration.

Figs. 3.19 and 3.20 represent the TGA traces and corresponding DTG curves of the F series. The data obtained from the TGA is presented in table 3.5.

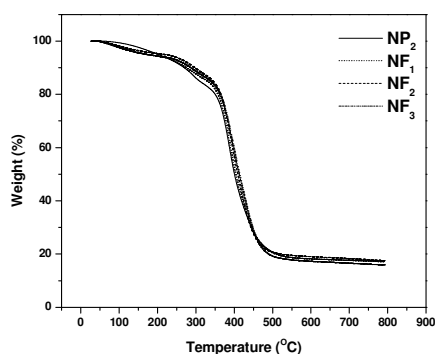


Fig. 3.19 TGA traces of F series CPCs

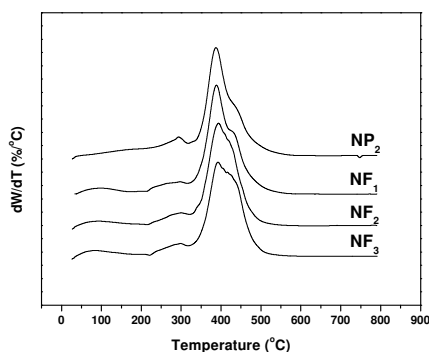


Fig. 3.20 DTG curves of F series CPCs

Table 3.5 Thermal degradation data of F series CPCs

	Degradation	NP <sub>2</sub>	NF <sub>1</sub>	NF <sub>2</sub>	NF <sub>3</sub>
Onset temperature (°C)	First	201.7	212.8	216.9	220.8
	Second	319.7	315.7	321.9	316.8
Peak degradation temperature (°C)	First	297.0	297.3	299.6	298.8
	Second	387.2	388.4	393.7	392.3
Weight loss (%)	First	11.0	7.8	7.6	6.9
	Second	65.6	67.9	68.1	69.6
Temperature at 50 % weight loss (°C)		400.6	403.3	409.0	412.9

As in the case of P series, three degradations are seen in F series also. The onset temperature of the first degradation due to the PANI dopant evolution increases on increasing the PANI-N concentration. There is no change in the degradation pattern on increasing the PANI-N concentration. The peak degradation temperature and the weight loss remain almost constant because of the fixed concentration of PANI in these composites. The second degradation is much more complex than in the case of P series due to the additional PANI-N degradation, overlapping in the same temperature range. The PANI-N degrades in the temperature range 293-523 °C (section 2.3.3.6). The second degradation of the CPCs starts at around 315 °C. The maximum temperature of this degradation shifts slightly to higher temperatures with increasing PANI-N content but the intensity of this degradation is unaltered. It is rather difficult to distinguish the PANI chain degradation and the PANI-N degradation. To conclude, the thermal stability of the composites increases with PANI-N concentration.

### 3.3.7.1 Thermal degradation kinetics

The kinetics of the thermal degradation reaction was followed using TGA. The Coats and Redfern (CR) equation (equation 3.22) for different values of  $n$  were applied for each CPC in the P and F series. Best fit is obtained for  $n = 1$ . Representative plots of one CPC from each series for  $n = 1, 2$  and 3 are given in figs. 3.21 and 3.22. The activation energies obtained from the corresponding plots are presented in table 3.6.

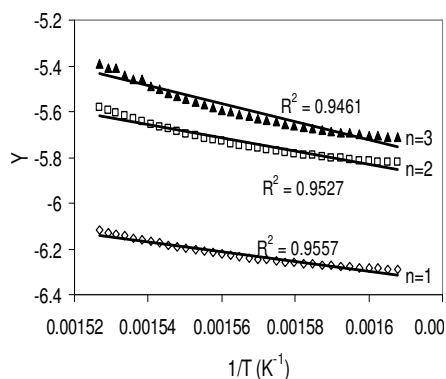


Fig. 3.21 Representative plot of Coats and Redfern equation for the CPC NP<sub>2</sub>

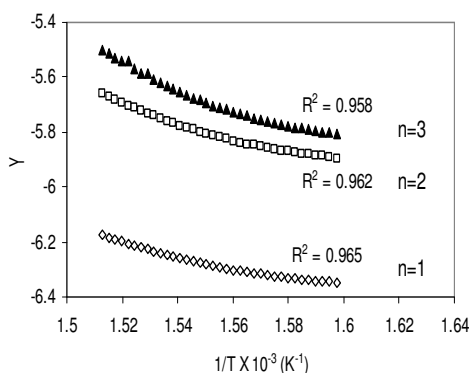


Fig. 3.22 Representative plot of Coats and Redfern equation for the CPC NF<sub>3</sub>



The Freeman and Carroll (FC) method (equation (3.17)) and the Chan and Balke (CB) method (equation (3.19)) were also applied and the corresponding activation energies are given in table 3.6. Representative graphs of the two methods are shown in figs. 3.23 and 3.24. Application of the Chan and Balke equation (equation 3.19) gives a perfect straight line and no deviation from linearity is observed. Hence it can be said that the degradation reaction follows first order kinetics. As shown in table 3.6, the estimates of activation energy vary widely amongst the three methods. There are several obvious sources of error that can be responsible for this variation. For the integral methods, i.e. CR equation, the different approximations to the integral of the Arrhenius equation lead to systematic errors in the values of the activation energy [63]. The precision of the quantities plotted according to the Freeman and Carroll equation can be poor because of the error-propagation effects resulting when two experimentally determined values are ratioed [64]. The CB equation treats the data as a pseudo first order reaction and any deviation from the first order kinetics results in a non-linear plot. Hence it can be presumed that this method is a reliable one. In summary, all the methods indicate the order of the degradation reaction to be one. No trend for the change in activation energy can be derived from table 3.6.

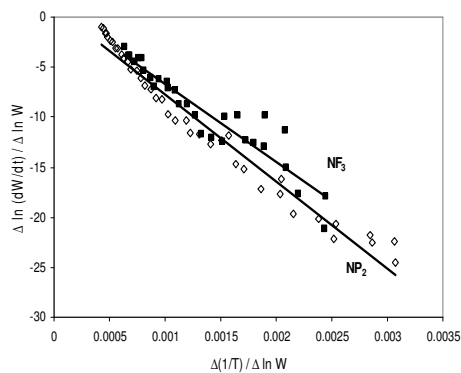


Fig. 3.23 Representative plot of Freeman and Carroll equation for NP<sub>2</sub> and NF<sub>3</sub>

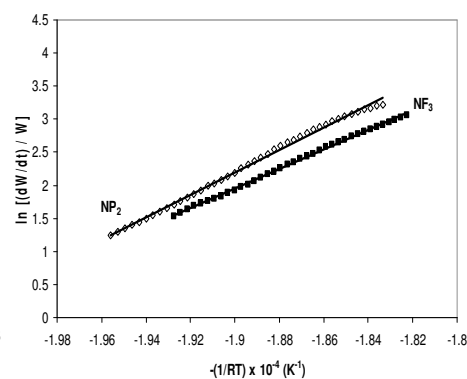


Fig. 3.24 Representative plot of Chan and Balke equation for NP<sub>2</sub> and NF<sub>3</sub>

Table 3.6 Kinetic parameters obtained from various methods

CPC	CR equation	FC equation		CB equation
	E <sub>a</sub> (kJ/mol)	n	E <sub>a</sub> (kJ/mol)	E <sub>a</sub> (kJ/mol)
NP <sub>0</sub>	167.0	0.96	190.2	209.1
NP <sub>1</sub>	83.2	1.0	194.3	194.7
NP <sub>2</sub>	62.9	0.97	160.7	170.0
NP <sub>3</sub>	43.9	1.0	170.3	163.7
NF <sub>1</sub>	64.3	1.0	156.8	159.1
NF <sub>2</sub>	67.0	1.0	123.7	145.8
NF <sub>3</sub>	62.0	0.97	143.1	147.5

### 3.4 Conclusions

Conducting natural rubber/polyaniline/polyaniline coated short Nylon fiber composites (NR/PANI/PANI-N CPCs) with sufficient mechanical properties can be prepared by mechanical mixing. Addition of pristine PANI to NR improves its cure characteristics. The cure reaction follows first order kinetics. Fine dispersion of PANI particles in the NR matrix is not achieved by mill mixing. Thermal stability and electrical conductivity increases with PANI concentration. The tensile strength decreases drastically with increase in PANI concentration. The tensile strength of the NR/PANI system can be improved by adding PANI coated short Nylon fibers. The addition of PANI coated short Nylon fiber not only brings about a significant improvement in the mechanical properties, but increases the cure rate, shear modulus, viscosity and thermal stability as well. The DC electrical conductivity of the composites decreases on addition of polyaniline coated short Nylon fiber. Higher conductivity values are obtained at higher loadings. A conductivity of  $\sim 2 \times 10^{-6}$  S/cm is obtained for 120 phr PANI-coated short Nylon fiber loaded composite. The thermal degradation process follows first order kinetics.

### References

1. Blackley DC. Polymer latices: Science and technology. Vol. 2, Types of latices, 2<sup>nd</sup> edition. Chapman and Hall, 1997.

2. Davis W. Fortune 1997;4:86-95.
3. Nielson LE. Mechanical properties of polymers and composites. Marcel Dekker, 1974.
4. Kraus G. Reinforcement of elastomers. Wiley, 1965.
5. Hundiware DG, Kapadi UR, Desai MC, Bidkar SH. J Appl Polym Sci 2002;85:995.
6. Saad ALG, Younan AF. Polym Degrad Stab 1995;50(2):133-140.
7. Gazeley KF, Fuller KNG. In: Roberts AD, editor. Natural rubber science and technology. Oxford University Press, MRPRA, U K, 1988, chapters 4 and 19.
8. Guth EJ Appl Phys 1944;16:20.
9. Kurian T, De PP, Khastgir D, Tripathy DK, De SK, Peiffer DG. Polymer 1995;36:3875.
10. Yatsuyanagi F, Suzuki N, Ito M, Kaidou H. Polymer 2001;42:9523.
11. Alberola ND, Benzarti K, Bas C, Bomal Y. Polym Compos 2001;22:312.
12. Zhang A, Wang L, Lin Y, Mi X. J Appl Polym Sci 2006;101:1763.
13. Seto J. Rubber Chem Technol 1977;50:333.
14. Smit PPA. Rubber Chem Technol 1968;41:1194.
15. Ahmed S, Jones FR. J Mater Sci 1990;25:4933.
16. Edwards DC. J Mater Sci 1990;25:4175.
17. Payne AR, Whittaker RE. Rubber Chem Technol 1971;44:440.
18. Janecek J. Rubber Chem Technol 1962;35:833.
19. Dizon ES, Hicks AE, Chirico VE. Rubber Chem Technol 1974;47:231.
20. Bokobza L, Rapoport O. J Appl Polym Sci 2002;85:2301.
21. Hepburn C. Plast Rubber Int 1984;9:11.
22. Parkinson D. Reinforcement of rubber. Lakeman and Co., 1957.
23. Goettler LA, Shen KS. Rubber Chem Technol 1983;56:620.
24. Setue DK, De SK. J Mater Sci 1984;19:983.
25. Fitzner E, Gkogkids A, Heine M. High Temp High Pressure 1984;16:363.
26. Zhan ZJ, Magnus FL, Halasa AF. Rubber Chem Technol 1993;66:456.
27. Sreeja R, Pradeep P, Rossamma Alex. In: Proceedings of the 15<sup>th</sup> Kerala Science Congress, India, 2003.

28. Blow CM, Hepburn C. Rubber technology and manufacture. 2<sup>nd</sup> edition, London; Butterworths, 1982.
29. Wazzan AA. Int J Polym Mat 2005;54:783-794.
30. Mathew G, Nah C, Rhee JM, Singh RP. J Elastomers and Plast 2006;38:43-63.
31. Fujimoto K, Nishi T, Okamoto T. Int Polym Sci Technol 1981;8:T/30.
32. Mathew G, Singh RP, Nair NR, Thomas S. J Mater Sci 2003;38:2469-2481.
33. Gonzalez L, Rodriguez A, Marcos A, Chamorro C. Rubber Chem Technol 1996;69:203.
34. Lee BL. Rubber Chem Technol 1979;52:1019-1029.
35. Costa HM, Visconte LLY, Nunes RCR, Furtado CRG. Int J Polym Mat 2004;53:475-479.
36. Wolf S. Rubber Chem Technol 1996;69:325-346.
37. Kraus G. Rubber Chem Technol 1978;51:297-321.
38. Sobhy MS, El-Nashar DE, Maziad NA. Egypt J Sol 2003;26(2):241-257.
39. Westlinning H, Wolf S. Kautsch Gummi Kustst 1966;19:470.
40. Wolf S, Meng-Jio Wang. Rubber Chem Technol 1992;65:329-342.
41. Freeman ES, Carroll B. J Phys Chem 1958; 62:394-397.
42. Chan JH, Balke ST. Polym Degrad Stab 1997;57(2):135-149.
43. Coats AW, Redfern JP. Nature 1964;201:68-69.
44. Sreeja TD, Kutty SKN. Polym Plast Technol Eng 2003;42(2):239-252.
45. Seema A, Kutty SKN. J Appl Polym Sci 2006;99:532-539.
46. Van Drumpt JP. Rubber World 1988;197:33.
47. Keller RC. Rubber Chem Technol 1988;61:238-254.
48. Faez R, Gazotti WA, De Paoli M-A. Polymer 1999;40:5497-5503.
49. Mathew G, Kuriakose B, Thomas S. J Elastomers Plast 1997;29:163.
50. da Silva ALN, Rocha MCG, Moraes MAR, Valente CAR, Coutinho FMB. Polym Test 2002;21:57-60.
51. Poh BT, Ismail H, Quah EH, Chin PL. J Appl Polym Sci 2001;81:47-52.
52. Deghaidy FS. Egypt J Sol 2000;23(1):167-177.
53. Chipara M, Hui D, Notingher PV, Chipara MD, Lau KT, Sankar J, Panaitescu D. Composites Part B 2003;34:637.

54. Choda'kI. Omastova' M, Pionteck J. J Appl Polym Sci 2001;82:1903.
55. Faez R, De Paoli M-A. Eur Polym J 2001;37:1139-1143.
56. Faez R, Martin IM, De Paoli M-A, Rezende MC. J Appl Polym Sci 2002;83(7):1568-1575.
57. Zilberman M, Siegmman A, Narkis M. J Macromol Sci Phys 1998;B37(3):301-318.
58. Zilberman M, Siegmman A, Narkis M. J Macromol Sci Phys 2000;B39(3):333-337.
59. Narkis M, Zilberman M, Siegmman A. Polym Adv Technol 1997;8(8):525-528.
60. Lennartz W, Mietzner T, Nimtz G, Wessling B. Synth Met 2001;119(1-3):425-426.
61. Wessling B. Chem Innovat 2001;31(1):34-40.
62. Faez R, Schuster RH, De Paoli M-A. Eur Polym J 2002;38:2459-2463.
63. Perez-Maqueda LA, Sanchez-Jimenez PE, Criado JM. Polymer 2005;46:2950-2954.
64. Balke ST. Quantitative column liquid chromatography. Amsterdam; Elsevier, 1984.

*Chloroprene rubber/polyaniline/polyaniline coated short Nylon fiber conducting composites were prepared and its cure characteristics, filler dispersion, mechanical properties, conductivity and thermal stability were evaluated. PANI and PANI-N increased the rate of cure reaction. The composite showed higher tensile strength, tear strength and modulus values and lower elongation. Characterization of the composites using scanning electron microscopy showed that there were changes in the morphology of the fracture surface with filler loading. The DC electrical conductivity and the thermal stability of the composites increased with PANI and PANI-N concentration. The kinetic parameters of thermal degradation were estimated by different methods.*

---

## Chapter 4

### PANI coated short fiber reinforced chloroprene rubber conducting composites

#### Preparation and characterization\*

#### 4.1 Chloroprene rubber

Chloroprene rubber (CR) or polychloroprene was the first mass-produced synthetic rubber. Its common name is Neoprene. (fig. 4.1). Among the speciality elastomers, chloroprene rubber is one of the most important with an annual consumption of

---

\* A. Saritha Chandran, Sunil K. Narayanankutty. *European Polymer Journal* 2008;44(7):2418-2429.

A part of the work described in this chapter has been presented at

- ✓ *International Conference on Materials Science Research and Nanotechnology, ICMSRN – 2008, Feb 27-29, 2008, Mother Teresa Women's University, Kodaikanal, India*
- ✓ *International Symposium, Polymers-Prospect and Challenges, POLYMSYM'08, April 4-5, 2008, National Institute of Technology, Calicut, India*

nearly 300,000 tons worldwide. First production was in 1932 by DuPont. Since then, CR has an outstanding position due to its favourable combination of technical properties. From the beginning until the 1960s, chloroprene was produced by the older “acetylene process”. This process has the disadvantages of being very energy-intensive and having high investment costs. The modern chloroprene process, which is now used by nearly all manufacturers, is based on butadiene, which is readily available. Butadiene is converted into the monomer chloroprene (2-chloro-1,3 butadiene).

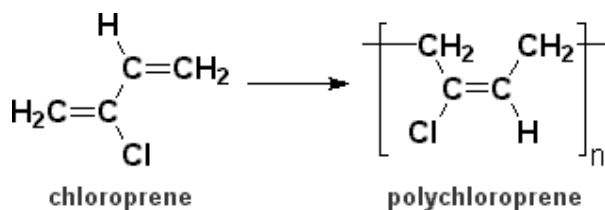


Fig. 4.1 Structure of chloroprene rubber

CR is used in different technical areas, mainly in the rubber industry (~ 61%), but is also important as a raw material for adhesives (both solvent based and water based, ~ 33%) and has different latex applications (~ 6%) such as dipped articles (e.g. gloves) and molded foam. Application areas in the elastomer field are widely spread, such as molded goods, cables, transmission belts, conveyor belts, profiles etc.

CR is not characterized by one outstanding property, but its balance of properties is unique among the synthetic elastomers. It is a polar rubber with good mechanical strength, high ozone and weather resistance, good ageing resistance, low flammability, good resistance toward chemicals, moderate oil and fuel resistance and adhesion to many substrates.

Incorporation of the conducting polymer modifies the properties of the elastomer enhancing its potential for many applications. An appropriate selection of the conducting polymer and the matrix can result in CPCs with desired properties for different applications. The processability and properties of the CPCs depend on the nature of the elastomer *viz.*, polar/non polar and the type of elastomer *viz.*,

natural/synthetic. It also depends on the properties of the conducting polymer incorporated into it. The processability studies are indispensable for the evaluation of the physical and mechanical properties of the CPCs or in fact, any composites. In this chapter, the preparation, processability and mechanical properties of CR based polyaniline/polyaniline coated short Nylon fiber CPCs are discussed. The cure characteristics and cure kinetics, filler dispersion, mechanical properties and morphological characterization of the composites are described. The DC electrical conductivity and thermal analysis of the composites are presented. The thermal degradation kinetics of the CPCs is also discussed.

## 4.2 Conducting chloroprene rubber composites

### 4.2.1 Composite preparation

Table 4.1 Formulation for the preparation of CPCs

Ingredients (phr <sup>*</sup> )	P series				F series		
	CP <sub>0</sub>	CP <sub>1</sub>	CP <sub>2</sub>	CP <sub>3</sub>	CF <sub>1</sub>	CF <sub>2</sub>	CF <sub>3</sub>
CR	100	100	100	100	100	100	100
PANI	0	50	100	150	100	100	100
PANI-N <sup>#</sup>	0	0	0	0	40	80	120

\* parts per hundred rubber

<sup>#</sup> PANI coated etched fiber

All the mixes contain Stearic acid- 1 phr and DCP- 3 phr

Chloroprene rubber was supplied by Toyo Soda Manufacturing Co. Ltd., Tokyo. The sample had a Mooney viscosity ML1+4 (@100 °C) 50. The prepared polyaniline (PANI) and PANI coated short Nylon fiber (PANI-N) (sections 2.2.2, 2.2.3 and 2.2.4) were incorporated into chloroprene rubber according to the formulation given in table 4.1. Two series of CPCs were prepared, first series with PANI alone (P series) and the second with PANI and PANI-N (F series). The composites were prepared in a laboratory size (15 × 33 cm) two-roll mill at a friction ratio of 1:1.25 as per ASTM D 3184 (1980) and compression molded at 150 °C. They were vulcanized to their respective optimum cure times (section 3.2.2).



#### 4.2.2 Characterization

The cure characteristics of the vulcanizates were monitored using a Rubber Process Analyzer as explained in *section 3.2.3*. The cure time;  $T_{90}$ , scorch time;  $T_{10}$ , maximum torque;  $D_{max}$  and minimum torque;  $D_{min}$  values were determined at 150 °C. The cure rate index (CRI) [1, 2] and the kinetic rate constant of cure reaction, were determined from the rheometric data. The vulcanization kinetics was studied by the method [3-5] described in *section 3.2.3 of this thesis*. The filler dispersion and formation of filler agglomerates in polymer matrices were studied by the methods proposed by Lee [6, 7] and Wolf [7-12] as described in *section 3.2.4 of this thesis*. The mechanical properties of the CPCs were determined using a Shimadzu Universal Testing Machine (model AG1) (*see section 3.2.5*). Average of atleast six sample measurements were taken to represent each data point. Scanning electron microscopic images (SEM) of tensile fracture surfaces and the DC electrical conductivity of the CPCs were measured as explained in *sections 3.2.6 and 3.2.7*, respectively. Thermogravimetric studies and the evaluation of the kinetic parameters of thermal degradation were also done (*section 3.2.8*). The thermal degradation parameters like activation energy and order of the degradation reaction was determined by various methods *viz.*, Freeman Carroll method [13], Chan and Balke method [14] and using Coats Redfern equation [15]. These different methods are described in detail in *section 3.2.8.1*.

### 4.3 Results and discussion

#### 4.3.1 Cure characteristics

Figures 4.1 and 4.2 show the cure curves of P series (CPCs with PANI) and F series (CPCs with PANI and PANI-N), respectively. The nature of the cure curves is different for both series, which indicates that in the matrix PANI and PANI-N react differently.

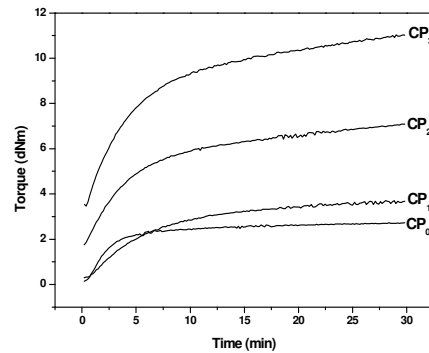


Fig. 4.1 Cure curves of the  
P series CPCs

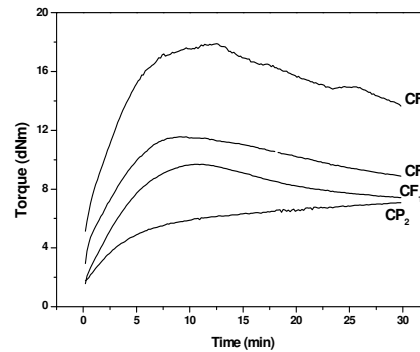


Fig. 4.2 Cure curves of the  
F series CPCs

Figures 4.3 and 4.4 presents the variation of cure time;  $T_{90}$ , and scorch time;  $T_{10}$ , respectively with PANI loading (P series) and PANI-N loading (F series). Cure time represents the time corresponding to the development of 90 % of the maximum torque. Initially, cure time is found to increase with the incorporation of PANI, which then stabilizes upon further addition; whereas it decreases on PANI-N loading initially but further additions do not affect the cure time significantly. This means that incorporation of PANI to the elastomer retards the cure reaction slightly whereas addition of PANI-N accelerates the cure reaction. This is supported by the cure kinetic studies and cure rate index values, which will be discussed in the following sections. Similar results in the case of natural rubber/short Nylon fiber composites have been reported earlier [16]. The initial increase in cure time for the P series may be due to the adsorption of the curatives on the surface of PANI, which results in a decrease in the effective concentration of the curatives. Hence, the time required for optimum cure increases. Again, between the P and F series, F series show lower cure time values. This means that the PANI-N has a much stronger influence on the cure reaction than PANI.

Scorch time is the time required for the torque value to reach 10 % of maximum torque. It is a measure of the scorch safety of the rubber compound. For P series, scorch time increases with filler loading; this indicates better processing safety. For

the F series, scorch time decreases with loading. Such a decrease is attributed to the heat of mixing resulting in the premature curing of the compounds.

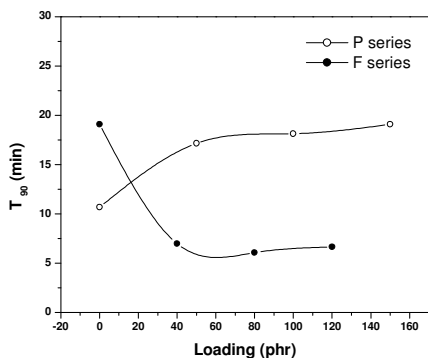


Fig. 4.3 Variation of cure time with loading

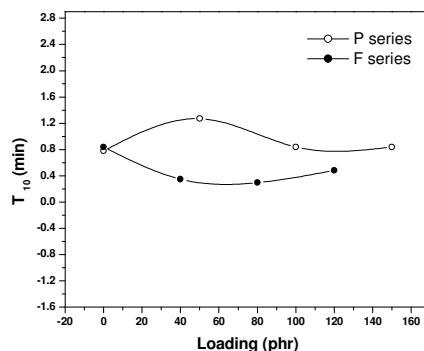


Fig. 4.4 Variation of scorch time with loading

The maximum torque is an index of the extent of crosslinking reactions and represents the shear modulus of the fully vulcanized rubber at the vulcanization temperature. It is also a measure of the filler-polymer interaction. The variation of maximum torque with filler loading is presented in fig. 4.5. The value is found to increase for both the series, indicating that the final matrix stiffness has a contribution from the filler-matrix interaction as well, apart from the crosslink density. The higher values of maximum torque for the F series compared to the P series indicate that the fiber-matrix interaction is stronger than the interaction of the matrix with PANI.

The minimum torque;  $D_{min}$ , a measure of the viscosity of the compound, is found to increase with filler loading for both the series (fig. 4.6).  $D_{min}$  can be considered as a measure of stiffness of the unvulcanized compound. The increase in viscosity with the addition of filler suggests a reduced mobility of the rubber chains in the presence of these fillers.

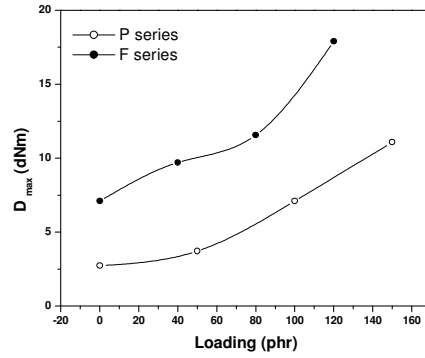


Fig. 4.5 Variation of maximum torque with loading

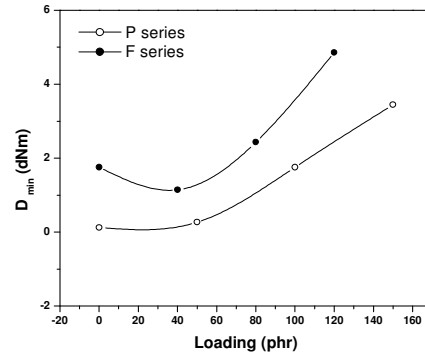


Fig. 4.6 Variation of minimum torque with loading

#### 4.3.2 Cure kinetics

The plot of  $\ln (D_{max} - D_t)$  against time  $t$  of the P series and F series at  $150^\circ\text{C}$  is presented in figures 4.7 and 4.8. The plots are found to be linear which proves that the cure reactions proceed according to first order kinetics.

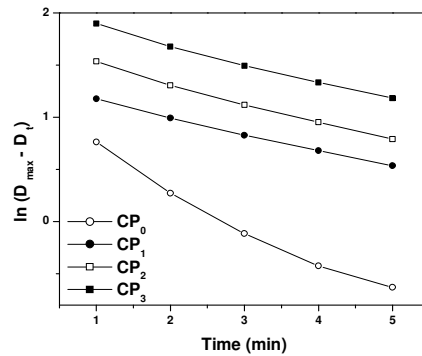


Fig. 4.7 Plot of  $\ln (D_{max} - D_t)$  vs. time for the P series

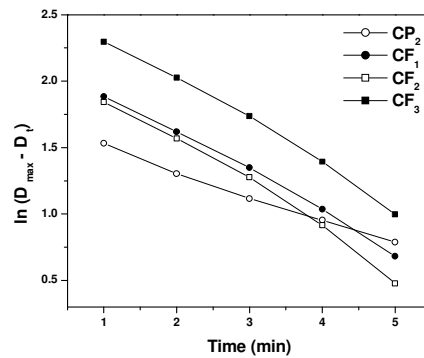


Fig. 4.8 Plot of  $\ln (D_{max} - D_t)$  vs. time for the F series

The cure rate constants were computed from their slope and the cure rate index (CRI) values were determined according to *equation (3.1)* for both series. The variation of these with filler loading is presented in fig. 4.9 and 4.10.

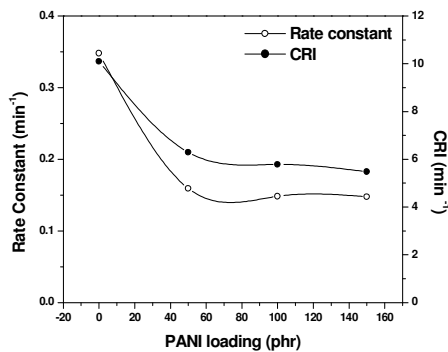


Fig. 4.9 Plot of rate constant and CRI vs. loading for the P series

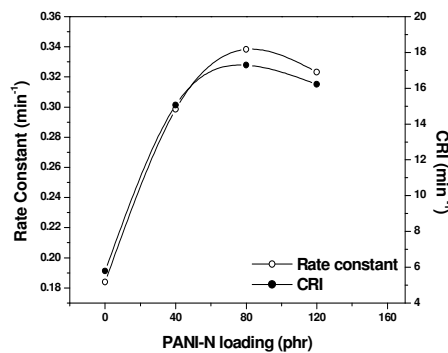


Fig. 4.10 Plot of rate constant and CRI vs. loading for the F series

For the P series, both rate constant and CRI decrease with PANI incorporation initially, and then levels off. Similar trend was seen for cure time (*fig. 4.3*). The rate constant and CRI increases with PANI-N loading for the F series, again, according to the trend seen in the variation of cure time. The increase in CRI and cure rate constant with PANI-N loading indicates the activation of cure reaction [17-19].

#### 4.3.3 Filler dispersion

The  $\eta_r$  and  $M_r$  values of both the series were computed and are given in table 4.2. For the vulcanizates with PANI i.e. for P series, it was observed that  $\eta_r > M_r$  which means that PANI is not well dispersed in the matrix. Figure 4.11 shows the variation of the index  $L$  with filler loading. The figure shows sharp increase in the value of  $L$  with PANI loading for the P series indicating predominance of agglomerates in the matrix. But for the F series,  $L$  changes less rapidly. The value of  $L$  is found to be higher for PANI-loaded samples compared to PANI-N-loaded ones. This indicates poor dispersion of PANI particles compared to PANI-N in the CR matrix.

Table 4.2  $\eta_r$  and  $M_r$  values of the CPCs

CPC	$\eta_r$	$M_r$
CP <sub>1</sub>	2.16	1.35
CP <sub>2</sub>	14.15	2.59
CP <sub>3</sub>	27.75	4.04
CF <sub>1</sub>	0.651	1.367
CF <sub>2</sub>	1.385	1.629
CF <sub>3</sub>	2.767	2.521

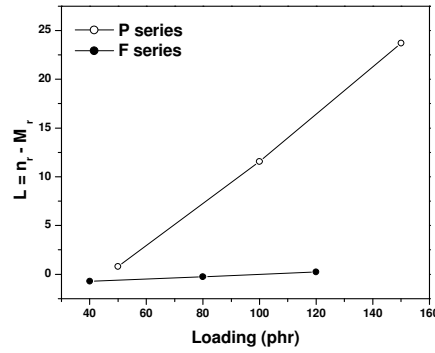


Fig. 4.11 Variation of index  $L$  with loading

In fig. 4.12, Wolf equation is applied for the PANI-loaded and PANI-N-loaded compounds. Since  $\alpha_f$  is a measure of the structure of the fillers in the matrix, the higher  $\alpha_f$  value found for the PANI-loaded compounds ( $\alpha_f = 1.16$ ) would be an evidence for this filler to be more viable to agglomeration in the vulcanizates when compared to the PANI-N-loaded compounds ( $\alpha_f = 1.13$ ). The absolute value of  $\alpha_f$  for each composite was calculated using equation (3.8) and is plotted in fig. 4.13. The value of  $\alpha_f$  increases with PANI loading for the CPCs of P series, indicating that PANI particles form agglomerates in the elastomer. But for the F series CPCs,  $\alpha_f$  decreases first and then increases. This means, PANI-N do not form agglomerates in the matrix up to 80 phr loading. With further additions, there is a tendency for agglomeration. These observations are in agreement with those obtained from Lee's approach.

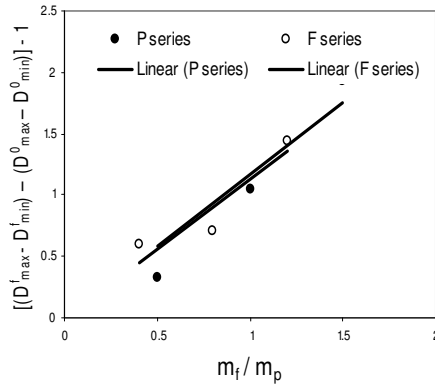


Fig. 4.12 Plot of relative torque as a function of filler loading

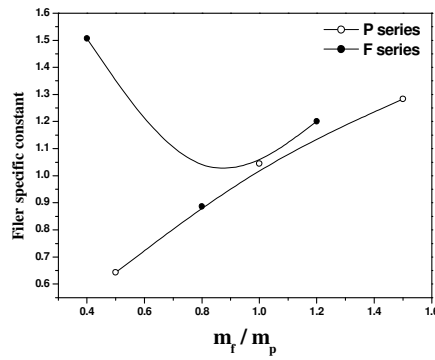


Fig. 4.13 Variation of the filler specific constant with filler loading

#### 4.3.4 Mechanical properties

The variation of tensile strength of PANI-loaded and PANI-N-loaded CPCs are shown in fig. 4.14. For the P series, tensile strength decrease initially with loading and after 50 phr, it increases whereas for F series, it increases sharply at lower loadings and at higher loadings, it decreases and reaches almost the same value as that of the composite without PANI-N. As discussed in *chapter 3*, the tensile strength of most PANI composites shows a decreasing trend, especially at low loadings. The increase in tensile strength beyond this can be attributed to probable interaction of PANI-N with the matrix. At very high loadings, the relative proportion of the matrix is low and the reinforcement becomes ineffective. With EPDM/PANI-DBSA

composite, Faez *et al.* [20] could achieve a tensile strength of approximately 7.2 MPa with a 30 % (w/w) PANI-DBSA loading. Beyond this, the tensile strength decreased to ~ 4.8 MPa at 40 % (w/w) loading. This decreasing trend was attributed to the mixture being more susceptible to imperfections due to the large PANI-DBSA agglomerates and poor interfacial adhesion. The increase in tensile strength of the CPCs denotes the reinforcing nature of the fillers. As the filler loading is increased, more surface area is available for interaction between filler particles and the rubber matrix; hence reinforcement increases with an increase in filler loading. Eventually a maximum reinforcement level is reached; at 40 phr of PANI-N (CPC CF<sub>1</sub>) for F series; after which dilution effect predominates, which tends to decrease the tensile strength. The presence of PANI-N in the matrix along the longitudinal direction of the application of force requires that greater force be applied to pull out the fiber from the fiber/rubber interface. This is the reason for the higher tensile strength values for the F series even though PANI particle possess more surface area than PANI-N. With the addition of 100 phr PANI (CPC CP<sub>2</sub>), there is ~ 12 % increase in tensile strength and on addition of 40 phr PANI-N (CPC CF<sub>1</sub>), almost 60 % increase is attained. For PANI composites, the maximum value obtained is 7.8 MPa for the composite CP<sub>3</sub> and for PANI-N composites, the maximum value of 10.6 MPa is obtained for composite CF<sub>1</sub>. Hence the percolation limit for the PANI-N CPCs is assumed to be 40 phr.

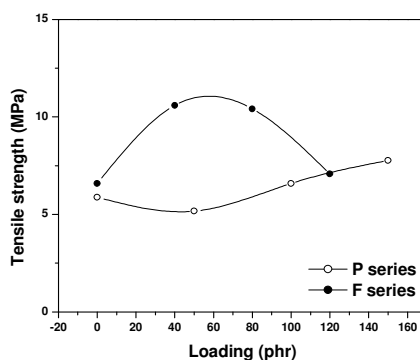


Fig. 4.14 Variation of tensile strength with loading



Fig. 4.15 shows the variation in tear strength of the composites with loading. For the P series, tear strength increases sharply up to 50 phr loading, which then shows a marginal decrease. For the F series, tear strength shows a sharp increase initially, after which, the increase slows down. PANI-N oriented perpendicular to the direction of propagation of the crack front deviates or arrests the crack more effectively. The result is that the PANI-N CPCs show higher tear strength than the PANI CPCs.

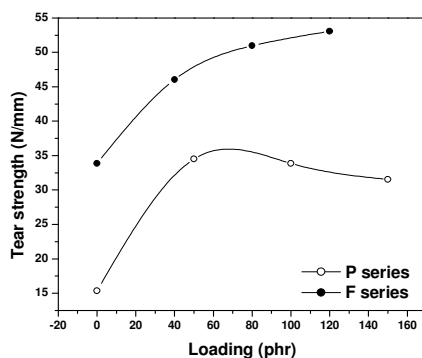


Fig. 4.15 Variation of tear strength with loading

Elongation at break for both sets of CPCs was estimated and is shown in figure 4.16. For the P series, there is a sharp decrease on addition of 50 phr of PANI. Further additions again lower elongation at break, but to a lesser extent. In the case of PANI-N-loaded compounds too, there is a rapid fall in the value initially, which then levels off. This means that both the fillers lack the ability to elongate to high strains. The decrease in elongation at break with filler loading is due to the decrease in the stress bearing capacity of the filler-matrix interface. In the PANI-N CPCs, the total loading of the filler ranges from 100 to 220 phr. Hence, the dilution effect outweighs the reinforcing effect of PANI-N and it shows lower elongation at break values. Tensile strength and elongation are properties that depend on the interfacial phase adhesion. If the adhesion is not perfect, the fissure that causes the rupture can originate in the interfacial region. The absence of interface adhesion makes this region weak and at higher loadings, the sample becomes weaker due to large agglomerates.

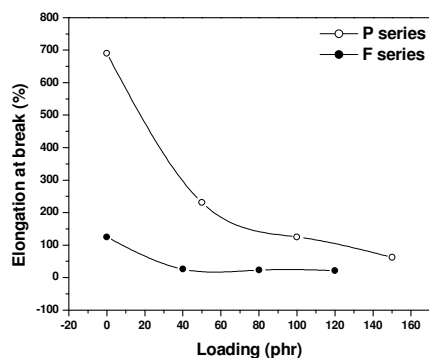


Fig. 4.16 Variation of elongation at break with loading

Variation of modulus at 25 % elongation with loading is plotted in fig. 4.17. It shows a slight increasing trend in the case of P series. This effect is assigned to the rigidity of PANI, acting as a reinforcing filler and changing the viscoelastic behavior of the rubber to a rigid material. Whereas for the F series, it increases sharply at 40 phr PANI-N loading, which then shows a decreasing trend and finally reaches almost the same value as that of the compound without PANI-N as seen in the variation of tensile strength.

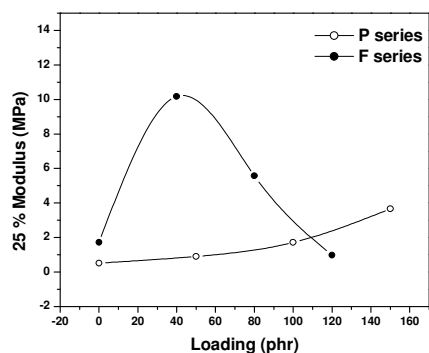


Fig. 4.17 Variation of modulus with loading

### 4.3.5 Morphology

The SEM micrographs of the tensile fracture surfaces of the CPCs are shown in fig. 4.18. In the gum compound (4.18a), minor cracks are seen. The rubber particles are found to peel of leaving flakes on the surface. A change in morphology of the fracture surface from regular to rough is observed on PANI loading. Even though there seems to be some aggregates of PANI particles in the composite with 100 phr PANI (fig. 4.18b) (CPC CP<sub>2</sub>), it is found that PANI has good dispersibility in the CR matrix. The PANI particles link with each other to form conductive chains or network in the matrix. Hence the conductivity is also expected to increase with PANI loading. The 40 phr PANI-N-loaded CPC (4.18c) shows better adhesion between the filler and the matrix resulting in better tensile strength. Detachment of the PANI-N from the fractured surface and the formation of grooves are observed in the micrographs of the composite CF<sub>3</sub> (4.18d). This results in poor tensile strength values for this composite. The increasing fiber-fiber contact with increasing loading, helps in forming a closed network of PANI and PANI-N leading to better conduction. Thus, conductivity increases with PANI-N loading.

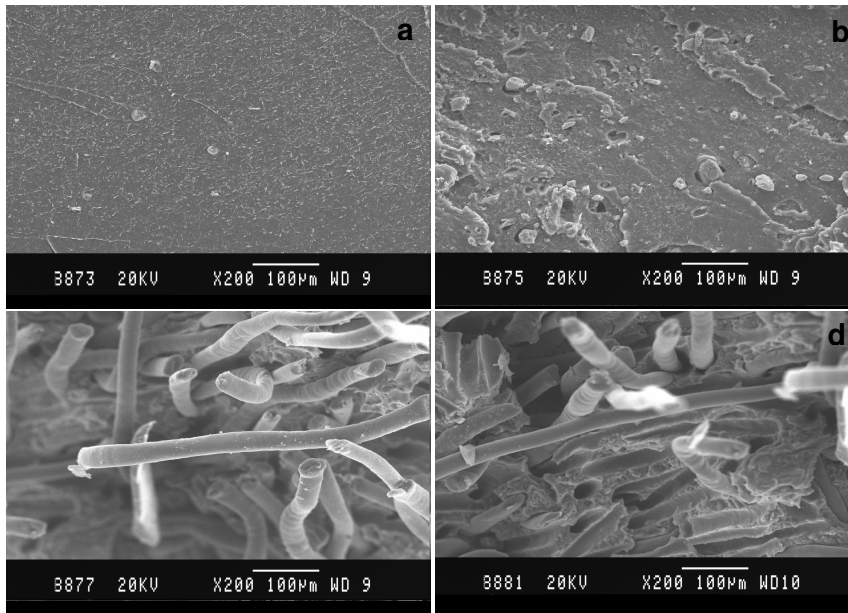


Fig. 4.18 SEM micrographs of (a) CP<sub>0</sub>, (b) CP<sub>2</sub>, (c) CF<sub>1</sub> and (d) CF<sub>3</sub> CPCs

#### 4.3.6 DC electrical conductivity

The room temperature DC electrical conductivity of the CPCs is presented in fig. 4.19. As expected, there is an increase in conductivity of the composites on PANI addition, though the increase is not significant upto 50 phr loading. Afterwards, conductivity increases sharply and reaches percolation at 100 phr loading (CPC CP<sub>2</sub>). Addition of PANI-N decreases the conductivity initially, which then shows a steady increase. A conductivity of  $1.44 \times 10^{-7}$  S/cm is obtained at a loading of 120 phr PANI-N. As discussed earlier, the increasing fiber-fiber contact with increasing loading helps in forming a closed network of PANI and PANI-N leading to better conduction.

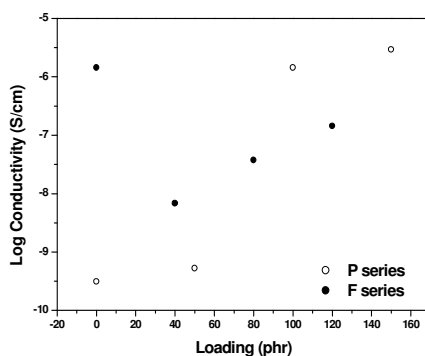


Fig. 4.19 Variation of DC electrical conductivity of the CPCs with loading

#### 4.3.7 Thermal analysis

The TG curves of the PANI-loaded samples can be seen in fig. 4.20 and the data are presented in table 4.3. CPCs with higher contents of PANI present complex thermal decomposition processes and several weight losses are observed, which could be related to the degradation of the elastomer and the conducting polymer. The onset of thermal degradation shifts to higher temperatures with increasing PANI content. The temperature at maximum degradation does not show any regular trend. The weight loss during the degradation decreases with PANI loading pointing to the improved

thermal stability of the CPCs. The temperature at which 50 % weight loss is recorded increases with PANI loading. All these results ascertain that the thermal stability of the CPCs increase steadily with PANI loading.

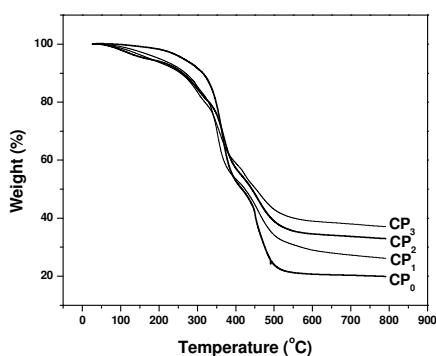


Fig. 4.20 TG curves of CPCs of P series

Table 4.3 Thermal degradation data of the CPCs of P series

	Degradation	CP <sub>0</sub>	CP <sub>1</sub>	CP <sub>2</sub>	CP <sub>3</sub>
Onset temperature (°C)	First	182.5	183.5	180.5	203.7
	Second	304.6	314.7	322.8	320.8
	Third	413.6	405.5	415.6	403.5
Peak degradation temperature (°C)	First	-	295.9	303.1	300.1
	Second	364.4	352.9	369.6	357.5
	Third	451.7	458.8	457.2	424.1
Weight loss (%)	First	7.45	13.03	13.6	14.88
	Second	50.8	58.1	60.3	62.1
	Third	29.5	24.1	20.2	7.1
Temperature at 50 % weight loss (°C)		416.3	424.1	442.1	452.6

Dependence of degradation of the CPCs on PANI loading is better visualized in the DTG curves (fig. 4.21). Pure CR presents its maximum weight losses at 364 °C and 452 °C. The composite CP<sub>1</sub>, with 50 phr PANI shows the same weight loss process,

but at lower temperature. This means that, for this composite, the conducting polymer acts as pro-degrading for the elastomer. Presumably, free radicals formed in the PANI, accelerate the formation of volatile oligomers in the CR chains. On increasing the PANI content, other processes are observed. The weight losses at 364 °C and 452 °C are still observed, but their relative intensities reduce with PANI content. By increasing the PANI content, other weight losses are observed at 303 °C and 424 °C. These can be assigned to the removal of PANI dopant and the chain degradation of PANI.

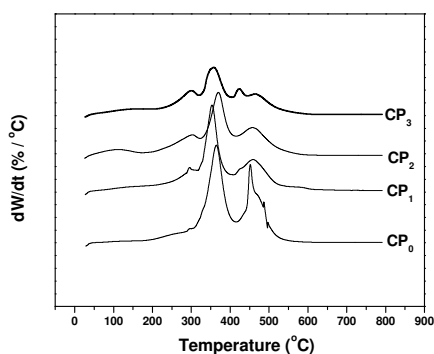


Fig. 4.21 DTG curves of the P series CPCs

Fig. 4.22 presents the thermograms of the PANI-N-loaded composites (F series) and table 4.4 presents the data. Three degradations are seen in the PANI-N composites with peak maximum at 303 °C, 376 °C and 451 °C. The peak degradation temperature shifts to higher values on PANI-N loading pointing to the increased thermal stability of these composites. The PANI-N shows maximum degradation at 451 °C (*chapter 2, section 2.3.3.6*). The intensity of the peak at 369 – 381 °C increases with PANI-N loading as evident from the DTG curves (fig. 4.23). This leads to the possibility that the third degradation with peak maximum at 451 °C is due to the overlapping of the degradations of PANI-N and CR. The presence of the PANI-N in the composite helps in enhancing the thermal stability of the composites.

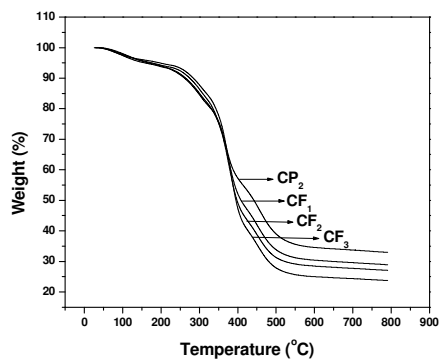


Fig. 4.22 TGA traces of the F series CPCs

Table 4.4 Thermal characteristics of the CPCs of F series

	Degradation	CP <sub>2</sub>	CF <sub>1</sub>	CF <sub>2</sub>	CF <sub>3</sub>
Onset temperature (°C)	First	180.5	314.8	217.9	219.9
	Second	322.8	314.7	313.7	314.7
	Third	415.6	422.7	425.7	427.8
Peak degradation temperature (°C)	First	303.1	301.4	303.2	303.8
	Second	369.6	376.4	377.5	381.5
	Third	457.2	451.7	450.8	451.3
Weight loss (%)	First	13.6	10.6	9.6	8.8
	Second	60.3	35.5	40.8	45.7
	Third	20.2	16.8	14.6	14.7
Temperature at 50 % weight loss (°C)		442.1	408.4	397.9	395.1

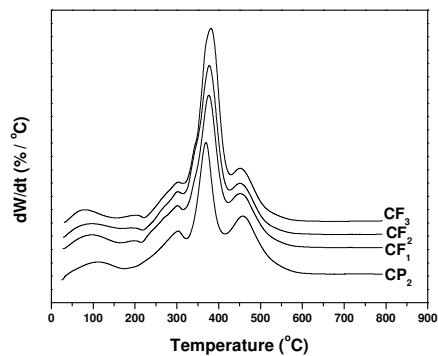


Fig. 4.23 DTG curves of the CPCs of F series

#### 4.3.7.1 Thermal degradation kinetics

The kinetics of the thermal degradation reaction was followed using TGA. The Coats and Redfern (CR) equation (equation (3.22)) for different values of  $n$  were applied for each CPC in the P and F series. Best fit is obtained for  $n = 1$ . Representative plots of CPCs from each series for  $n = 1, 2$  and  $3$  are given in figs. 4.24 and 4.25. The activation energies obtained from the corresponding plots are presented in table 4.5.

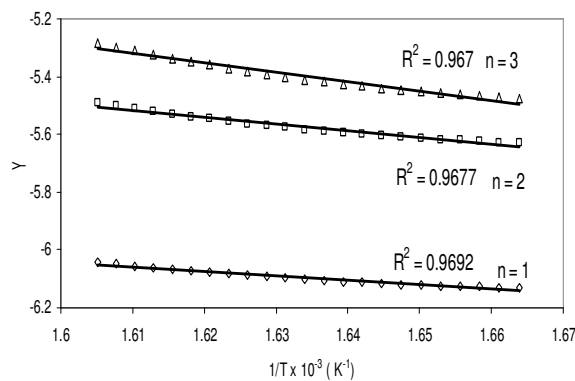


Fig. 4.24 Representative plot of Coats and Redfern equation for the CPC CP<sub>1</sub>



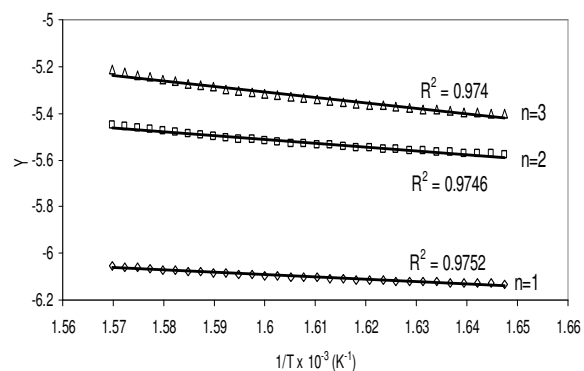


Fig. 4.25 Representative plot of Coats and Redfern equation for the CPC CF<sub>1</sub>

The Freeman and Carroll (FC) method (equation (3.17)) and the Chan and Balke (CB) method (equation (3.19)) were also applied and the corresponding order of reaction and activation energies are given in table 4.5. Representative graphs of the two methods are shown in figs. 4.26 and 4.27.

Table 4.5 Thermal degradation kinetic parameters of the CPCs

CPC	CR equation	FC equation		CB equation
	E <sub>a</sub> (kJ/mol)	n	E <sub>a</sub> (kJ/mol)	E <sub>a</sub> (kJ/mol)
CP <sub>0</sub>	73.00	1.04	132.35	133.8
CP <sub>1</sub>	60.73	0.99	173.54	166.7
CP <sub>2</sub>	54.27	1.04	129.57	132.6
CP <sub>3</sub>	44.34	0.96	118.86	134.7
CF <sub>1</sub>	49.35	1.02	100.09	99.59
CF <sub>2</sub>	48.64	1.00	97.90	96.10
CF <sub>3</sub>	48.64	0.99	143.94	143.43

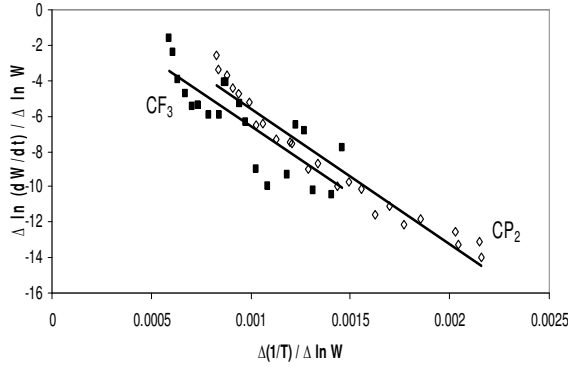


Fig. 4.26 Representative plot of Freeman and Carroll equation for CP<sub>2</sub> and CF<sub>3</sub>

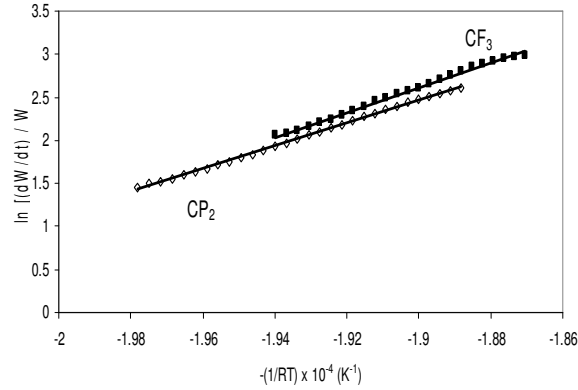


Fig. 4.27 Representative plot of Chan and Balke equation for CP<sub>2</sub> and CF<sub>3</sub>

The estimates of both  $E$  and  $n$  vary amongst the three methods. This variation is caused by several obvious sources of error: the finite difference approximation to the rate will depend on the increment and can be very inaccurate; and the precision of the quantities plotted according to Freeman and Carroll equation can be poor because of the error-propagation effects resulting when two experimentally determined quantities are ratioed [21]- the error in the intercept of *equation (3.17)* and hence in the determined value of  $n$  from this equation is very large because the experimental data points are remote from the intercept. These differential methods in general, tend to produce ‘scattered’ results because of the inherent noise in the  $dW/dt$  term. However, all the three methods point to an order,  $n = 1$ . The method of Chan and Balke (*equation (3.19)*) seems to be more accurate than these two methods. In this

method, a non-linearity in the plot indicates that the reaction deviates from first order kinetics. No such non-linearity is observed in our results and the data conformed to a first-order fit.

#### 4.4 Conclusions

The cure characteristics, cure kinetics, filler dispersion and mechanical properties of Chloroprene rubber-polyaniline-polyaniline coated short Nylon fiber CPCs prepared by mechanical mixing were investigated. Cure rate index and cure rate constants indicate that incorporation of PANI to CR retards the cure reaction slightly whereas addition of PANI-N accelerates the cure reaction. The shear modulus and viscosity of the CPCs is found to increase with filler loading for both series. The cure reaction follows first order kinetics. Higher loadings of the filler causes agglomeration, which is predominant for PANI-loaded composites. The tensile strength, tear strength and modulus of the CPCs increase marginally with PANI loading for the PANI composites. As was the aim of this work, better mechanical properties could be obtained by the addition of fiber. There is a good distribution of PANI particles in the composites. The PANI particles link with each other to form conductive chains or network in the matrix, increasing the conductivity. The percolation limit of the PANI composites is at 100 phr loading. Addition of PANI-N decreases the conductivity initially, but it increases with further additions. There is an enhancement in the thermal stability of the composites on filler addition. The activation energy of the thermal degradation reaction was estimated by various methods and the results show variations due to the different approximations made in the derivations. Degradation reactions followed first order kinetics.

#### References

1. Blow CM, Hepburn C. Rubber technology and manufacture. 2<sup>nd</sup> edition London: Butterworths, 1982.
2. Wazzan AA. Int J Polym Mat 2005;54:783-794.
3. Mathew G, Nah C, Rhee JM, Singh RP. J Elastomers Plast 2006;38:43-63.
4. Fujimoto K, Nishi T, Okamoto T. Int Polym Sci Technol 1981;8:T/30.

5. Mathew G, Singh RP, Nair NR, Thomas S. *J Mater Sci* 2003;38:2469-2481.
6. Lee BL. *Rubber Chem Technol* 1979;52:1019-1029.
7. Costa HM, Visconte LLY, Nunes RCR, Furtado CRG. *Int J Polym Mat* 2004;53:475-479.
8. Wolf S. *Rubber Chem Technol* 1996;69:325-346.
9. Kraus G. *Rubber Chem Technol* 1978;51:297-321.
10. Sobhy MS, El-Nashar DE, Maziad NA. *Egypt J Sol* 2003;26(2):241-257.
11. Westlinning H, Wolf S. *Kautsch Gummi Kustst* 1966;19:470.
12. Wolf S, Meng-Jio Wang. *Rubber Chem Technol* 1992;65:329-342.
13. Freeman ES, Carroll B. *J Phys Chem* 1958; 62:394-397.
14. Chan JH, Balke ST. *Polym Degrad Stab* 1997;57(2):135-149.
15. Coats AW, Redfern JP. *Nature* 1964;201:68-69.
16. Sreeja TD, Kutty SKN. *Polym Plast Technol Eng* 2003;42(2):239-252.
17. da Silva ALN, Rocha MCG, Moraes MAR, Valente CAR, Coutinho FMB. *Polym Test* 2002;21:57-60.
18. Poh BT, Ismail H, Quah EH, Chin PL. *J Appl Polym Sci* 2001;81:47-52.
19. Deghaidy FS. *Egypt J Sol* 2000;23(1):167-177.
20. Faez R, De Paoli M-A. *Eur Polym J* 2001;37(6):1139-1143.
21. Balke ST. In: *Qualitative column liquid chromatography*. Amsterdam: Elsevier, 1984.



*The dielectric properties of PANI, and NR and CR based CPCs were measured in the frequency range 0.1 to 8 MHz and in the temperature range 303 to 393 K. Both NR and CR based CPCs showed Maxwell-Wagner type of polarization. The conduction mechanism in the composites was primarily hopping. CR based composites exhibited better dielectric properties due to its polar nature. At 303 K and 0.1 MHz, a dielectric permittivity as high as 177 was obtained for the composite CP<sub>3</sub>, which was almost double the value obtained for NR-PANI composite. The F series CPC of CR, CF<sub>1</sub> had a permittivity of 70 at the same frequency and temperature. At 303 K, a maximum conductivity of  $6.2 \times 10^{-3}$  S/m at 5 MHz was obtained for CR based CPC, CP<sub>3</sub>. The composite CF<sub>3</sub> of the F series gave a conductivity of  $1.01 \times 10^{-3}$  S/m. The dielectric dispersion could be fitted well with well known empirical equations.*

---

## Chapter 5

### Dielectric properties of conducting elastomer composites

#### 5.1 Introduction

Development of electronic devices working at high operating frequencies, such as fast computers, cellular phones, etc. requires new high-dielectric constant materials that combine good dielectric properties with sufficient mechanical strength and ease of processing. In particular, high dielectric constant materials are required for making embedded capacitors for integrated electronic devices [1, 2]. The unique combination of dielectric and mechanical properties is hard to achieve in a one-component material. Pure polymers are easy to process into mechanically robust components but generally suffer from low dielectric constants [3]. On the other hand, typical high dielectric constant materials, such as ferroelectric ceramics, are brittle and require high-temperature processing, which is often not compatible with current circuits integration technologies [4]. The ideal solution for developing such a one-component material would be designing a high dielectric constant material that is mechanically

robust and processable at ambient temperatures. This has raised a great interest in hybrid materials, such as polymer/ceramic composites and conducting polymer/polymer composites, which combine desired properties of the components.

Polymer/ceramics composites have been of great interest as embedded capacitor material because they combine the processability of polymers with the high dielectric constant of ceramics [5-7]. Some novel nanostructure composites made of epoxy and lead magnesium niobate-lead titanate (PMN-PT)/BaTiO<sub>3</sub> were reported to have very high dielectric constant ( $\epsilon' = 110$ ) [5]. A similar epoxy-based composite with an ultra high dielectric constant ( $\epsilon' = 1000$ ) has been developed by the same group, which was claimed by these researchers to be the highest  $\epsilon'$  value of the polymer based composite ever reported, while no experimental details were disclosed except the volume fraction of ceramics [7]. The high dielectric constant ceramics employed in the polymer composites generally belongs to the categories of niobates, titanates, zirconia (ZrO<sub>2</sub>), tantalum oxide (Ta<sub>2</sub>O<sub>5</sub>) and aluminum oxide (Al<sub>2</sub>O<sub>3</sub>), etc. The adhesion between these ceramics and polymer matrix is poor, especially when ceramics loading is high [8]. Conducting polymer systems constituted by a conducting polymer dispersed inside an insulating polymer matrix have been extensively investigated in the last decades in the electronics industry. The good mechanical properties and intriguing electronic properties and high dielectric constants of these materials indicate that they can be used in many device applications.

Some studies observed that PANI and some PANI/polymer blends are capable of obtaining a high dielectric constant. As a consequence, its conducting composites are very close to applications on a large scale in electromagnetic shielding and microwave absorption [9-12] and many studies are going on the dielectric behavior of PANI and PANI composites. For instance, a dielectric constant  $\geq 10^4$  can be observed in a partially crystalline PANI sample system [13]. An inhomogeneous disorder model was proposed for this system, in which ordered (crystalline) region, described by three-dimensional metallic states, is connected through amorphous region of polymer chains where one-dimensional disorder-induced localization is dominant. High dielectric constant values ranging between 200-1000 have been

reported for a PANI/polyvinyl alcohol (PVA) composite by Dutta and co-workers [14]. The frequency range investigated was 1 kHz - 5 kHz from room temperature to 80 K. This report gave no structural analysis results for the composite, but just stated that the dispersed submicronic PANI particles are suspended in the insulating PVA matrix. They reported that the temperature dependence of DC conductivity followed variable range hopping (VRH) and that the hopping transport occurred between the superlocalised states of polymer. The frequency dependence of conductivity satisfied the  $\omega^s$  law and the AC conduction was reported to be due to correlated barrier hopping (CBH). High dielectric constant PANI/polyurethane (PU) blends were synthesized by using the technique of *in situ* polymerization of aniline in an aqueous dispersion of PU (ISP blends) by Chwang *et al.* [15]. A dielectric constant of  $\sim 1120$  was obtained for the PANI/PU blend containing 17 wt % of PANI, which surpassed the highest value of  $\epsilon'$  ever reported for the high dielectric constant polymer composites. A parallel study was carried out with a similar PANI/PU blend prepared by simple mixing of PANI dispersed solution with an aqueous solution of PU. The totally different microstructures exhibited by these two types of blends could adequately explain their discrete dielectric behavior. Based on the results of morphological study as well as the existence of a percolation threshold for the conductivity of the ISP blends, the enhancement of dielectric constant in the ISP blends was established to be chiefly due to electrode polarization.

Tabellout *et al.* studied the dielectric properties of conducting polymer composite films based on doped and dedoped PANI located in a thin layer in the vicinity of the surface of some insulating polymer matrices like polyamide and poly(ethylene terephthalate), using dielectric relaxation spectroscopy over a wide temperature and frequency range [16]. Several relaxation processes related to the film surface conductivity and influenced by the nature of the polymer matrix were found in these composites. At low temperature, in addition to sub-glass relaxation processes occurring in the polymer matrix and in the non-doped composite as well, three relaxation processes were observed in the doped one related to its conductive properties. In the low frequency region, interfacial polarization relaxations were observed arising due to the layered and clustered structure. At higher frequency,



conductivity relaxation was connected to the conductivity in the PANI clusters. They found that the nature of the polymer matrix, especially matrix crystallinity, influenced the relaxations by frequency shift, change in relaxation strength and activation energy.

The dielectric properties of the styrene-butadiene-styrene (SBS) triblock copolymer matrix loaded with different amounts of PANI in the protonated conducting form and in non-protonated, non-conducting form, emeraldine base, prepared by mechanical mixing, were studied by Leyya and co-workers [17]. They reported that the dielectric constant and loss factor increased with increase in PANI-DBSA concentration. The dielectric loss factor data of SBS and their blends with PANI-DBSA revealed a sharp increase at temperatures above the glass transition because of interfacial polarization and ionic conductivity contributions. These phenomena were important at low frequency measurements. The electrical properties of polyaniline/polyimide blends [18], polyaniline/polychloroprene composite [19], polyaniline/polyvinyl chloride blends [20] were also reported by different authors.

The dielectric behavior of conducting composites depends mainly on the method of preparation, conductivity, molecular structure, particle size and crystal structure. It also depends on external factors such as frequency of the applied voltage, temperature, pressure and humidity [21]. Since the properties of the conducting polymers and CPCs are very much dependent on the microstructure, nature of dopant used, type of matrix and the processing variables, study of dielectric properties of these materials assume significance. Dielectric properties of polymers and polymer composites, like those of other dielectric materials are usually expressed in terms of its resistivity, conductivity and complex permittivity. These quantities are functions of temperature and the type i.e. AC/DC and magnitude of the voltage applied. Frequency and temperature dependence of dielectric properties of the CPCs throw light on the dielectric polarization and on the conduction mechanisms. The frequency and temperature dependence of dielectric properties of PANI, as well as CR and NR based PANI/PANI coated short Nylon fiber composites are presented in this chapter. Different theoretical equations and mixture equations are applied to fit the observed dielectric data of the CPCs.

## **5.2 Dielectric measurements**

### **5.2.1 Method of measurements**

The dielectric constant or permittivity is defined as the ratio of the field strength in vacuum to that in the material for the same distribution of charges. Dielectric constant is dependent on parameters like temperature, orientation, molecular structure of the material and frequency of the applied field. An electrical conductor charged with a quantity of electricity  $q$  at a potential  $V$  is said to have a capacity  $C=q/V$ . The capacity of a sample parallel plate capacitor is given by:

$$C = \epsilon A / d \quad (5.1)$$

where  $A$  is the area of the parallel plates,  $d$  is the separation between the plates and  $\epsilon$  is the ratio of dielectric constant of the medium between the plates to that of free space. When a parallel plate capacitor with a dielectric in between is charged, then the capacitance,  $C$  is given by:

$$C = \epsilon_0 \epsilon_r A / d \quad (5.2)$$

where  $A$  is the area of the sample,  $d$  is the separation between the plates,  $\epsilon_0$  is the permittivity of free space and  $\epsilon_r$  is the dielectric constant of the material between the plates. Dielectric constant of the samples can thus be calculated if the capacitance, area and thickness of the samples are known. Thus, dielectric constant,

$$\epsilon_r = Cd / \epsilon_0 A \quad (5.3)$$

The AC electrical conductivity can be calculated utilizing the dielectric parameters using the formula:

$$\sigma_{AC} = 2\pi f \tan \delta \epsilon_0 \epsilon_r \quad (5.4)$$

where  $f$  is the frequency of the applied field and  $\tan \delta$  is the loss factor. The principle and theory underlying the evaluation of  $\sigma_{AC}$  from dielectric measurements is based on a treatment dealt by Goswamy [22].

### 5.2.2 Cell for the measurements

The schematic design of the cell employed for the electrical measurements is given in fig. 5.1. All the necessary facilities like temperature sensing facility, high vacuum facility, facility for measuring the pressure inside the cell and facility to carry out optical and electrical studies have been incorporated. The cell is made up of mild steel with a cylindrical stem having provisions for fixing various attachments such as electrical connections and vacuum gauges. The cell is connected to a rotary pump to maintain a pressure of  $10^{-2}$  Torr inside the chamber. The inner diameter of the cell is about 18 cm and the length of the cell is 30 cm. The sample holder assembly consists of a mild steel stem of diameter 5 cm with mild steel flange and O-rings. The sample holder is fixed at the bottom of a one-end closed metallic tube to be embedded to the top flange. It consists of two copper disc electrodes. For high temperature measurements, a solderon heater is kept at the back side of the sample holder. An Fe-K thermocouple is placed on the sample to sense the temperature and is controlled by a digital temperature controller.

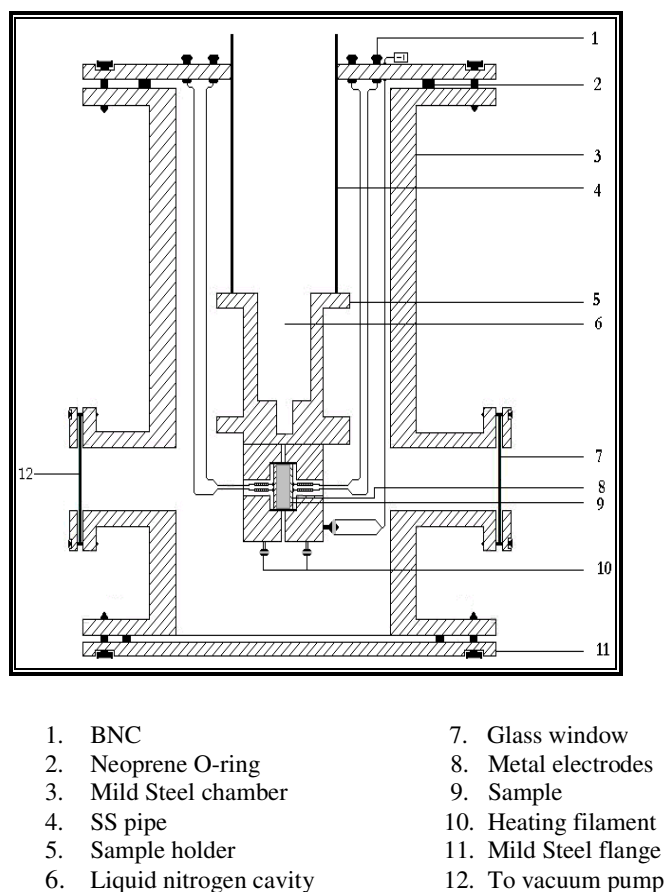


*Fig. 5.1 Schematic of the cell for dielectric and conductivity measurements*

The dielectric properties of the CPCs were studied using the dielectric cell and an impedance analyzer, Hewlett Packard 4192A. The cell was standardized using Teflon pellets and lead. The fringe capacitance was eliminated by employing a procedure suggested by Ramasasthry *et al.* [23]. The samples, in the form of pellets of diameter 12 mm and ~ 2 mm thickness were mounted in between two copper disc electrodes. The capacitance of the samples was measured in the frequency range 0.1 to 8 MHz and in the temperature range 303 to 393 K. The data acquisition was automated by interfacing the impedance analyzer with a computer. For this, a virtual instrumentation package, based on a graphical programme was employed. This package is called LabVIEW (Laboratory Virtual Instrument Engineering

Workbench), a base software package for implementing virtual instrumentation and G programming. LabVIEW is a programming language for data acquisition, analysis, simulation or computer control of instruments and techniques or processes. Appropriate modifications were incorporated in the software so as to enable the data acquisition automatic and visual observation of the graphs on the computer screen. The characteristic feature of this automatic data acquisition is that it is possible to acquire 20,000 data points or more in a matter of 5 to 10 minutes. By using the modified package, the data can be plotted and analyzed. After obtaining capacitance and dielectric loss from the instrument, the LabVIEW software first calculates the dielectric constant and then evaluates the AC conductivity of the samples.

### **5.3 Results and discussion**

#### **5.3.1 Dielectric permittivity**

##### **5.3.1.1 Frequency dependence of pristine PANI**

Fig. 5.2 presents the variation of dielectric permittivity;  $\epsilon'$ , i.e. the real part of complex permittivity, of pristine PANI with frequency. The permittivity decreases with increase in frequency at all temperatures. This is more pronounced at low frequencies. Finally, it reaches a constant value at all temperatures. The decrement in permittivity with increase of frequency reveals that the systems exhibit strong interfacial polarization at low frequencies. As reported by other authors, the strong low frequency dispersion of permittivity is a characteristic of charged carrier systems [24]. This is the normal behavior found in the case of PANI [25]. This kind of behavior can be explained on the basis of Maxwell-Wagner theory for interfacial polarization.

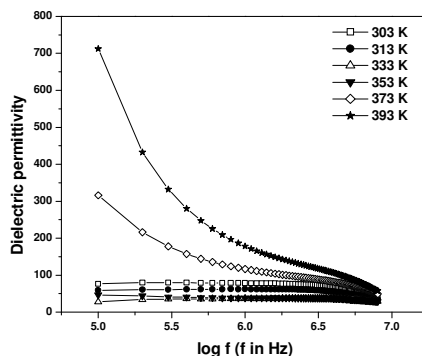


Fig. 5.2 Variation of dielectric permittivity of PANI with frequency

### 5.3.1.2 Temperature dependence of pristine PANI

Fig. 5.3 shows the variation of dielectric permittivity of pristine PANI with temperature at different frequencies. Generally, at any particular frequency, the dielectric permittivity decreases with temperature up to 333 K and then increases with increasing temperature. This behavior is more pronounced at lower frequencies.

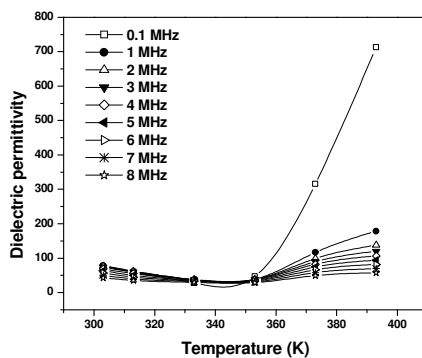


Fig. 5.3 Variation of dielectric permittivity of PANI with temperature

Dielectric behavior of conducting polymers depends on their structure. PANI aggregates are made up of small grains, which are formed from still smaller primary particles. These primary particles have a metallic core surrounded by an amorphous

non-metallic shell. This forms a heterogeneous structure as put forward by Maxwell-Wagner. In the Maxwell-Wagner model, well conducting grains are separated by poorly conducting grain boundaries. The increasing permittivity value with increasing temperature is in accordance with Maxwell-Wagner theory, which means that at higher temperatures, Maxwell-Wagner type of polarization is predominant. It can be seen from fig. 5.3 that at 303 K, PANI has a permittivity of 76 and at 393 K, the value is 712 at 0.1 MHz. The high values of dielectric permittivity at lower frequencies can be accounted for by employing Koop's theory, which is based on Maxwell-Wagner model for heterogeneous double layer dielectric structures [26-28].

### 5.3.1.3 Frequency dependence of dielectric loss factor of pristine PANI

The variation of dielectric loss factor;  $\varepsilon''$ , i.e. the imaginary part of complex permittivity with frequency is presented in fig. 5.4. It decreases with frequency at all temperatures as in the case of dielectric permittivity and reaches a constant value. The decrease is more pronounced at lower frequencies. It is interesting to observe that the dependence of loss factor of PANI with frequency appears as straight lines at lower frequencies, at low temperatures. Beyond 353 K, deviation from straight line is observed.

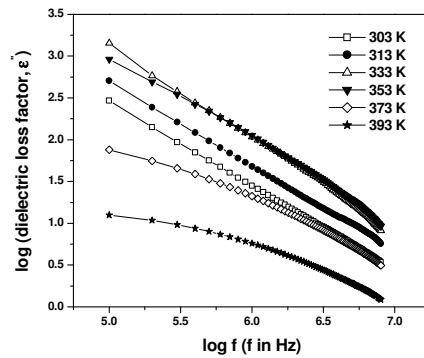


Fig. 5.4 Variation of dielectric loss factor with frequency

The loss factor;  $\epsilon''_{obs}$ , must be regarded as the sum of contributions of three distinct effects as [29]:

$$\epsilon''_{obs} = \epsilon''_{DC} + \epsilon''_{MW} + \epsilon''_D \quad (5.5)$$

where  $\epsilon''_{DC}$  is due to DC conductance,  $\epsilon''_{MW}$  is due to interfacial polarization and  $\epsilon''_D$  is the usual dipole orientation or Debye loss factor.

Different mathematical equations have been developed to distinguish between loss arising from a DC conductivity process and from other sources of different processes. These equations were developed by considering the sample as parallel resistor-capacitor circuit [29-31]. The loss factor due to DC conductance;  $\epsilon''_{DC}$ , is given by the equation [30]:

$$\epsilon''_{DC} = \frac{1.8 \times 10^{12} [G_{spec}]}{f} \quad (5.6)$$

where  $G_{spec}$  is the specific conductivity (S/cm) of the sample. The loss factor due to the Maxwell-Wagner or interfacial polarization;  $\epsilon''_{MW}$ , is given by [32]:

$$\epsilon''_{MW} = \epsilon_{\infty} \left[ 1 + \frac{K}{1 + \omega^2 \tau^2} \right] \quad (5.7)$$

where  $\epsilon_{\infty}$  and  $K$  are calculated considering two different dielectric permittivity of the sample at the interfaces and  $\tau$  is the relaxation time of the interfacial polarization. By expressing the above two equations in logarithm form and making the plot of  $\log \epsilon''_{DC}$  and  $\log \epsilon''_{MW}$  vs. logarithm of frequency, two different curves will be obtained. The  $\log \epsilon''_{DC}$  vs.  $\log f$  represents a straight line and the  $\log \epsilon''_{MW}$  vs.  $\log f$  represents a sigmoidal curve.

Fig. 5.4 shows that at lower frequencies and temperatures, the loss factor;  $\epsilon''_{obs}$ , decrease linearly with increasing frequency. These results suggest that DC conductivity process is more significant than interfacial polarization at these frequencies and temperatures. Similar results have been reported elsewhere [25].



Generally it is believed in dielectric analysis that the high frequency permittivity (dielectric constant) is mainly associated with dipolar relaxation, whereas at lower frequency and higher temperature, the contributions of interfacial polarization (Maxwell-Wagner type of polarization) and DC conductivity become more significant in both  $\epsilon'$  and  $\epsilon''$ . Interfacial polarization arises mainly from the existence of polar and conductive regions dispersed in relatively less polar and insulating matrix. This phenomenon is particularly important in conjugated polymers and may interfere on the relaxation process analysis. Therefore, many authors prefer to describe the dielectric properties of these systems by using the electric modulus formalism [24, 33-36]. The complex electric modulus is derived from the complex permittivity, according to the relationship defined by Macedo *et al.* [37]. The real and imaginary parts of the electric modulus ( $M'$  and  $M''$ ) can be calculated from  $\epsilon'$  and  $\epsilon''$ , as follows [38]:

$$M' = \frac{\epsilon'}{(\epsilon')^2 + (\epsilon'')^2} \quad (5.8)$$

$$M'' = \frac{\epsilon''}{(\epsilon')^2 + (\epsilon'')^2} \quad (5.9)$$

The electric modulus representations of dielectric process give us some idea of relaxation of dipoles that exists in different energy environments, independent of the strong effect of DC conductivity, which often mask the actual dielectric relaxation processes active in these types of systems. Figs. 5.5 and 5.6 show the isothermal and isochronal dependence of the imaginary part of electric modulus,  $M''$  with frequency and temperature, respectively, of pristine PANI. PANI exhibits only one broad peak, both in isothermal and isochronal plots with a narrow distribution of the relaxation, indicating a uniform system and a single relaxation process. The peak shifts to higher frequencies in the isothermal plots with increasing temperature upto 333 K. With increasing frequency (fig. 5.6), the peak height increases initially upto 3 MHz which then decreases.

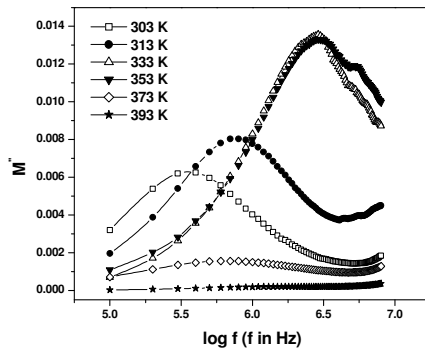


Fig. 5.5 Isothermal plots of the imaginary part of electric modulus of pristine PANI

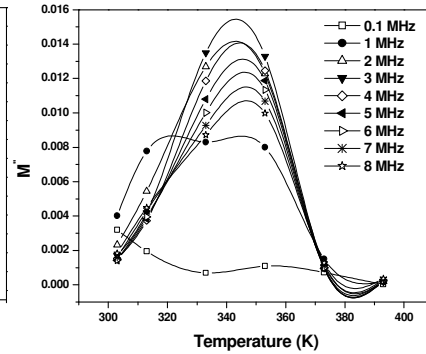


Fig. 5.6 Isochronal plots of the imaginary part of electric modulus of pristine PANI

#### 5.3.1.4 Effect of frequency of NR gum vulcanizate

Variation of dielectric permittivity of NR gum vulcanizate is shown in fig. 5.7. As the frequency increases, dielectric permittivity decreases at all temperatures. The decrease is gradual at lower frequencies and more significant at higher frequencies. The dielectric constant of the unvulcanized NR is reported to be in the range 2.6 to 3.04 [39]. A dielectric constant of 2.3 is obtained at 0.1 MHz in the present study.

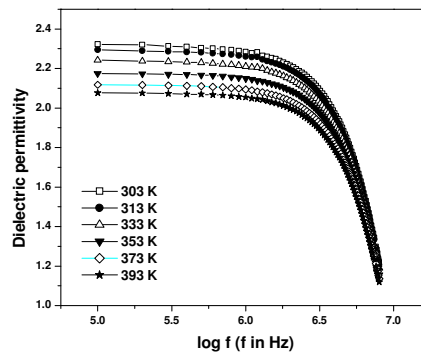


Fig. 5.7 Variation of dielectric permittivity of NR gum vulcanizate with frequency

The dielectric behavior of a polymeric material under the influence of an external electric field depends on the polarization effect that occurs within the material. The total polarization is the sum of the deformational polarization and orientational polarization. At low applied frequencies, both factors contribute to the total polarization. As the frequency is increased, the orientation polarization becomes out of phase with the applied field i.e. the dipolar motion can no longer follow the rapid vibration in the electric field. So the dielectric permittivity of polymeric materials decreases with increase in applied frequency. The polarization and hence the dielectric permittivity must be regarded as a complex quantity,

$$\epsilon^* = \epsilon' - i\epsilon'' \quad (5.10)$$

The complex dielectric permittivity;  $\epsilon^*$ , is given by the Debye equation as follows:

$$\epsilon^* = \epsilon_\infty + \frac{\epsilon_0 - \epsilon_\infty}{1 + i\omega\tau} \quad (5.11)$$

where  $\omega$  is the angular frequency,  $\epsilon_0$  is the static dielectric permittivity and  $\epsilon_\infty$  is the dielectric permittivity at infinite frequency. The real and imaginary components  $\epsilon'$  and  $\epsilon''$  are given by [40-42]:

$$\epsilon' = \epsilon_\infty + \frac{\epsilon_0 - \epsilon_\infty}{1 + (\omega\tau)^2} \quad (5.12)$$

$$\epsilon'' = \frac{(\epsilon_0 - \epsilon_\infty)\omega\tau}{1 + (\omega\tau)^2} \quad (5.13)$$

According to equation (5.12), the dielectric permittivity decreases with increase in frequency, and the decrease is more pronounced at higher frequencies.

#### 5.3.1.5 Effect of temperature of NR gum vulcanizate

The effect of temperature on the dielectric permittivity of NR gum vulcanizate at selected frequencies is presented in fig. 5.8. The dielectric permittivity is found to

decrease with increase in temperature at all frequencies. When the temperature increases, due to thermal expansion of matter, the ratio of the number of molecules to the effective length of the dielectric diminishes and as a result, dielectric permittivity decreases [43, 44]. In other words, as the temperature increases, the polymer density reduces which, in turn causes a decrease in dielectric permittivity.

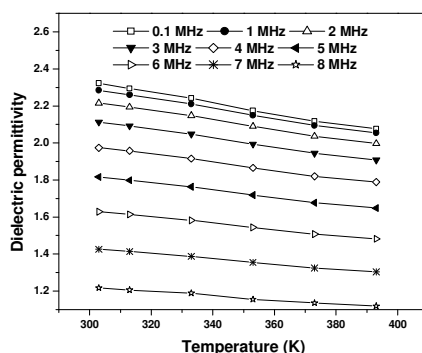


*Fig. 5.8 Variation of dielectric permittivity of NR gum vulcanizate with temperature*

### **5.3.1.6 Frequency dependence of the NR based CPCs**

The dielectric properties of NR/PANI and NR/PANI/PANI-N composites containing different loadings of PANI and PANI-N, respectively, were studied. Effect of frequency on the dielectric permittivity of NR composites NP<sub>2</sub>, NP<sub>3</sub> and NF<sub>3</sub> at some selected temperatures is represented in figures 5.9, 5.10 and 5.11, respectively. The variation pattern shows almost similar behavior as that of PANI. The dielectric permittivity decreases with increasing frequency for all the composites. This indicates that more and more PANI dipoles can no longer keep up with the increasing frequency. This behavior is in accordance with Maxwell-Wagner interfacial polarization. As the frequency of the applied field increases, interfacial polarization decreases and hence dielectric permittivity decreases.

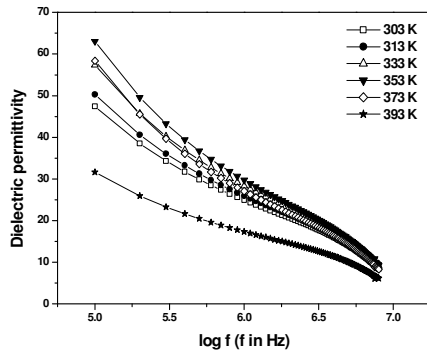


Fig. 5.9 Variation of dielectric permittivity with frequency of NR/PANI CPC NP<sub>2</sub>

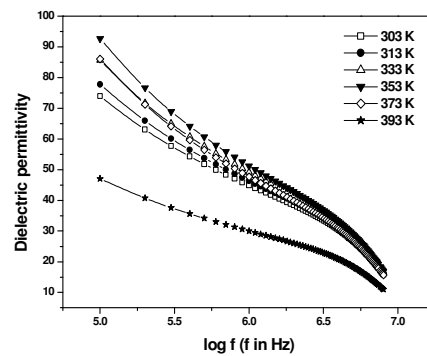


Fig. 5.10 Variation of dielectric permittivity with frequency of NR/PANI CPC NP<sub>3</sub>

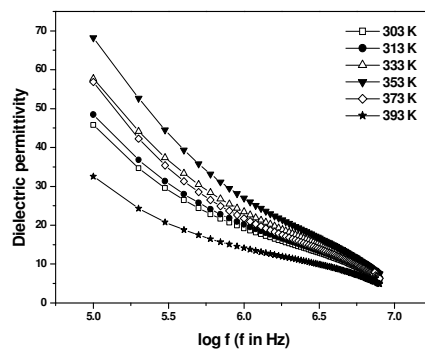


Fig. 5.11 Variation of dielectric permittivity with frequency of NR/PANI/PANI-N CPC NF<sub>3</sub>

The absolute value of the dielectric permittivity of the CPCs is found to be much greater than the gum vulcanizate. Higher values are obtained for composites with higher PANI loading. Dielectric constants as high as 47, 73 and 45 are obtained for NP<sub>2</sub>, NP<sub>3</sub> and NF<sub>3</sub> composites, respectively at 0.1 MHz. Compared to most of the polymers which have  $\epsilon'$  values between 2 and 10 ( $\epsilon' = 10$  for poly(vinylidene fluoride), PVDF;  $\epsilon' = 5.6$  for polyurethane, PU) and many common ceramics such as SiO<sub>2</sub> ( $\epsilon' = 4.0$ ) and Si<sub>3</sub>N<sub>4</sub> ( $\epsilon' = 7.0$ ), the results obtained by NR based CPCs are quite remarkable.

### 5.3.1.7 Temperature dependence of the NR based CPCs

Variation of dielectric permittivity with temperature of NR based composites NP<sub>2</sub>, NP<sub>3</sub> and NF<sub>3</sub> are presented in figures 5.12, 5.13 and 5.14, respectively. In all the three composites, the dielectric permittivity is found to increase initially with temperature up to 353 K, and then decreases. This effect is more pronounced at lower frequencies and nominal at higher frequencies.

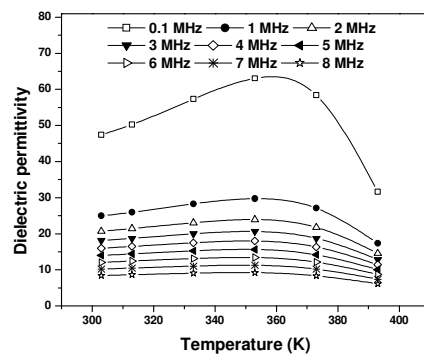


Fig. 5.12 Variation of dielectric permittivity with temperature of 90 phr PANI-loaded NR/PANI CPC (NP<sub>2</sub>)

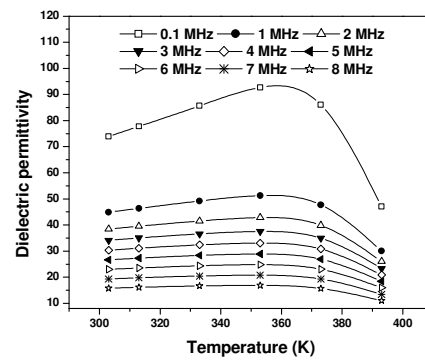


Fig. 5.13 Variation of dielectric permittivity with temperature of 140 phr PANI-loaded NR/PANI CPC (NP<sub>3</sub>)

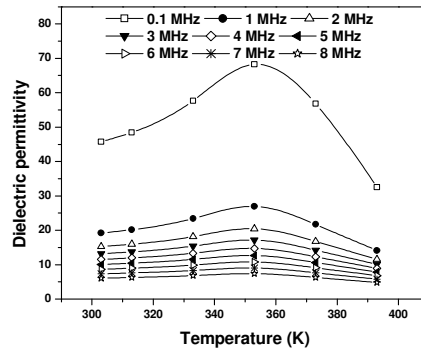
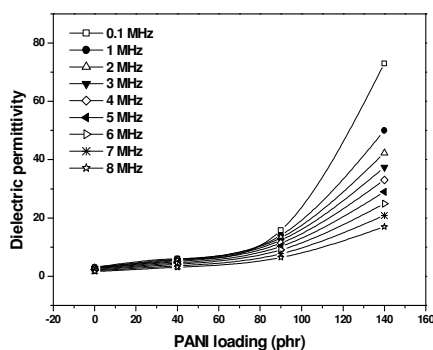


Fig. 5.14 Variation of dielectric permittivity with temperature of 120 phr PANI-N-loaded NR/PANI/PANI-N CPC (NF<sub>3</sub>)

The high dielectric permittivity at low frequencies found at high temperatures may be explained by the presence of permanent dipole moments indicating a small effective charge separation. Such a small separation must be due to asymmetry in the fields experienced by the presence of charged ions. In most cases, the atoms or molecules in the samples cannot orient themselves at low temperature region. When the temperature rises, the orientation of these dipoles is facilitated and this increases the dielectric polarization. At even high temperatures, the chaotic thermal oscillations of molecules are intensified and the degree of orderliness of their orientation is diminished and thus the permittivity passes through a maximum value. In the present case, this maximum temperature is 353 K. At very high temperatures, the dielectric permittivity decreases. This is due to the thermal expansion of the matrix as discussed earlier. At high frequencies, the temperature has little effect on dielectric permittivity [43, 44].

#### ***5.3.1.8 Effect of loading of NR based CPCs***

Variation of dielectric permittivity with the loading of PANI and PANI-N at 303 K was followed and is presented in figs. 5.15 and 5.16, respectively. It is found to increase with increase in PANI and PANI-N content at all frequencies. The increase is more pronounced at lower frequencies. At 0.1 MHz, a maximum value of 73 is obtained at 140 phr PANI loading (CPC NP<sub>3</sub>) and a value of 45 at 120 phr PANI-N loading (CPC NF<sub>3</sub>). Thus, it is clear that the dielectric properties of the NR matrix gets modified by addition of PANI and PANI-N and the required dielectric constant can be achieved by varying their concentration.



*Fig. 5.15 Variation of dielectric permittivity with PANI loading at 303 K*

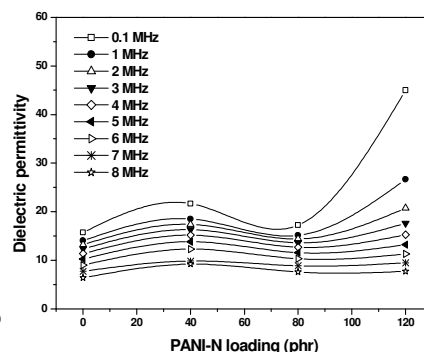


*Fig. 5.16 Variation of dielectric permittivity with PANI-N loading at 303 K*

#### **5.3.1.9 Effect of frequency and temperature of CR gum vulcanizate**

The frequency and temperature dependence of CR gum vulcanizates is shown in figures 5.17 and 5.18, respectively. The dielectric permittivity of CR gum vulcanizate is found to be 5.3 at 0.1 MHz and it decreases with increase in frequency. The decrease is nominal at lower frequencies and significant at higher frequencies. The higher dielectric permittivity of the CR gum vulcanizate compared to NR vulcanizate may be due to its polar nature. It indicates that CR possesses better dielectric characteristics than NR. The decrease in permittivity with frequency is due to the decrease in polarization. At higher frequencies, the orientation polarization lags behind the applied frequency and hence the total polarization and the dielectric permittivity decrease with increase in frequency. Another factor that affects the dielectric permittivity of the polymer is its crystallinity. The dielectric permittivity of a semi crystalline polymer is the average of their respective values in the amorphous and crystalline phases.

The permittivity increases up to 333 K and then decreases with further increase in temperature. The initial increase in dielectric permittivity is more pronounced at higher frequencies. The initial increase at low temperature is due to the increase in



polarity of the C-Cl bond. At very high temperature, the increased polymer chain mobility decreases the density of the matrix and hence the dielectric permittivity decreases.

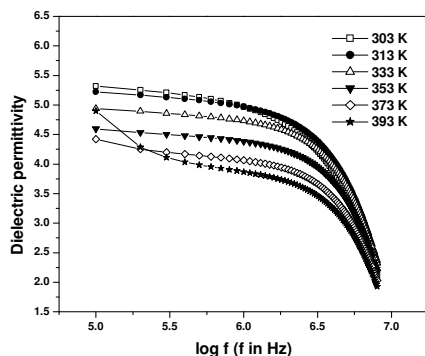


Fig. 5.17 Variation of dielectric permittivity with frequency of CR gum vulcanizate

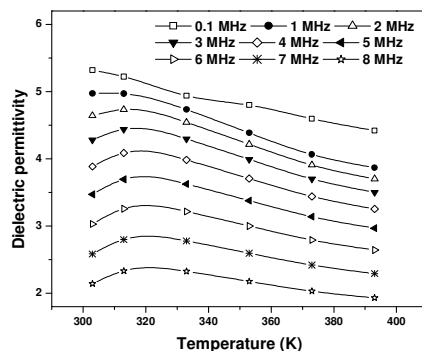
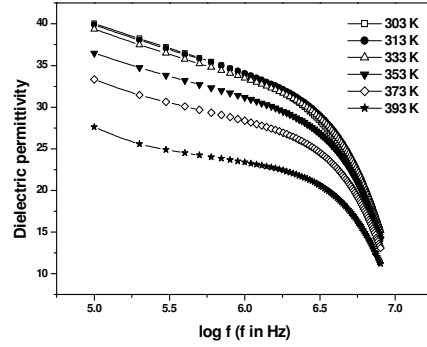


Fig. 5.18 Variation of dielectric permittivity with temperature of CR gum vulcanizate

#### 5.3.1.10 Frequency dependence of CR based CPCs

The dielectric properties of CR/PANI and CR/PANI/PANI-N composites containing different loadings of PANI and PANI-N at different temperatures were measured in the frequency range 0.1-8 MHz. Effect of frequency on the dielectric permittivity of CR/PANI composites at different temperatures with 100 phr (CP<sub>2</sub>) and 150 phr (CP<sub>3</sub>) PANI loadings and 120 phr PANI-N loading (CF<sub>3</sub>) is represented in figures 5.19, 5.20 and 5.21, respectively. Frequency dependence of dielectric permittivity of CR based CPCs shows similar behavior as that of NR based CPCs. In the conducting polymer composites, the conducting particles are covered with the insulating matrix and space charge polarization occurs at the interfaces. This can also be explained by Maxwell-Wagner model. The interfacial polarization can take place at lower frequency. As the frequency is increased, the time required for the interfacial charges to be polarized or for the dipoles to be arranged is delayed, thus the dielectric permittivity decreases with frequency. Dielectric permittivity as high as 177 is obtained for the composite CP<sub>3</sub> at 0.1 MHz and 303 K, which is greater than double the value observed for NR composite. The composite CF<sub>3</sub> gives a permittivity of 30

at 0.1 MHz and 303 K. The  $\epsilon'$  values are comparable to those reported by Chwang *et al.* ( $\epsilon' = 167$ ) for PANI/PU blends at 0.1 MHz [15].



*Fig. 5.19 Effect of frequency on the dielectric permittivity of CR/PANI composite CP<sub>2</sub>*

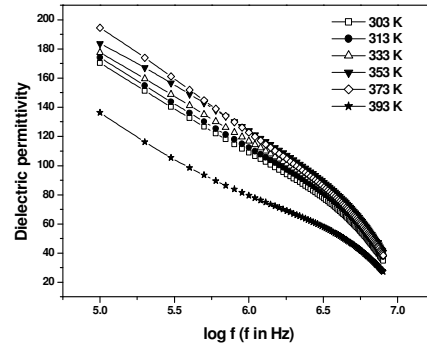


*Fig. 5.20 Effect of frequency on the dielectric permittivity of CR/PANI composite CP<sub>3</sub>*

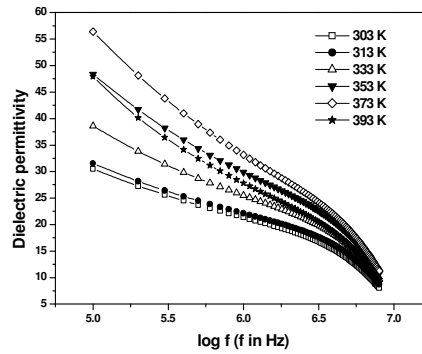


*Fig. 5.21 Effect of frequency on the dielectric permittivity of CR/PANI/PANI-N CPC CF<sub>3</sub>*

#### **5.3.1.11 Temperature dependence of CR based CPCs**

The effect of temperature on the dielectric permittivity of CR based CPCs with different loadings of PANI and PANI-N at some selected frequencies is presented in figs. 5.22, 5.23 and 5.24. The dielectric permittivity of 100 phr PANI-loaded CPC CP<sub>2</sub> increases marginally up to 313 K and then decreases at higher temperatures. For

150 phr PANI-loaded composite  $CP_3$ , the dielectric permittivity marginally increases up to 353 K, and then decreases. For 120 phr PANI-N-loaded CPC  $CF_3$ , the increase is up to 373 K. The initial increase in dielectric permittivity may be due to the increase in interfacial polarization, which is facilitated by the increase in temperature. But, as the temperature increases, the density of the polymer matrix decreases, which outweighs the increase in interfacial polarization. Thus, the dielectric permittivity decreases. Since the volume percentage of the matrix in the CPCs is lesser, this effect is less predominant for the higher loaded composites. Hence, the temperature at which the dielectric permittivity decreases is shifted to higher values.

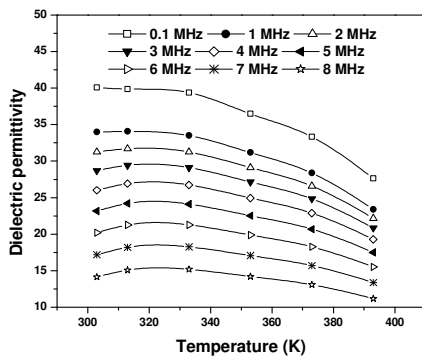


Fig. 5.22 Temperature dependence of dielectric permittivity of CR/PANI composite  $CP_2$

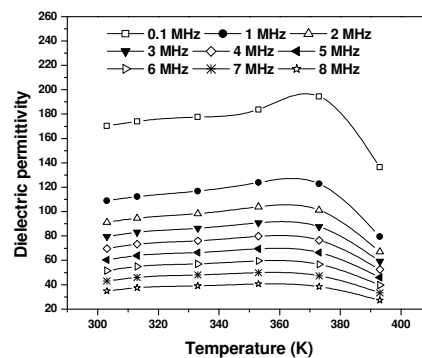


Fig. 5.23 Temperature dependence of dielectric permittivity of CR/PANI composite  $CP_3$

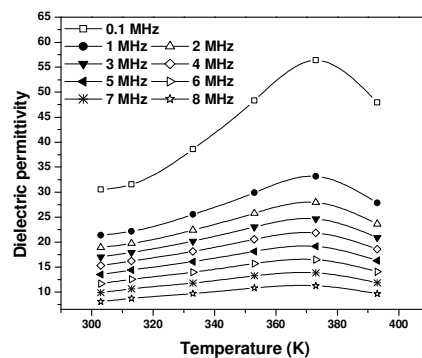


Fig. 5.24 Temperature dependence of dielectric permittivity of CR/PANI/PANI-N CPC  $CF_3$

### 5.3.1.12 Loading dependence of CR based CPCs

Variation of dielectric permittivity with loading of PANI of CR/PANI CPCs and PANI-N loading of CR/PANI/PANI-N CPCs at 303 K are shown in figs. 5.25 and 5.26. The dielectric permittivity increases with increase in weight percentage of PANI at all frequencies for CR/PANI composites. The increase is more rapid at lower frequencies. A dielectric permittivity of 177 is obtained for the composite CP<sub>3</sub> at 0.1 MHz at 303 K. For CR/PANI/PANI-N composites, the dielectric permittivity tends to increase with the introduction of PANI-N loading but it decreases with further loading. A maximum dielectric permittivity value of 70 is obtained for 40 phr PANI-N-loaded composite CF<sub>1</sub>.

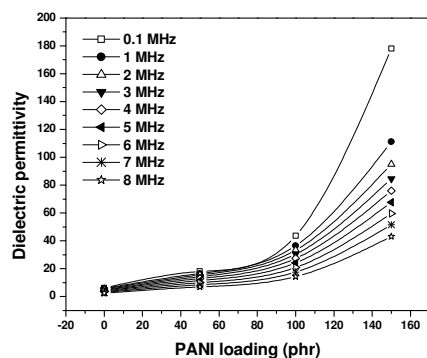


Fig. 5.25 Dielectric permittivity vs. PANI loading of CR/PANI CPCs at 303 K

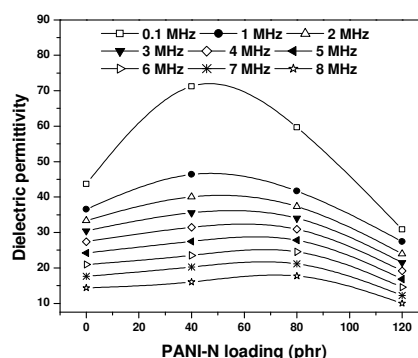


Fig. 5.26 Dielectric permittivity vs. PANI-N loading of CR/PANI/PANI-N CPCs at 303 K

### 5.3.1.13 Tailoring of dielectric permittivity of the CPCs

Efforts were made to correlate the dielectric constant of the composite samples with those of pristine PANI, and gum NR and gum CR. Several mixture equations exist which can be employed to predetermine the dielectric permittivity of the composites correctly [45]. For this, the dielectric has to be considered as a mixture of several components. The observed permittivity of the CPCs can be predicted in terms of the permittivity of the host matrix and that of the conducting polymer by using well-known empirical equations with certain modifications. Among the different mixture

equations, the simplest one is the Lichtenecker equation [43, 46-48], which can be written as:

$$\log \varepsilon_{eff} = (1 - V_f) \log \varepsilon_m + V_f \log \varepsilon_f \quad (5.14)$$

where  $\varepsilon_{eff}$  is the dielectric permittivity of the composite,  $V_f$  is the volume fraction of the filler,  $\varepsilon_m$  and  $\varepsilon_f$  are the dielectric permittivity of the matrix and the filler respectively. The best-known formula for  $\varepsilon_{eff}$  for a binary mixture is associated with Maxwell and Wagner. Maxwell developed the idea of effective conductivity of a binary system consisting of spheres of a particular conductivity distributed uniformly in a continuum of different conductivity. Wagner adopted Maxwell's expression to

the dielectric case and

the equation is as follows [49]:

$$\varepsilon_{eff} = \varepsilon_m \frac{\left[ 1 - 2V_f \frac{(\varepsilon_m - \varepsilon_f)}{(2\varepsilon_m + \varepsilon_f)} \right]}{\left[ 1 + V_f \frac{(\varepsilon_m - \varepsilon_f)}{(2\varepsilon_m + \varepsilon_f)} \right]} \quad (5.15)$$

Another mixture equation of the form [50]:

$$\varepsilon_{eff} = \frac{\varepsilon_m \varepsilon_f}{\varepsilon_m y_2 + \varepsilon_f y_1} \quad (5.16)$$

is also found to be useful in predicting the loading dependence of dielectric permittivity of the CPCs. Here,  $y_1$  and  $y_2$  represent the weight fractions of the matrix and the filler respectively. For CPCs, the equations (5.14), (5.15) and (5.16) did not fit well with the experimental data. Deviations may have occurred due to the formation of agglomerates of PANI particles in the matrix. Hence modified versions of the equations were derived assuming that spherical shaped conducting particles are well distributed in the non-conducting medium. These modified equations are employed to fit the experimental data. For convenience, logarithmic values were calculated and plotted. The modified form of equation (5.14) used to calculate the dielectric permittivity of the CPCs is:

$$\log \epsilon_{eff} = (1 - W_f)(\log \epsilon_m)^k + W_f(\log \epsilon_f)^k \quad (5.14a)$$

Equations (5.15) and (5.16) were also modified with an exponential factor as:

$$\log \epsilon_{eff} = \log \epsilon_m \frac{\left(1 - 2W_f \frac{(\epsilon_m - \epsilon_f)}{(2\epsilon_m + \epsilon_f)}\right)}{\left(1 + W_f \frac{(\epsilon_m - \epsilon_f)}{(2\epsilon_m + \epsilon_f)}\right)} + \log k \quad (5.15a)$$

$$\log \epsilon_{eff} = \log \frac{\epsilon_m \epsilon_f}{\epsilon_m y_2 + \epsilon_f y_1} + \log k \quad (5.16a)$$

$W_f$  is the weight fraction of the filler. Using equations (5.14a), (5.15a) and (5.16a),  $\log \epsilon_{eff}$  was calculated and plotted against  $\log f$ . Figures 5.27 to 5.32 shows the plots along with the plots of the experimentally observed values. It can be seen that, as the loading increases, the calculated permittivity deviates from the observed one at lower frequencies. For NR composites, the value of  $k$  in equation (5.14a) lies in the range 0.6-1.3, in equation (5.15a), in the range 0.38-0.73 and in equation (5.16a) between 0.2-0.7. For CR composites, the values lie between 0.23-0.88. The marginal variation of the empirical constant and the deviation from the observed value at higher loadings may be due to the difference in filler distribution and filler matrix interactions.

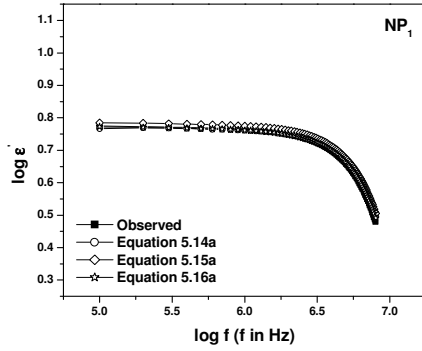


Fig. 5.27  $\log \epsilon'$  vs.  $\log f$  for the observed and calculated permittivity of NR/PANI CPC with 40 phr PANI ( $NP_1$ ) at 303 K

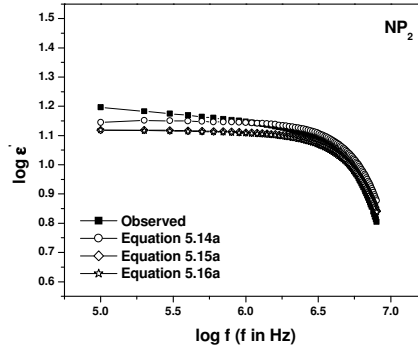


Fig. 5.28  $\log \epsilon'$  vs.  $\log f$  for the observed and calculated permittivity of NR/PANI CPC with 90 phr PANI ( $NP_2$ ) at 303 K

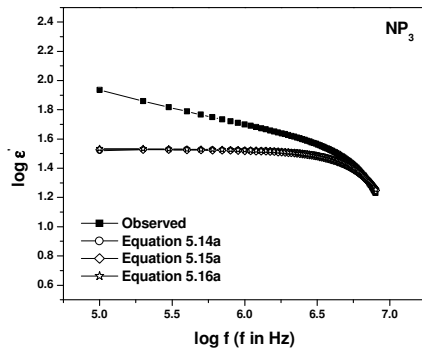


Fig. 5.29  $\log \epsilon'$  vs.  $\log f$  for the observed and calculated permittivity of NR/PANI CPC with 140 phr PANI ( $NP_3$ ) at 303 K

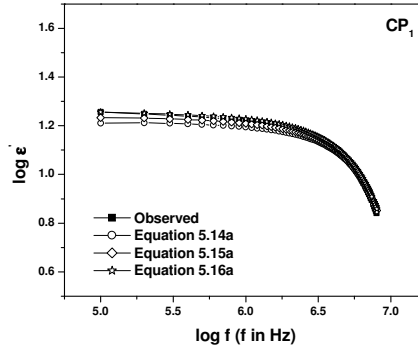


Fig. 5.30  $\log \epsilon'$  vs.  $\log f$  for the observed and calculated permittivity of CR/PANI CPC with 50 phr PANI ( $CP_1$ ) at 303 K

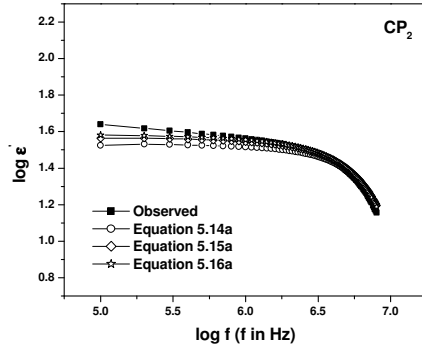


Fig. 5.31  $\log \epsilon'$  vs.  $\log f$  for the observed and calculated permittivity of CR/PANI CPC with 100 phr PANI ( $CP_2$ ) at 303 K

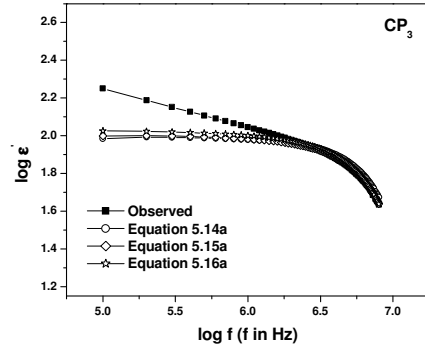


Fig. 5.32  $\log \epsilon'$  vs.  $\log f$  for the observed and calculated permittivity of CR/PANI CPC with 150 phr PANI ( $CP_3$ ) at 303 K

### 5.3.2 AC conductivity

Taking into consideration the wide range of electrical conductivity of dielectric materials, there are many mechanisms of carrier transport to explain the conductivity over the entire range. Many mechanisms have been proposed, reflecting the evolution of the underlying electronic structure in the various regimes. The room temperature DC conductivity value is insufficient to differentiate among these various models. Measurements of the frequency and temperature dependence of the AC conductivity;  $\sigma_{AC}$ , provides important means to distinguish between the various conduction mechanisms. The AC conductivity values of the samples were computed from the dielectric data using equation (5.4).

The current passing through a sample of thickness  $h$  and cross-sectional area  $A$  can be determined from Ohm's law and has two components, the in-phase component  $I \cos \Phi$  and the out-of-phase component  $I \sin \Phi$ . The real and imaginary AC electrical conductivities are given by  $\sigma'_{AC} = (h/A) I \cos \Phi$  and  $\sigma''_{AC} = (h/A) I \sin \Phi$ , respectively. The real part of AC conductivity  $\sigma'_{AC}$  consists of two terms, which can be written as:

$$\sigma'_{ac} = \sigma_1(T) + \sigma_2(\omega) \quad (5.17)$$



$$\sigma_1(T) = \sigma_0 \exp\left(\frac{-E}{kT}\right) \quad (5.18)$$

$$\sigma_2(\omega) = B\omega^n \quad (5.19)$$

The first term;  $\sigma_1(T)$  is related to drift electric charge carriers. It is frequency independent and temperature dependent, and is really the DC electrical conductivity. The second term;  $\sigma_2(\omega)$ , is related to the dielectric relaxation caused by bound charge carriers.  $k$  is the Boltzmann's constant and  $E$  is the activation energy in eV.  $\sigma_0$ ,  $B$  and  $n$  are constants, where  $n$  is temperature dependent and  $\omega$  is the angular frequency of the applied field [51].

### 5.3.2.1 Frequency dependence of pristine PANI

Variation of AC conductivity of pristine PANI with frequency at different temperatures is plotted in fig. 5.33. It shows a nominal increase initially up to 2 MHz, and then decreases at higher frequencies.

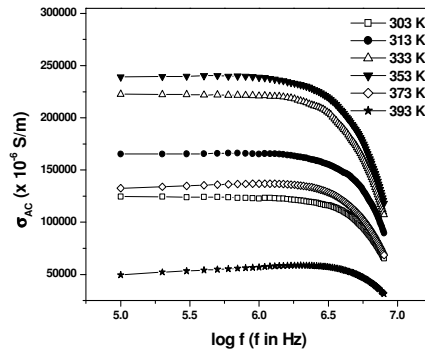


Fig. 5.33 Variation of AC conductivity of PANI with frequency

This can be explained using Maxwell-Wagner two layers or the heterogeneous model. The heterogeneities of the material as described by the Maxwell-Wagner model consist of two layered capacitors i.e. well conducting grains separated by layers of lower conductivity. The low-frequency AC conductivity is related to the

resistive grain boundaries, where as the high frequency AC conductivity is due to the conductive grains. Electrical conductivity in conducting polymers is due to the hopping of charge carriers. As the frequency of the applied field increases, the hopping of the charge carriers also increases thereby increasing the conductivity. Equations (5.4) and (5.18) also explain the increase in  $\sigma_{AC}$  with increase in frequency. At high frequencies, greater than 2 MHz, AC conductivity decreases with increase in frequency as the hopping of charge carriers lags behind the applied frequency.

A plot of  $\log \sigma_{AC}$  against  $\log f$  from 2 MHz to 8 MHz at different temperatures is presented in fig. 5.34. This can be understood on the basis of equation (5.19),  $\sigma(\omega) = B\omega^n$  where  $n$  is an index less than or equal to unity which is used to understand the type of conduction/relaxation mechanism dominant in amorphous materials. The variation of the exponent  $n$  with temperature gives information on the specific mechanism involved in the conduction process. This behavior has been ascribed to the inhomogeneity within the solid caused by the absence of long range crystalline order [52]. Carrier transport via hopping can be identified with this type of dielectric response. Jonscher [53] has proposed that such a dependence on frequency and temperature represents a universal law, applicable to a very wide range of materials irrespective of their chemical and physical structure and the type of dominant charge carriers. The value of  $n$  obtained from the plots lies between -0.36 and -0.46 (table 5.1). This value is in accordance with the theory of hopping conduction in amorphous materials. The observed frequency dependence suggests that the mechanism responsible for AC conduction in pristine PANI is hopping [54].

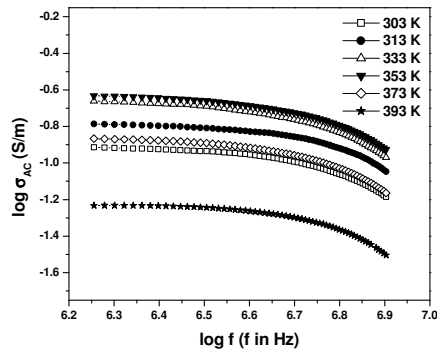


Fig. 5.34 log AC conductivity vs. log frequency of pristine PANI

Table 5.1 *n* values of pristine polyaniline

Temperature (K)	<i>n</i> values
300	-0.40
313	-0.36
333	-0.46
353	-0.43
373	-0.44
393	-0.38

### 5.3.2.2 Temperature dependence of pristine PANI

The effect of temperature on the AC electrical conductivity of pristine PANI is presented in fig. 5.35. As the temperature increases, the conductivity increases, reaches a maximum and then decreases. The increase in conductivity with temperature can be related to the increase in the drift mobility of thermally activated electrons, which increases the hopping conduction [55]. Mott's variable range hopping mechanism (VRH) has been applied with varying degree of success to conducting organic systems [56-58]. Reghu *et al.* have shown the applicability of Mott's VRH model in polyaniline film [59]. The thermal variation of conductivity with time and temperature in polyaniline has also been explained in terms of a

conduction mechanism consisting of electron tunneling between conducting grains embedded in an insulating matrix [60-62]. The thermal degradation was attributed to a decrease of the grain size with a simultaneous broadening of the barriers.

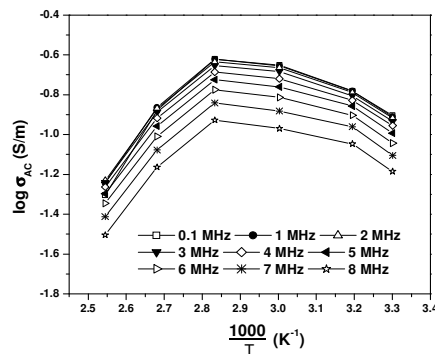


Fig. 5.35 log AC conductivity as a function of  $1000/T$  for pristine PANI

### 5.3.2.3 Effect of frequency of NR based CPCs

Fig. 5.36 presents the frequency dependence of NR gum vulcanizate ( $NP_0$ ) and figs. 5.37 to 5.39 that of the corresponding CPCs at temperatures ranging from 303-393 K. Most of the polymeric materials are insulators and practically no conductivity is observed in unvulcanized elastomers.

The CPCs with different loadings of PANI and PANI-N show similar frequency dependence at different temperatures. With the incorporation of PANI and PANI-N, the AC conductivity increases with increase in frequency and drops after reaching a maximum at higher frequencies. The increase in AC conductivity with increase in frequency is due to the increase in hopping conduction. With increase in PANI loading, the AC conductivity shows an increase.

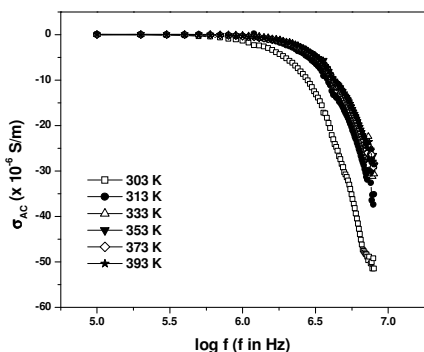


Fig. 5.36 Effect of frequency on the AC conductivity of NR gum vulcanizate

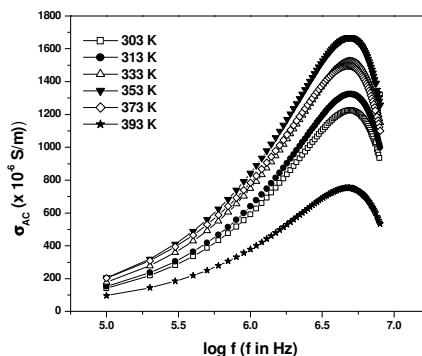


Fig. 5.37 Effect of frequency on the AC conductivity of NR based CPC with 90 phr PANI (NP<sub>2</sub>)

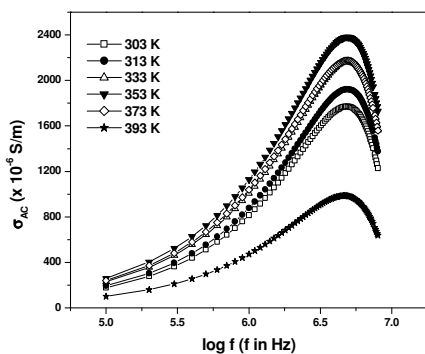


Fig. 5.38 Effect of frequency on the AC conductivity of NR based CPC with 140 phr PANI (NP<sub>3</sub>)

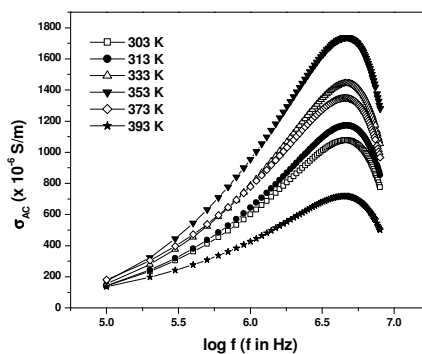


Fig. 5.39 Effect of frequency on the AC conductivity of NR based CPC with 120 phr PANI-N (NF<sub>3</sub>)

#### 5.3.2.4 Effect of temperature of NR based CPCs

Effect of temperature on the AC conductivity at different frequencies for different loadings of PANI and PANI-N are shown in figs. 5.40, 5.41 and 5.42. The AC conductivity increases with temperature up to 353 K and then decreases. The temperature dependence of AC conductivity is similar to that of dielectric permittivity of these samples (figs. 5.12-5.14). The initial increase in conductivity is

due to the increase in hopping conduction, though at very high temperatures, the increased segmental mobility of the polymer may insulate the PANI particles and decrease the conductivity.

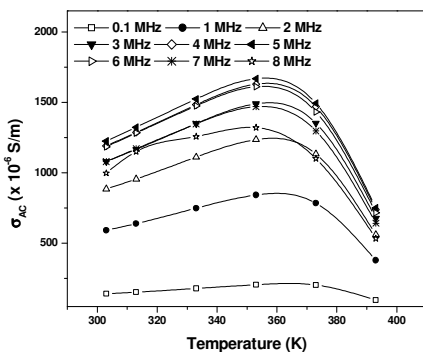


Fig. 5.40 Effect of temperature on the AC conductivity of NR/PANI CPC NP<sub>2</sub>

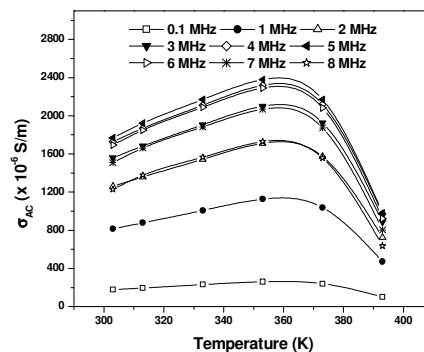


Fig. 5.41 Effect of temperature on the AC conductivity of NR/PANI CPC NP<sub>3</sub>

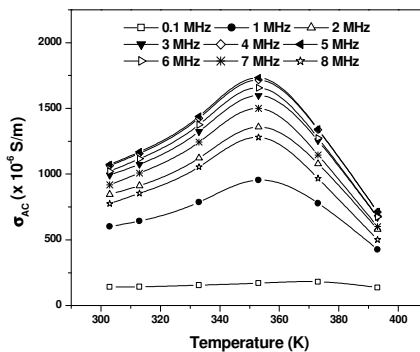


Fig. 5.42 Effect of temperature on the AC conductivity of NR/PANI/PANI-N CPC NF<sub>3</sub>

### 5.3.2.5 Loading dependence of NR based CPCs

The loading dependence of AC conductivity of NR based CPCs at 303 K at different frequencies is presented in figs. 5.43 and 5.44. As expected, it increases with increase in PANI and PANI-N loadings. The maximum conductivity ( $2.13 \times 10^{-3}$  S/m at 5 MHz) is observed for CPC with 140 phr PANI loading (NP<sub>3</sub>). The 120 phr

PANI-N-loaded composite (NF<sub>3</sub>) gives conductivity very close ( $1.68 \times 10^{-3}$  S/m) to the NP<sub>3</sub> composite.

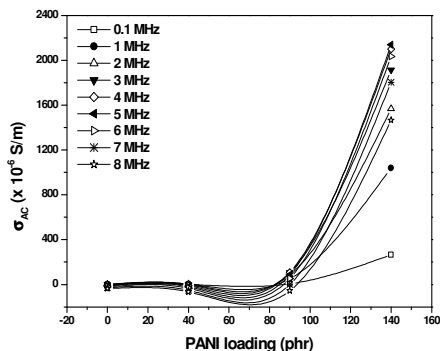


Fig. 5.43 Loading dependence of AC conductivity of NR/PANI CPCs at 303 K

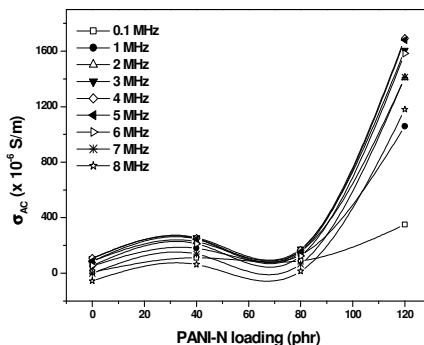


Fig. 5.44 Loading dependence of AC conductivity of NR/PANI/PANI-N CPCs at 303 K

### 5.3.2.6 Frequency dependence of CR based CPCs

Figs. 5.45 to 5.48 present the effect of frequency on the AC conductivity of gum CR, CR/PANI and CR/PANI/PANI-N composites at 303 K. The conductivity of gum vulcanizate is due to the different ingredients added during vulcanization. CR is a semi-crystalline polymer and can be considered as a continuous matrix of an amorphous polymer in which the crystalline regions are randomly distributed. The crystallite centers tend to lower the conductivity. The elastomer can be visualized as a double layer made up of crystalline and non-crystalline centers, analogous to Maxwell-Wagner two layer model. If the conduction is ionic, ion mobility through the crystalline region will be low and in the case of electronic conduction, the crystalline-amorphous interface may act as a trapping region. At lower frequencies, the crystalline/non-crystalline interface may be more active and as the frequency increases, the ions cross over to the interface leading to an increase in conductivity. High frequency limit is reached when the applied frequency is greater than the hopping rate. Further increase in applied frequency leads to decrease in conductivity.

The CPCs with different loading of PANI and PANI-N show the same behavior as that of the gum vulcanizate on frequency variation. The conductivity increases with increase in frequency, reaches a maximum and then decreases at higher frequencies. However, the rate of increase is higher for the CPCs compared to the gum vulcanizate. The AC conductivity is found to be higher for CR based CPCs compared to NR based composites. This might be due to the presence of polar C-Cl bonds in chloroprene rubber. However, the behavior patterns with respect to frequency and temperature are the same for both.

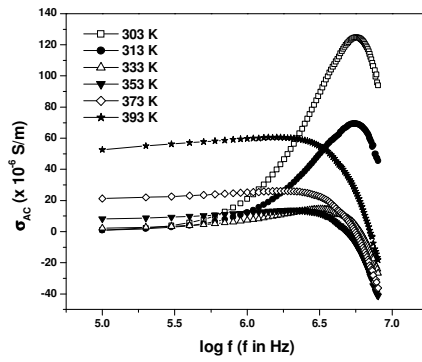


Fig. 5.45 Effect of frequency on the AC conductivity of CR gum vulcanizate

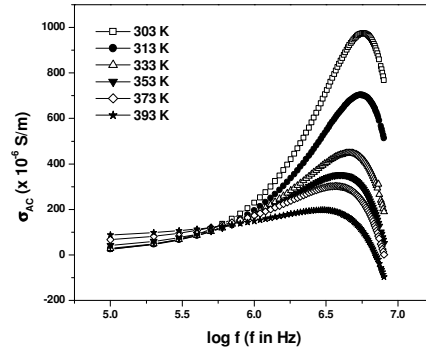


Fig. 5.46 Effect of frequency on the AC conductivity of CR/PANI CPC with 100 phr PANI loading (CP<sub>2</sub>)

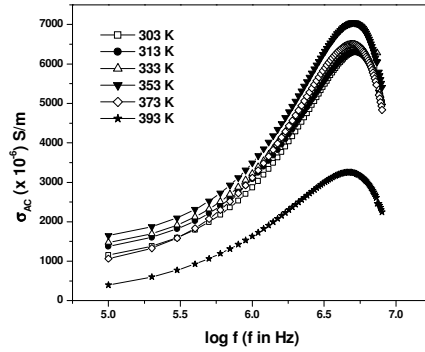


Fig. 5.47 Effect of frequency on the AC conductivity of CR/PANI CPC with 150 phr PANI loading (CP<sub>3</sub>)

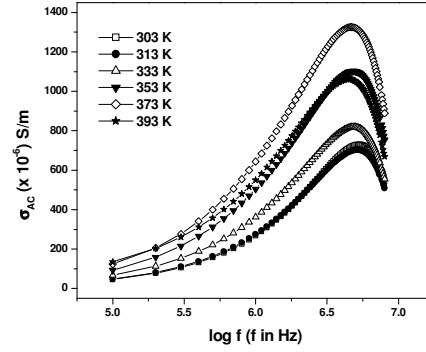


Fig. 5.48 Effect of frequency on the AC conductivity of CR/PANI/PANI-N CPC with 120 phr PANI-N loading (CF<sub>3</sub>)



### 5.3.2.7 Effect of temperature of CR based CPCs

The effect of temperature on AC conductivity of CR based CPCs is plotted in figs. 5.49, 5.50 and 5.51. For the composite  $CP_2$  (fig. 5.49), the conductivity increases nominally with temperature. But as the frequency increases, the conductivity decreases with temperature and reaches a constant value. As the loading is increased to 150 phr (CPC  $CP_3$ ), the conductivity shows an increase up to a temperature of 353 K and then decreases. For the composite  $CF_3$ , the conductivity increases with temperature up to 373 K, and then decreases. The initial increase in conductivity is due to the increase in hopping conduction, though at very high temperatures, the polymer chain mobility increases, which decreases the conductivity. The point beyond which the conductivity decreases is shifted to higher temperature for the CR/PANI-N composite, compared to the CR/PANI composite.

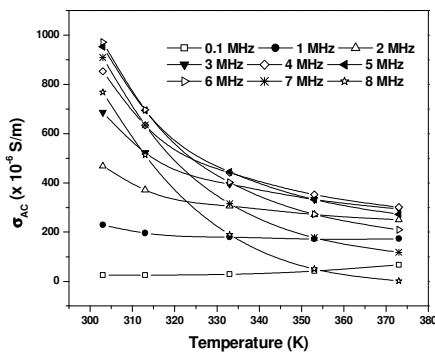


Fig. 5.49 Effect of temperature on the AC conductivity of CR/PANI CPC with 100 phr PANI loading ( $CP_2$ )

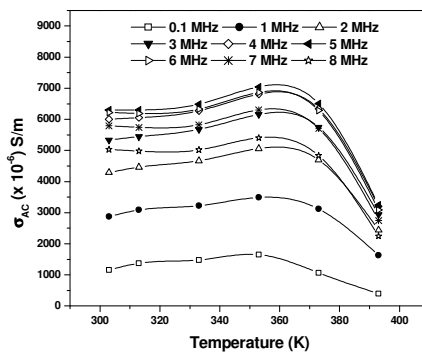


Fig. 5.50 Effect of temperature on the AC conductivity of CR/PANI CPC with 150 phr PANI loading ( $CP_3$ )

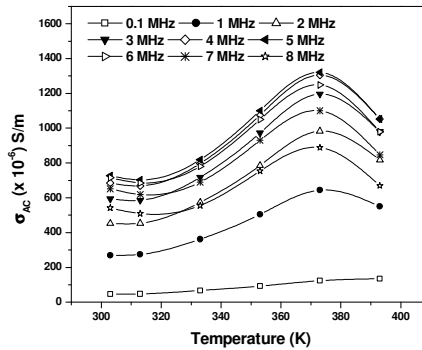


Fig. 5.51 Effect of temperature on the AC conductivity of CR/PANI/PANI-N CPC with 120 phr PANI-N loading ( $CF_3$ )

### 5.3.2.8 Loading dependence of CR based CPCs

The effect of loading of PANI and PANI-N on AC conductivity of CR based CPCs are shown in figs. 5.52 and 5.53.

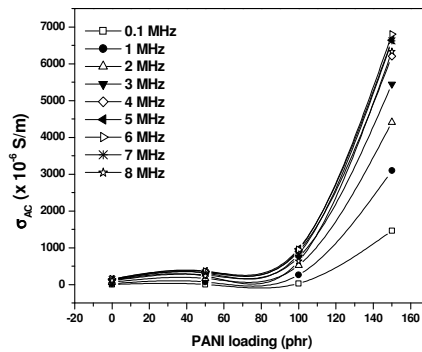


Fig. 5.52 AC conductivity vs. PANI

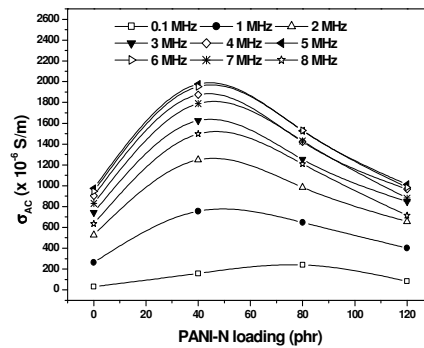


Fig. 5.53 AC conductivity vs. PANI-N

loading for CR/PANI CPCs at 303 K loading for CR/PANI/PANI-N CPCs at 303 K

The conductivity increases with PANI content, as expected. The increment is sharper at higher frequencies. For CR/PANI/PANI-N composites, the AC conductivity tends to increase with PANI-N loading but it decreases at higher loadings as seen in the case of dielectric permittivity (fig. 5.26). The conductivity is slightly higher than that observed for NR/PANI CPCs (section 5.4.5). A maximum conductivity of

$6.20 \times 10^{-3}$  S/m at 5 MHz is recorded for CPC CP<sub>3</sub>. The PANI-N-loaded composite gives a maximum conductivity of  $1.01 \times 10^{-3}$  S/m for 120 phr loading (CPC CF<sub>3</sub>).

## 5.4 Conclusions

The dielectric properties of PANI and the CPCs were measured in the frequency range 0.1 to 8 MHz and in the temperature range 303 to 393 K. The dielectric permittivity of pristine PANI decreases with increase in frequency revealing that PANI exhibit interfacial polarization at low frequencies. At 0.1 MHz, PANI shows a permittivity of 76 at 303 K and at 393 K, the permittivity is as high as 712. At low frequencies and temperatures, the loss factor of pristine PANI decreases linearly with increasing frequency suggesting that DC conductivity process is more significant than interfacial polarization at these frequencies and temperatures. The dielectric permittivity of the CPCs decreases with frequency owing to a decrease in interfacial polarization and increases with PANI and PANI-N loading. With increasing temperature it increases, reaches a maximum and then decreases. At 303 K and 0.1 MHz, a dielectric permittivity as high as 177 is obtained for 150 phr PANI-loaded CR CPC, which is almost double the value obtained for NR composite. The dielectric dispersion could be fitted well with the well known empirical equations. The effective permittivity of the CPCs can be predicted by employing one of these equations.

The conductivity in the CPCs is mainly due to hopping of charge carriers. AC conductivity increases with increase in frequency and temperature and drops after reaching a maximum for the CPCs due to an increase in hopping conduction. In the case of NR based CPCs, a maximum conductivity of  $2.13 \times 10^{-3}$  S/m at 5 MHz is observed for CPC with 140 phr PANI loading. The 120 phr PANI-N-loaded CPC gives conductivity ( $1.68 \times 10^{-3}$  S/m) very close to the 140 phr PANI-loaded CPC at the same frequency. The AC conductivity is found to be higher for CR based CPCs compared to NR based composites. A maximum conductivity of  $6.20 \times 10^{-3}$  S/m at 5 MHz is obtained for CPC with 150 phr PANI loading. The 120 phr PANI-N-loaded composite gives a conductivity of  $1.01 \times 10^{-3}$  S/m at the same frequency. Better dielectric properties are exhibited by CR based composites due to its polar nature.

Thus, the dielectric properties of the rubber matrix can be modified by appropriate loadings of PANI and PANI-N according to the intended operating temperature and frequency.

## References

1. Bhattacharya SK, Tummala RR. J Mater Sci: Mater Electron 2000;11:25-268.
2. Chahal P, Tummala RR, Allen MG, Swaminathan M. IEEE Trans Comput Pack Manuf Technol Part B: Adv Packaging 1998;21(2):184-193.
3. Polymer Handbook. 2<sup>nd</sup> edition, New York: Wiley-Interscience, 1974. p. VIII-7.
4. Dimos D, Lockwood SJ, Schwarz RW, Rodgers MS. IEEE Trans Comput Hybrids Manufact Technol 1994;18:174.
5. Rao Y, Ogitani S, Kohl P, Wong CP. J Appl Polym Sci 2002;83:1084.
6. Rao Y, Yue J, Wong. Active Passive Elec Comp 2002;25:123.
7. Rao Y, Wong CP. Novel ultra-high dielectric constant polymer based composite for embedded capacitor application. In: Proceedings of the Polytronic 2002, the 2<sup>nd</sup> International Conference of Polymers and Adhesive in Microelectronics and Photonics, Zalaegerszeg, Hungary, 23-26 June 2002.
8. Wong CP, Bollampally RS. J Appl Polym Sci 1999;14:3396.
9. Bhattacharya A, De A. Prog Solid State Chem 1996;24(3):141-81.
10. Taka T. Synth Met 1991;41(3):1177-1180.
11. Cottevieille D, Le Mehaute A, Challioui C, Mirebeau P, Demay JN. Synth Met 1999;101(1-3):703-704.
12. Makela T, Sten J, Hujanen A, Isotalo H. Synth Met 1999;101(1-3):707.
13. Joo J, Long SM, Pouget JP, Oh EJ, MacDiarmid AG, Epstein AJ. Phys Rev B 1998;57(16):9567.
14. Dutta P, Biswas S, De SK. Mater Res Bull. 2002;37:193-200.
15. Chwang CP, Liu CD, Huang SW, Chao DY, Lee SN. Synth Met 2004;142:275-281.

16. Tabellout M, Fatyeyeva K, Baillif PY, Bardeau JF, Pud AA. *J Non-Cryst Solids* 2005;351:2835-2841.
17. Leyya ME, Soares BG, Khastgir D. *Polymer* 2002;43:7505-7513.
18. Gyu HM, Soon IMS. *J Appl Polym Sci.* 1999;7(1):2169-2178.
19. Mangali PS, Marcia D, Marianna G, Soares BG. *J Appl Polym Sci* 1999;71:2329-2334.
20. Piellichowski K. *J Therm Anal Calorim* 1998;54:171-175.
21. Mateveeva ES. *Synth Met* 1996;79:127.
22. Goswamy A. *Thin film fundamentals*. New Age International Publishers Ltd., New Delhi, 1996.
23. Ramasasthry C, Syamasundra Rao. *J Phys E Sci Instrum* 1979;12:1023.
24. Lee HT, Liao CS, Chen SA. *Macromol Chem* 1993;194:2443.
25. Soares BG, Leyva ME, Barra GMO, Khastgir D. *Eur Polym J* 2006;42:676-686.
26. Koops CG. *Phys Rev* 1951;83:121-124.
27. Maxwell J. *Electricity and magnetism*. Vol 1, Oxford University Press, London, 1873, section 328.
28. Wagner K. *Ann Phys (Lipzig)* 1913;40:817.
29. Smyth CP. *Dielectric behavior and structure*. New York: McGraw-Hill Book Company Inc., 1955, p. 191.
30. McCrum NG, Read BE, Williams G. *Anelastic and dielectric effects in polymeric solids*. New York: John Wiley & Sons; 1967, p. 211.
31. Riande E, Calleja RD. *Electrical properties of polymers*. Munich: Hanser Publishers; 1987, p. 34.
32. Ku CC, Liepins D. *Electrical properties of polymers*. Munich: Hanser Publishers; 1987, p. 34.
33. Matveeva ES. *Synth Met* 1996;79:127.
34. Calleja RD, Matveeva Es, Parkhutik VP. *J Non-Cryst Solids* 1995;180:260.
35. Lee HT, Chuang KR, Chen SA, Wei PK, Hsu JH, Fann W. *Macromolecules* 1995;28:7645.
36. Han MG, Im SS. *J Appl Polym Sci* 2001;82:2760.
37. Macedo PB, Moynihan CT, Bose R. *Phys Chem Glasses* 1972;13:171.

38. Ram MK, Annapoorni S, Pandey SS, Malhotra BD. *Polymer* 1998;39:3399.
39. Malini KA, PhD Thesis, Department of Physics, Cochin University of Science and Technology, Cochin, India, 2001.
40. Jeffery AM, Damon DH. *IEEE Transactions on Dielectrics and Electrical Insulation* 1995;2:394.
41. Kenneth S, Cole, Cole RH. *J Chem Phy* 1941;9:341.
42. El-Lawidy AMY. *Egypt J Solids* 2005;28:97.
43. Tareev B. *Physics of dielectrics*. Mir Publishers, Moscow, 1979.
44. Karasz FE. *Dielectric properties of polymers*. Plenum Press, New York, 1972.
45. Chulhan K, Choi HD, Moon TJ, Kim WS, Kim KY. *J Mater Sci* 1995;30:3567-3570.
46. Lichtenecker K. *Phys Z* 1908;10:1005.
47. Choi HD, Shim HW, Cho KY, Lee HJ, Park CS, Yoon HG. *J Appl Polym Sci* 1999;72:75.
48. Achour ME, Malhi MEL, Miane JL, Carmona F, Lahjomri J *App Polym Sci* 1999;73:969.
49. Wagner KW. *Arch Electrochem* 1914;2:371.
50. George M. PhD Thesis, Department of Physics, Cochin University of Science and Technology, Cochin, India, 2004.
51. Ahmed MA, El Hiti MA, El Nimr MK, Amer MA. *J Magn Mater* 1996;152:391.
52. Mott NF, Davis EA. *Electronic processes in non-crystalline materials*. Clarendon Press, Oxford, 1971.
53. Jonscher AK. *Thin Solid Films* 1976;36:1.
54. Tauc J. *Optical properties of solids*. Ables A, North Holland, Amsterdam, 1970, p. 277.
55. Hiti MA. *J Phys D Appl Phys* 1996;29:501.
56. Singh R, Tandon RP, Singh GS, Chandra S. *Philos Mag B* 1992;66:285.
57. Singh R, Narula AK, Tandon RP, Mansingh A, Chandra S. *J App Phys* 1996;79:1476.

- 58. Punka E, Rubner MF, Hettinger JD, Brooks JS, Hannahs ST. Phys Rev B 1991;43:9076.
- 59. Reghu M, Cao Y, Moses D, Heeger AJ. Phys Rev B 1993;47:1758.
- 60. Sixou B, Mermilliod N, Travers JP. Phys Rev B 1996;53:4509.
- 61. Sixou B, Travers JP, Nicolau YF. Synth Met 1997;84:703.
- 62. Sakkapoulos S, Vitoratos E, Dalas E. Synth Met 1998;92:63.

*The measurement of dielectric parameters at microwave frequencies is a good means of understanding the mechanism of polarization of polymeric materials. The polarization is a function of frequency and temperature apart from material characteristics. Hence, an in-depth study of the microwave characteristics of a material assumes significance. The dielectric properties at microwave frequencies of the prepared CPCs were measured in the X (7-13 GHz) and S (2-4 GHz) band frequencies using the cavity perturbation technique. The important properties like dielectric permittivity, loss tangent, conductivity, and dielectric heating coefficient were evaluated. The electromagnetic interference shielding efficiency of the composites in the X band frequencies were also studied.*

---

## Chapter 6

### Microwave characteristics of conducting elastomer composites

#### 6.1 Introduction

An electromagnetic wave will undergo a combination of reflection, absorption and transmission when it encounters an absorbing material [1]. The exact behavior of the electromagnetic wave at the surface and in the bulk material critically depends on the dielectric and magnetic properties of the material. The complex permeability ( $\mu' - j\mu''$ ) and permittivity ( $\epsilon' - j\epsilon''$ ) of the constituent material of the microwave absorber determine the reflection and attenuation characteristics of the test material [2-5]. The complex permittivity ( $\epsilon' - j\epsilon''$ ), in the case of dielectric absorber, is an important parameter, which determines the absorption properties of the composite. These absorbers being resonant type, sample thickness is also an important parameter. Excessive loading of particulates in the matrix causes heavy cracks in the samples, as the matrix molecules are unable to bind the filler together, while low loading of fillers in the same matrix reduces absorption properties. By controlling the composition, fill factor and thickness, the performance of these absorbers can be optimized.



An EMI shield can be made up by attaching an absorbing layer on a metallic plate. The impedance of this layer ( $Z_{in}$ ), normalized by the impedance of free space is given by [5]:

$$Z_{in} = \frac{Z_i}{Z_0} = \left\{ \frac{\mu^*}{\epsilon^*} \right\}^{1/2} \tanh \left[ j \frac{2\pi}{c} (\mu^* \epsilon^*)^{1/2} f d \right] \quad (6.1)$$

where  $Z_i$  and  $Z_0$  are the impedance of absorber and that of free space, respectively,  $\mu^*$  and  $\epsilon^*$  are relative permeability and permittivity of the medium,  $c$  is the velocity of light in free space,  $f$  is the frequency of the microwave in free space and  $d$  is the thickness of the absorber. A perfect impedance match,  $Z_i = Z_0$  allows electromagnetic waves to propagate from the free space to the inside of the absorber without any reflection. Variations in matching of the two impedances give rise to reflections at the surface of the absorber. The process of absorption of microwaves within the material occurs as a result of various interactive processes of magnetization and polarization. This requires the imaginary parts of complex permeability and permittivity to be high. It is evident from equation (6.1) that the absorption depends on the thickness of the absorber. However, minimum sample thickness for maximum absorption also depends upon the permeability and permittivity of the material [6-8]. The shielding effectiveness (SE) is usually expressed by the attenuation experienced by the wave interacting with the shield itself. In turn, they are usually related by the reflection loss, which is a measure of the amount of electromagnetic wave reflected. The reflection loss;  $RL$ , is related to  $Z_{in}$  as follows:

$$RL = -20 \log \left( \frac{Z_{in} - 1}{Z_{in} + 1} \right) \quad (6.2)$$

Thus, lower the reflection loss, better is the shielding effectiveness, since a lesser amount of incident wave is reflected [9]. Generally, the thickness of the absorber is optimally reduced for maximum absorption. High conductivity and dielectric constant of materials contribute to high EMI shielding efficiency [10, 11]. These criteria can be achieved by fabricating CPCs, which can be molded into any desired shape and thickness.

## 6.2 Measurement of microwave properties by cavity perturbation technique

Different methods including transmission line coaxial method, free space propagation, cavity resonance and cavity perturbation techniques are generally used for microwave measurements. Among these, the cavity perturbation technique has been extensively employed for studying the dielectric properties of materials at microwave frequencies [12, 13]. In the cavity perturbation technique, generally rectangular or cylindrical wave-guide resonators are employed. When a dielectric material is introduced into a cavity resonator at the position of maximum electric field, the resonant frequencies of the cavity are perturbed. The contribution of magnetic field for the perturbation is minimum at this position. So, from the measurement of the perturbation due to the sample, the dielectric parameters can be determined. The microwave characteristics of the prepared CPCs were studied using Agilent Performance Network Analyzer E8362 B. The measurements were done in X (8-12 GHz) and S (2-4 GHz) band frequencies at room temperature.

### 6.2.1 Design of rectangular wave-guide cavities

The cavity resonators are constructed from brass or copper wave-guides. The inner walls of each cavity are silvered to reduce the wall losses. Both the resonators are of transmission type, since power is coupled into/out through separate irises. The design details of X and S band rectangular wave-guides used in the measurements are given in table 6.1.

Table 6.1 Design parameters of X and S band wave-guide resonators

Dimensions of the cavity (cm)	X band	S band
Length	14.1	34.5
Breadth	2.3	7.2
Height	1	3.4

The photographs of the X and S band wave-guide cavity resonators are shown in figs. 6.1 and 6.2, respectively. The network analyzer is shown in fig. 6.3.



*Fig. 6.1 The X band wave-guide cavity resonator*



*Fig. 6.2 The S band wave-guide cavity resonator*



*Fig. 6.3 Setup for the measurement of microwave properties*

### 6.2.2 Theory of microwave characterization

When a dielectric material is introduced into a cavity resonator at the position of maximum electric field, the contribution of magnetic field for the perturbation is minimum. The field perturbation is given by Kupfer *et al.* [14] as:

$$-\frac{d\Omega}{\Omega} \approx \frac{(\epsilon^* - 1) \int_{V_s} E \cdot E_0^* dV}{2 \int_{V_c} |E_0|^2 dV} \quad (6.3)$$

where  $d\Omega$  is the complex frequency shift,  $V_c$  and  $V_s$  are the volumes of the cavity and the sample, respectively.  $E$  and  $E_0$  are the perturbed and unperturbed fields in the cavity, and  $\epsilon^*$  is the relative complex permittivity of the sample material.  $\epsilon^* = \epsilon' - j\epsilon''$  where  $\epsilon'$  is the real part of the complex permittivity and  $\epsilon''$  is the imaginary part of the complex permittivity. Complex frequency shift is related to the quality factor,  $Q$  as:

$$\frac{d\Omega}{\Omega} \approx \frac{d\omega}{\omega} + \frac{j}{2} \left[ \frac{1}{Q_s} - \frac{1}{Q_0} \right] \quad (6.4)$$

$Q_s$  and  $Q_0$  are the quality factors of cavity with and without sample. Quality factor,  $Q$ , is given by  $Q = f/\Delta f$  where  $f$  is the resonant frequency and  $\Delta f$  is the corresponding 3 dB bandwidth. For small samples, we assume that  $E = E_0$  and for the dominant TE<sub>10p</sub> mode in a rectangular wave-guide,

$$E_0 = E_{0\max} \sin\left(\frac{\pi x}{a}\right) \sin\left(\frac{\pi p z}{d}\right), p = 1, 2, 3, \dots \quad (6.5)$$

$E_{0\max}$  is the peak value of  $E_0$ ,  $a$  is the broader dimension and  $d$  is the length of the wave-guide cavity resonator. From equations (6.3)-(6.4), the real and imaginary parts of the relative complex permittivity are given by

$$\epsilon' = 1 + \frac{f_0 - f_s}{2f_s} \left( \frac{V_c}{V_s} \right) \quad (6.6)$$

$$\epsilon'' = \frac{V_c}{4V_s} \left( \frac{Q_0 - Q_s}{Q_0 Q_s} \right) \quad (6.7)$$

The real part of the complex permittivity;  $\epsilon'$ , is generally known as the dielectric constant/dielectric permittivity and the imaginary part;  $\epsilon''$ , is related to the dielectric loss of the material. The dielectric constant represents the amount of dipole alignment, both induced and permanent, and the dielectric loss represents the energy required to align dipoles or move ions.

The loss tangent is given by:

$$\tan \delta = \frac{\sigma + \omega \epsilon''}{\omega \epsilon'} \quad (6.8)$$

Here,  $(\sigma + \omega \epsilon'')$  is the effective conductivity of the medium. When the conductivity;  $\sigma$ , due to free charge is negligibly small (good dielectric), the effective conductivity is due to electric polarization and is reduced to:

$$\sigma_e = \omega \epsilon'' = 2\pi f \epsilon_0 \epsilon'' \quad (6.9)$$

The efficiency of heating is usually compared by means of a comparison coefficient;  $J$ , which is defined as [15, 16]:

$$J = \frac{1}{\epsilon \tan \delta} \quad (6.10)$$

The absorption of electromagnetic waves when it passes through the medium is given by the absorption coefficient;  $\alpha_f$ , defined as [17]:

$$\alpha_f = \frac{\epsilon'' f}{nc} \quad (6.11)$$

where  $n = \epsilon'^*$  and  $c$  is the velocity of light.

Skin depth or penetration depth is the effective distance of penetration of an electromagnetic wave into the material, given as [18]:

$$\delta_f = \frac{1}{\alpha_f} \quad (6.12)$$

The quality factor;  $Q_0$ , of the cavity and resonance frequency;  $f_0$ , in the unperturbed conditions were measured. The samples in the form of thin rectangular rods, the length of which equals the height of the cavity, so that both the ends of the specimen are in contact with the cavity walls, were used. The samples were inserted into the cavity through a slot and positioned at the maximum electric field. The resonance frequency;  $f_s$ , and loaded quality factor;  $Q_s$ , of the samples were measured. Permittivity values were then calculated using the equations (6.6) and (6.7) [19, 20]. The procedure was repeated for all the available resonant frequencies.

### **6.3 Results and discussion**

#### **6.3.1 Permittivity measurements**

The dielectric permittivities of the CPCs were determined in the X and S band frequencies. From the measured parameters, the dielectric loss tangent, heating coefficient, conductivity and skin depth were calculated.

##### **6.3.1.1 Dielectric permittivity of NR based CPCs**

Figs. 6.4 and 6.5 show the frequency dependence of the real part of permittivity of PANI filled NR composites in X and S bands, respectively. In the X band, dielectric permittivity shows insignificant variation with frequency at low loadings; but increases with increase in frequency at higher loadings. In the S band, it remains constant over the whole frequency range studied. The dielectric properties of the CPCs arise mainly due to the interfacial polarization along with some contributions from intrinsic electric dipole polarization. Polyaniline, protonated with HCl, possess permanent electric dipoles. Therefore, orientation or dipolar polarization, which depends on the frequency of the applied field, is expected to contribute to the dielectric permittivity. Some contribution from atomic polarization may be expected,

but electronic polarization is completely ruled out since it occurs in the optical frequency range. Further, the prepared composites are a heterogeneous mixture of conducting PANI separated by highly resistive rubber matrix. The dielectric permittivity of such a heterogeneous composite also arises due to the interfacial polarization [19].

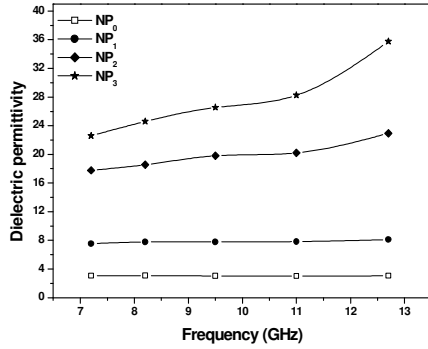


Fig. 6.4 Dielectric permittivity of NR/PANI CPCs in the X band

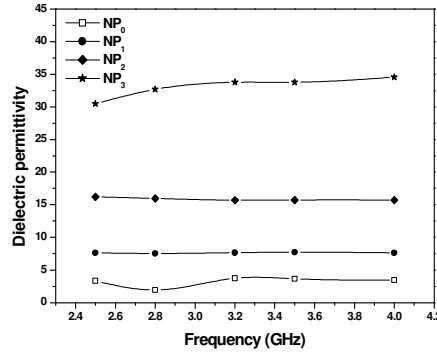


Fig. 6.5 Dielectric permittivity of NR/PANI CPCs in the S band

According to Koops, the dielectric permittivity is inversely proportional to the square root of resistivity [21]. The DC and AC conductivities of the NR based CPCs increase with loading and frequency (*see figs 3.16 and 5.37-5.39*). Therefore, the permittivity increases with frequency, especially at higher loadings. A dielectric permittivity of 35 is obtained for 140 phr PANI-loaded NR CPC NP<sub>3</sub> at 12.7 GHz. For a PANI/NR semi interpenetrating network (SIPN) from natural rubber latex, John *et al.* have reported a permittivity of  $\sim 20$  at a NR:PANI proportion of 2:1 [22].

Figs. 6.6 and 6.7 present the variation of dielectric permittivity of NR/PANI/PANI-N CPCs with frequency in X and S bands. The dielectric permittivity increases with frequency in the X band and the variation is insignificant in the S band, as observed in the case of NR/PANI composites.

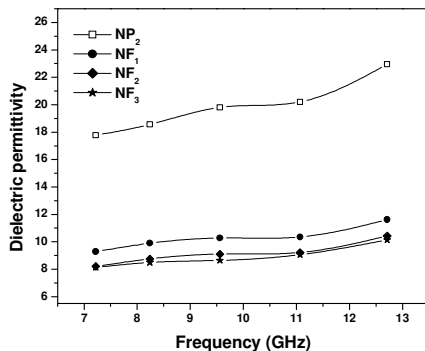


Fig. 6.6 Dielectric permittivity of NR/PANI/PANI-N CPCs in the X band

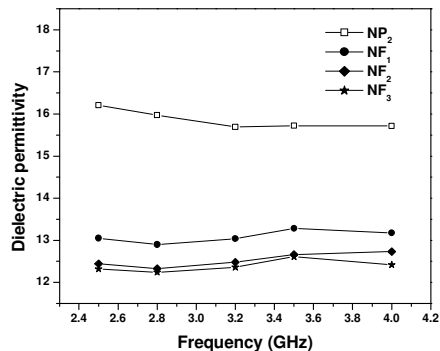


Fig. 6.7 Dielectric permittivity of NR/PANI/PANI-N CPCs in the S band

Figs. 6.8 and 6.9 present the loading dependence of dielectric permittivity of NR/PANI CPCs in X and S bands, respectively. Dielectric permittivity depends on the volume fraction of the conducting filler incorporated and hence increases with increase in PANI content. The higher value of permittivity at higher loaded composites may be attributed to the higher conductivity values of these samples.

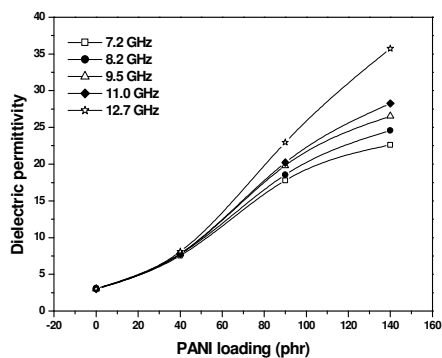


Fig. 6.8 Dielectric permittivity vs. loading of NR/PANI CPCs in the X band

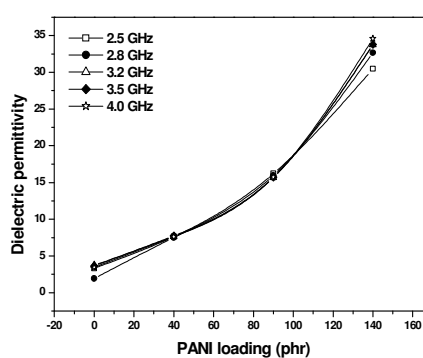


Fig. 6.9 Dielectric permittivity vs. loading of NR/PANI CPCs in the S band

The variation of dielectric permittivity with loading of PANI-N for the NR/PANI/PANI-N composites in the X and S bands are given in figs. 6.10 and 6.11, respectively. In both bands, it decreases with increase in PANI-N loading. The DC electrical conductivity decreases with PANI-N loading and increases only at very



high loadings in the case of NR/PANI/PANI-N CPCs (see fig. 3.16 of chapter 3). The decrease in dielectric permittivity can be assigned to the lesser conductivity of these composites. At 12.7 GHz, the 40 phr PANI-N-loaded CPC NF<sub>1</sub> shows the highest permittivity value of 11.6.

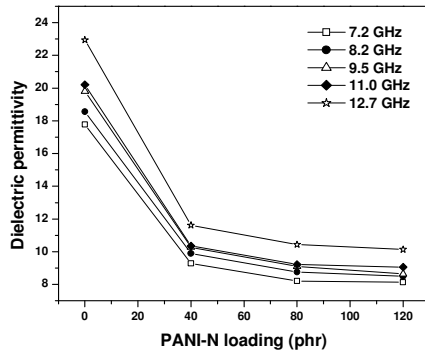


Fig. 6.10 Dielectric permittivity vs. loading of NR/PANI/PANI-N CPCs in the X band

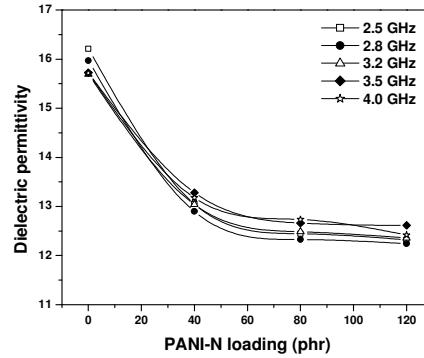


Fig. 6.11 Dielectric permittivity vs. loading of NR/PANI/PANI-N CPCs in the S band

### 6.3.1.2 Loss tangent of NR based CPCs

Loss tangent is the tangent of the angle  $\delta$  between the vector for the amplitude of the total current and that for the amplitude of charging current [15]. Figs. 6.12 and 6.13 show the frequency dependence of  $\tan \delta$  of the NR/PANI CPCs in X and S band frequencies, respectively, and figs. 6.14 and 6.15 present the variation of loss tangent with frequency of the NR/PANI/PANI-N composites in the X and S bands, respectively. Loss tangent of all the CPCs show similar behavior. It is found to increase with frequency in both bands, for both NR/PANI CPCs and NR/PANI/PANI-N CPCs. The dielectric loss at S band is due to the free charge motion within the material [23, 24]. The variation in loss tangent with frequency is a function of relaxation process and its origin is due to the local motion of polar groups. At lower frequencies, the dipoles synchronize their orientation with the field. As the frequency is increased, the inertia of the molecule and the binding forces become dominant and this is the basis for high dielectric loss at higher frequencies. The NR gum compound offers a very low permittivity ( $\epsilon' \sim 3$ ) and a very low loss

tangent ( $\tan \delta = 0.008$ ). This indicates that the dielectric properties and microwave absorption of the CPCs depend largely on the filler used i.e. PANI and PANI-N.

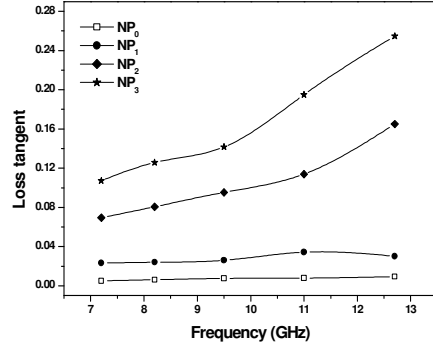


Fig. 6.12 Loss tangent of NR/PANI CPCs at X band frequencies

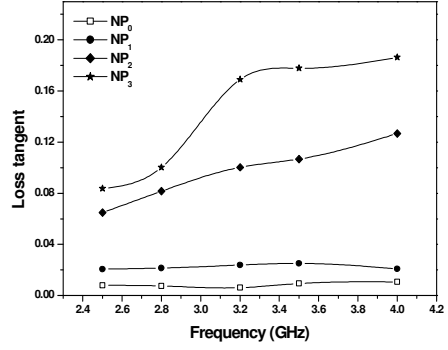


Fig. 6.13 Loss tangent of NR/PANI CPCs at S band frequencies

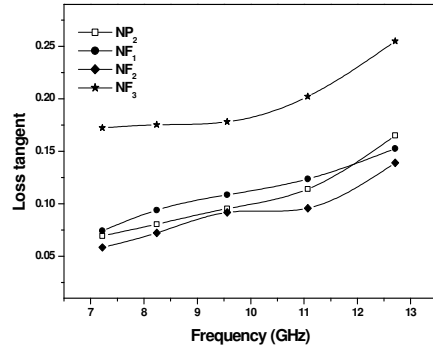


Fig. 6.14 Loss tangent vs. frequency of the NR/PANI/PANI-N CPCs in the X band

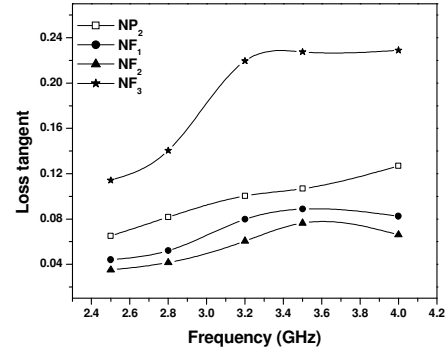


Fig. 6.15 Loss tangent vs. frequency of the NR/PANI/PANI-N CPCs in the S band

The loading dependence of loss tangent of NR/PANI composites in X and S bands are given in figs. 6.16 and 6.17, respectively. As the PANI loading increase, the loss tangent is also found to increase continuously. Figs. 6.18 and 6.19 show the loading dependence of loss tangent for the NR/PANI/PANI-N CPCs in X and S bands,

respectively. It shows the same behavior as in the case of dielectric permittivity in both bands.

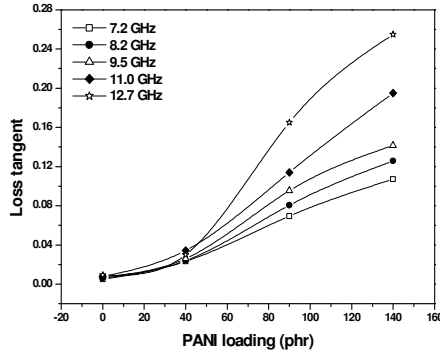


Fig. 6.16 Loading dependence of loss tangent of NR/PANI CPCs at X band frequencies

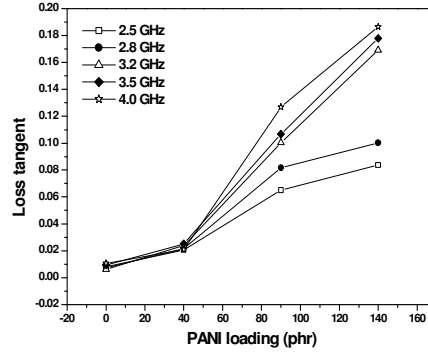


Fig. 6.17 Loading dependence of loss tangent of NR/PANI CPCs at S band frequencies

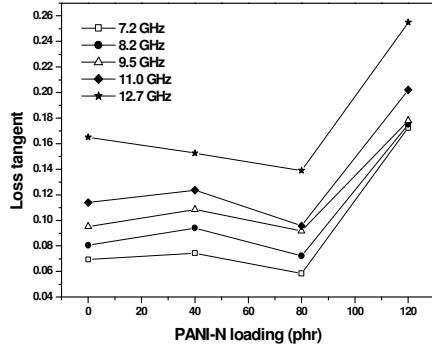


Fig. 6.18 Loading dependence of loss tangent of NR/PANI/PANI-N CPCs in the X band

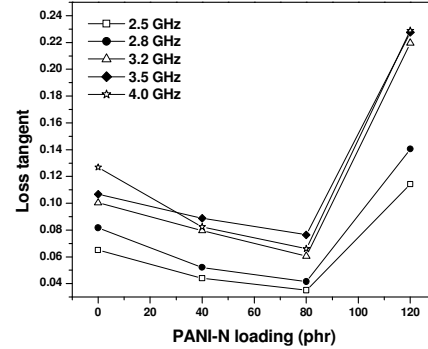


Fig. 6.19 Loading dependence of loss tangent of NR/PANI/PANI-N CPCs in the S band

### 6.3.1.3 Heating Coefficient of NR based CPCs

The heating coefficient;  $J$ , of microwave absorbing materials can be calculated using equation (6.10). The heat developed is proportional to both frequency and the product of  $\epsilon'$  and  $\tan \delta$ . A higher  $J$  value implies that the material is a poor choice for high frequency dielectric heating purposes. The heat generated in the material comes

from the tangent loss, but that loss may not come entirely from the relaxation loss. Rather, conductivity of the material may also contribute to  $\tan \delta$  [15].

The frequency and loading dependence of  $J$  of the NR based CPCs of P series at X band frequencies are presented in figs. 6.20 to 6.23. It decreases with increasing frequency and PANI loading. Lower the heating coefficient, better is the microwave attenuation. Hence, as the loading increases, microwave attenuation of the CPCs increases. For the F series composites, it decreases with increase in frequency, and increases with PANI-N loading, reaches a maximum and then decreases. Heating coefficient as low as 0.11 is obtained at 12.7 GHz for the CPC NP<sub>3</sub>. The lowest  $J$  value recorded for F series CPCs is 0.38 at 12.7 GHz for the composite NF<sub>3</sub>.

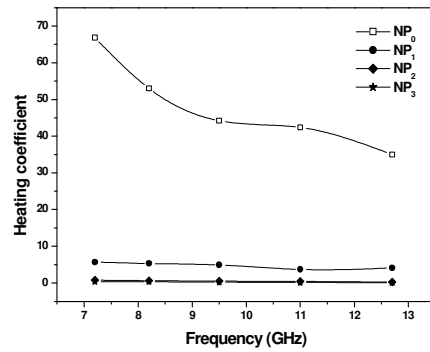


Fig. 6.20 Heating coefficient vs. frequency of NR/PANI CPCs in the X band

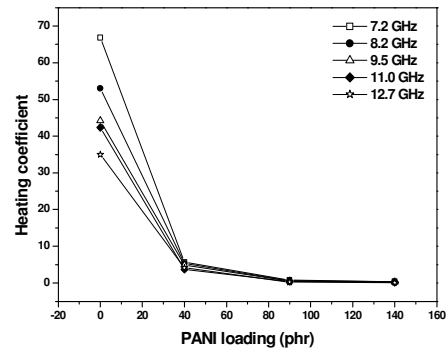


Fig. 6.21 Heating coefficient vs. loading of NR/PANI CPCs in the X band

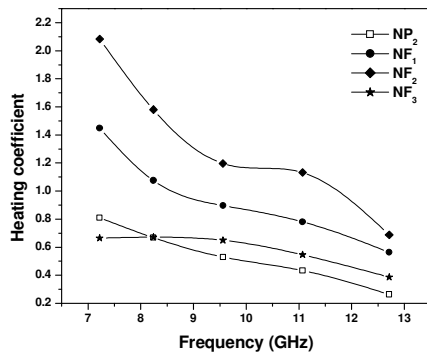


Fig. 6.22 Heating coefficient vs. frequency of NR/PANI/PANI-N CPCs in the X band

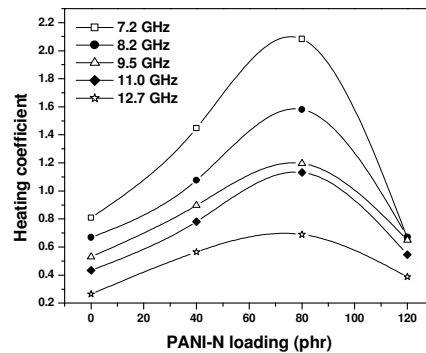


Fig. 6.23 Heating coefficient vs. loading of NR/PANI/PANI-N CPCs in the X band

#### 6.3.1.4 Conductivity, absorption coefficient and skin depth of NR based CPCs

The microwave conductivity and absorption coefficients are direct functions of dielectric loss according to equations (6.9) and (6.11). Hence, the variation of conductivity and absorption coefficients of the CPCs show the same variation pattern as that of the dielectric loss factor. Both these factors increase with frequency. As the absorption coefficient is derived from the complex permittivity and is a measure of propagation and absorption of electromagnetic waves when it passes through the medium, the dielectric materials can be classified in terms of this parameter indicating transparency of waves passing through it [17]. As the skin depth, also called penetration depth, is basically the effective distance of penetration of an electromagnetic wave into the material [18], it can be applied to a conductor carrying high frequency signals. The self-inductance of the conductor effectively limits the conduction of the signal to its outer shell and the shell's thickness is the skin depth, which decreases with increase in frequency. The highest values of conductivity and absorption coefficient and the lowest value of skin depth for the NR/PANI CPCs are recorded at 12.7 GHz for NP<sub>3</sub>. In the case of NR/PANI/PANI-N composites, the best values are recorded at 12.7 GHz for the CPC NF<sub>3</sub>. Table 6.2 shows the best values of these parameters recorded for both the P and F series composites of NR.

Table 6.2 Dielectric properties of NR based CPCs at 12.7 GHz

CPC	Conductivity (S/m)	Absorption coefficient (m <sup>-1</sup> )	Skin depth (m)
NP <sub>3</sub>	6.27	32.01	0.001
NF <sub>3</sub>	1.79	32.27	0.003

### 6.3.1.5 Dielectric permittivity of CR based CPCs

Figs. 6.24 and 6.25 show the frequency dependence of CR/PANI and CR/PANI/PANI-N composites in the X band and figs. 6.26 and 6.27 presents the corresponding loading dependence. All the plots show the same pattern as seen in NR based CPCs. But better dielectric properties are exhibited by CR based CPCs. The 150 phr PANI-loaded CR/PANI composite CP<sub>3</sub> gives a dielectric permittivity of 96 at 12.7 GHz whereas, the 140 phr PANI-loaded NR/PANI CPC NP<sub>3</sub> has a permittivity of only 35. At 12.7 GHz, the 40 phr PANI-N-loaded CR based CPC CF<sub>1</sub> has a permittivity of 23.6 whereas, at the same frequency, the 40 phr PANI-N-loaded NR based CPC NF<sub>1</sub> has a permittivity of 11.6.

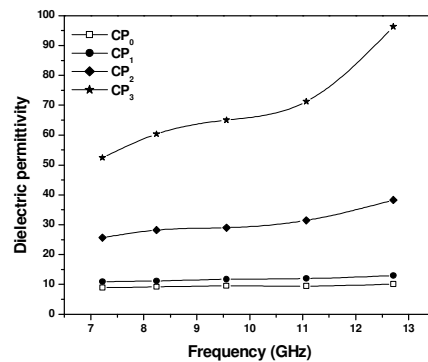


Fig. 6.24 Dielectric permittivity vs. frequency of CR/PANI composites in the X band

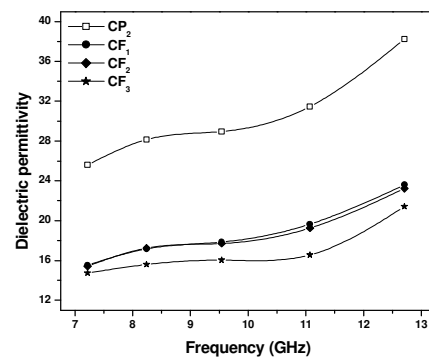


Fig. 6.25 Frequency dependence of dielectric permittivity of CR/PANI/PANI-N composites at X band frequencies

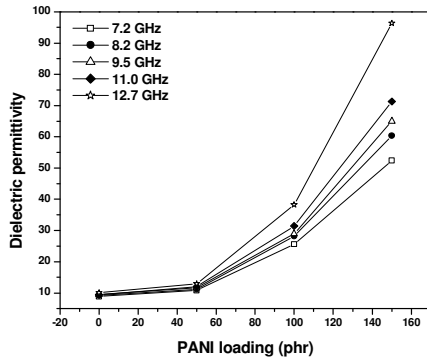


Fig. 6.26 Dielectric permittivity vs. PANI loading of CR/PANI CPCs at X band frequencies

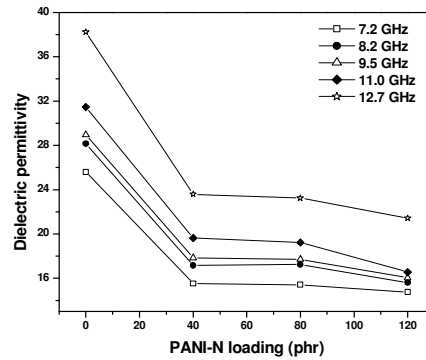


Fig. 6.27 Dielectric permittivity vs. PANI-N loading of CR/PANI/PANI-N CPCs at X band frequencies

### 6.3.1.6 Loss tangent of CR based CPCs

In heterogeneous dielectrics, the accumulation of virtual charge at the interface of two media having different dielectric constants  $\epsilon_1$  and  $\epsilon_2$ , and conductivities  $\sigma_1$  and  $\sigma_2$ , respectively, lead to interfacial polarization [25]. In the case of CR/PANI and CR/PANI/PANI-N composites, which consist of more than one phase, a charge build up can occur at the macroscopic interface as a result of the differences in the conductivity and dielectric permittivity of the components. This accumulation of charge then leads to field distortions and dielectric loss. This interfacial loss depends on the quantity of the weakly polar material present, as well as on the geometrical shape of its dispersion [26]. CR as a second phase in PANI, with a different dielectric permittivity and conductivity, contributes to the interfacial polarization and thereby a high dielectric loss is observed for the CPCs. Figs. 6.28 and 6.29 present the loss tangent vs. frequency graphs in X band of the P and F series composites of CR, respectively. The variation of loss tangent of the CPCs with PANI and PANI-N loading in the X band are presented in figs. 6.30 and 6.31.

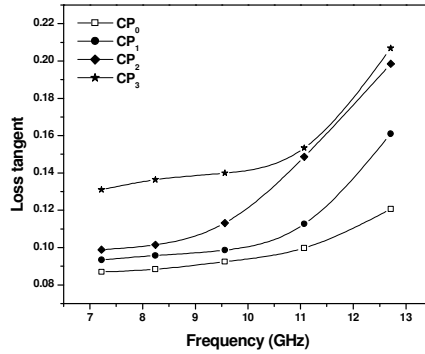


Fig. 6.28 Loss tangent vs. frequency of CR/PANI CPCs in the X band

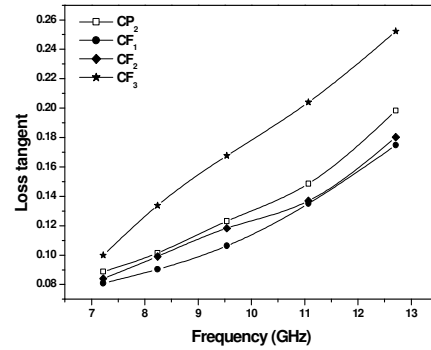


Fig. 6.29 Loss tangent vs. frequency of CR/PANI/PANI-N CPCs in the X band

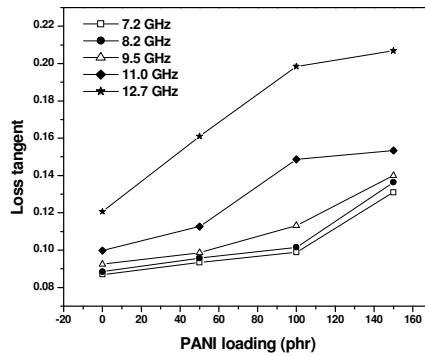


Fig. 6.30 Loss tangent vs. PANI loading of CR/PANI composites in the X band

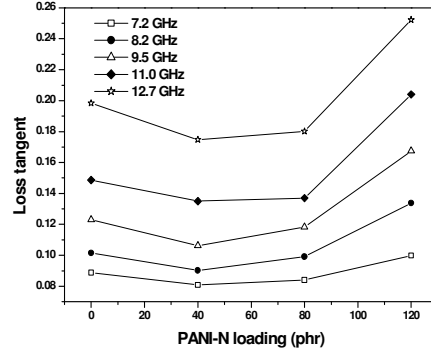


Fig. 6.31 Loss tangent vs. PANI-N loading of CR/PANI/PANI-N composites in the X band

### 6.3.1.7 Heating coefficient of CR based CPCs

Figs. 6.32 and 6.33 depict the frequency dependence of heating coefficient of CR/PANI and CR/PANI/PANI-N composites at X band frequencies. The variation of heating coefficient of the CPCs with loading are presented in figs. 6.34 and 6.35. The heating coefficient decreases with frequency and loading for the CPCs. Though the heating coefficient of F series CPCs increases with PANI-N loading initially, it shows lower values at higher loadings. CR gum vulcanizate has better heating properties than NR gum vulcanizate. At 12.7 GHz, the heating coefficient of CR and NR gum vulcanizates are 0.82 and 34.9, respectively. Hence CR based CPCs is a



better choice for high frequency heating applications. At 12.7 GHz and 150 phr PANI loading, CR has a  $J$ -value of 0.05 and at 120 phr PANI-N loading, the value is 0.18. The F series CPCs exhibits poorer heating properties than P series composites for both the matrices studied.

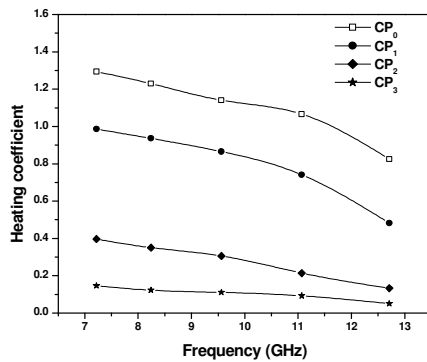


Fig. 6.32 Heating coefficient vs. frequency of P series composites of CR at X band frequencies

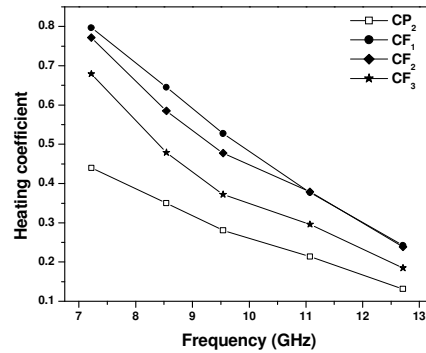


Fig. 6.33 Heating coefficient vs. frequency of F series composites of CR at X band frequencies

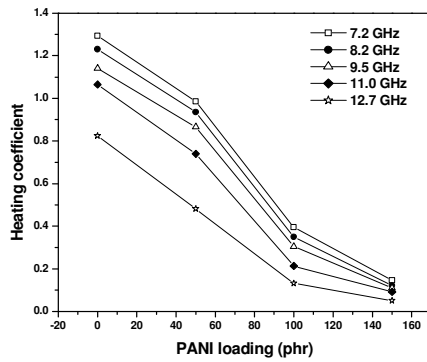


Fig. 6.34 Heating coefficient vs. PANI loading of CR/PANI CPCs

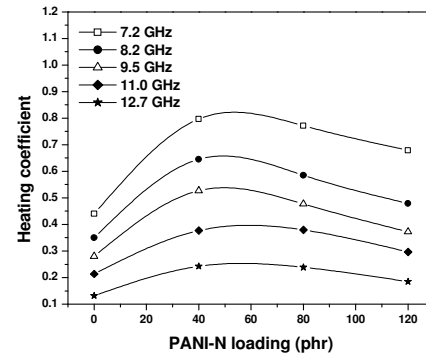


Fig. 6.35 Heating coefficient vs. PANI-N loading of CR/PANI/PANI-N CPCs

### **6.3.1.8 Conductivity, absorption coefficient and skin depth of CR based CPCs**

Conductivity and absorption coefficient of the CPCs increases with increase in frequency and loading as in the case of NR based CPCs. The skin depth decreases with both, frequency and loading, as expected. The dielectric properties of CR based CPCs at 12.7 GHz are presented in table 6.3. Comparing with table 6.2, it can be understood that conducting composites of CR exhibit superior microwave properties than composites of NR.

*Table 6.3 Dielectric properties of CR based CPCs at 12.7 GHz*

CPC	Conductivity (S/m)	Absorption coefficient (m <sup>-1</sup> )	Skin depth (m)
CP <sub>3</sub>	13.46	25.76	0.0012
CF <sub>3</sub>	3.71	31.6	0.0023

### **6.3.2 Electromagnetic interference shielding**

The EMI shielding efficiency (SE) of a composite material depends on many factors, including the filler's intrinsic conductivity, dielectric constant and aspect ratio [27, 28]. PANI and other conducting polymers are well known materials for shielding electromagnetic waves in both near and far fields [29, 30]. Polyaniline as well as other conducting polymers are excellent microwave absorbing materials [31]. The possibility of utilizing conducting polyaniline coated fibers for the application of EMI shielding is potentially very attractive, because they offer the promise of being low density, inexpensive and easily processable. Rubber radar absorbing materials (RAM) are also useful as shielding materials, which can reduce or weaken the EMI to a certain extent [32]. It is mainly made of a rubber matrix and some electromagnetic wave absorbents, which are usually conducting materials. The electromagnetic wave absorbents provide the necessary electromagnetic performances of the rubber RAM. Rubber is the carrier of the electromagnetic wave absorbents, which can make the RAM soft and flexible. Conducting rubber composites has inspired much interest because of their lightweight, hard corrosion,

good processability and easy control of conductivity. Since the shielding effectiveness at a specific wavelength depends up on the electrical conductivity of the shielding material and its ability to attenuate electrical and magnetic fields at the specific wavelength, there exists the possibility of producing selective filtering shielding. This part of the chapter deals with the measurement of EMI shielding efficiency of the conducting polymer composites prepared.

### 6.3.2.1 Theory of electromagnetic shielding

EMI shielding effectiveness is defined as the attenuation of an electromagnetic wave produced by its passage through a shield. It is measured as the ratio of the output energy to the input energy across the shielding material, expressed in decibels (dB), and is calculated according to [33, 34]

$$SE = 10 \log \frac{P_i}{P_0} = 20 \log \frac{E_i}{E_0} \quad (6.13)$$

where  $P_i$  and  $P_0$  mean the input and output energy, respectively and  $E_i$  and  $E_0$  represent the input and output electric fields, respectively. When a plane wave is incident on a shielding material, three phenomena such as reflection, absorption and multiple reflections are observed. Hence, the total shielding effectiveness is given as [34-37]

$$SE = SE_A + SE_R + SE_M \quad (6.14)$$

where  $SE_A$ ,  $SE_R$  and  $SE_M$  are the shielding efficiency due to absorption, reflection and multiple reflections in amplitude, respectively. Reflection loss arises due to the impedance mismatch between air and the sample at the frequency of interest. It is the result of interaction between conducting particles in the conducting material (free electron or vacancy) and the electromagnetic field and it has relationship with the value of  $\mu_r/\epsilon_r$ . Larger the conductivity and smaller the magnetic permeability, larger the reflection loss will be. This mechanism plays a major role in producing loss in EMI SE mechanisms. The absorption loss is due to the energy dissipation while the

electromagnetic wave interacts with the material. It is caused by the heat loss under the action between electric dipole and magnetic dipole in the shielding material and the electromagnetic field. Multiple reflection loss arises due to the inhomogeneity within the material. It occurs due to re-reflection from the shield. This loss is very low and is the correction term for the reflection loss [38]. They can be generally disregarded for shield thicknesses that are much greater than skin depth and only initial reflection and transmission at the left and right interfaces need to be considered. Higher the SE value in decibel, lesser will be the energy passing through the sample.

#### **6.3.2.2 Measurement technique**

EMI shielding measurements were performed using a wave-guide coupled to an Agilent Performance Network Analyzer E8362 B in the X band. The two test port cables of the network analyzer were connected via two wave-guide to coaxial adapters. The network analyzer was calibrated in the X band frequency range (7-13) GHz for the thru response. The sample was placed between the two sections of the wave-guide and the transmission loss was measured. This directly gave the shielding efficiency of the sample. The samples used were rectangular slices of dimensions  $2.3 \times 1 \times 0.18$  cm. The set-up is shown in fig. 6.36.



*Fig. 6.36 Set-up for EMI shielding measurements*

### 6.3.2.3 The shielding effectiveness

The EMI shielding effectiveness of the NR/PANI composites in the frequency range 7-13 GHz is shown in fig. 6.37. The gum NR has a very poor SE. The CPCs are found to have appreciable SE depending on loading of PANI and in turn, the conductivity. Increasing the percentage of conducting PANI in the host elastomer matrix increases the shielding effectiveness. There is only a nominal increase in SE on addition of 40 phr PANI (CPC NP<sub>1</sub>). On increasing the PANI loading to 90 phr (NP<sub>2</sub>), there is a sudden increase in SE from ~ 4 dB to ~ 15 dB at 7 GHz. At this loading, the SE is above 5 dB for the whole frequency range. Further additions do not have much effect on SE, indicating that the percolation has been achieved. A maximum SE of 16.1 dB is obtained for the 140 phr loaded CPC NP<sub>3</sub>.

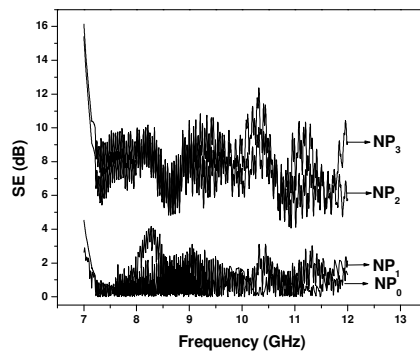


Fig. 6.37 Variation of SE with frequency of NR/PANI CPCs

The variation of SE of the PANI-N-loaded CPCs with frequency is shown in fig. 6.38. The perusal of the figure indicates that the SE decreases with PANI-N loading. But, at certain frequencies, the NF<sub>3</sub> composite has SE comparable to the 0 phr PANI-N-loaded NP<sub>2</sub> CPC. At 7 GHz, the NR/PANI/PANI-N composite NF<sub>1</sub> has a SE of 12.8 dB.

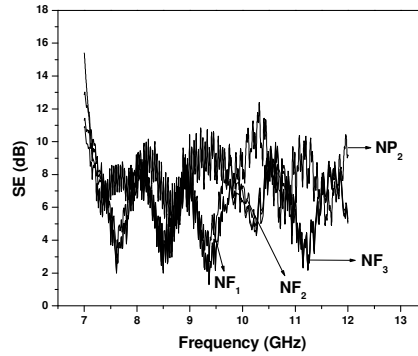


Fig. 6.38 Variation of SE with frequency of NR/PANI/PANI-N CPCs

The shielding efficiency of the CR/PANI composites increases with PANI loading (fig. 6.39). There is an appreciable increase in SE of the gum CR on 50 phr PANI incorporation ( $CP_1$ ). From there, a similar sharp increase is seen for 100 phr PANI-loaded CPC  $CP_2$ . On increasing the loading further, there is only a nominal increase, indicating the percolation limit. At this loading (100 phr), the SE is 21.3 dB at 7 GHz.

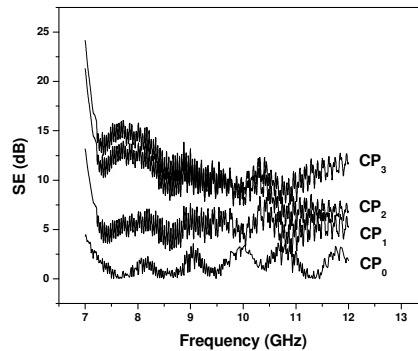


Fig. 6.39 Variation of SE with frequency of CR/PANI CPCs

The SE of CR/PANI/PANI-N CPCs vs. frequency is presented in fig. 6.40. The CPC  $CF_1$  gives higher SE than the CPC  $CP_2$ . But higher loadings of PANI-N decrease the

SE. At higher frequencies, CPC CF<sub>3</sub> gives higher SE than the other composites. Another feature to be noted is that the SE decreases with increase in frequency.

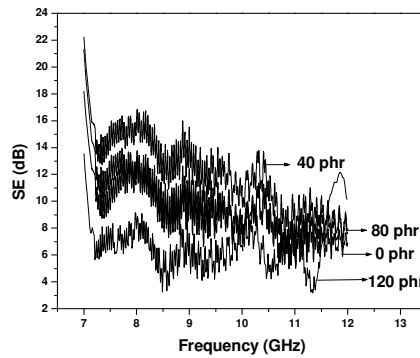


Fig. 6.40 Variation of SE with frequency of CR/PANI/PANI-N CPCs

Comparing these figures with *figs. 3.16* and *4.19*, the direct relationship between the conductivity and shielding efficiency can be followed. With increasing loading and hence conductivity, SE increases. The SE of the CPCs depends on the resistance loss and interfacial polarization loss as well. The conducting PANI particles are distributed in insulating matrix, which leads to interfacial polarization as discussed in previous sections [38]. As the PANI content increases, the size and number of the conducting islands increases, which contribute to stronger interfacial polarization of electromagnetic wave and larger electromagnetic loss [39].

The SE of the composites recorded at 7 GHz is tabulated in table 6.4. CPCs of CR show better shielding effectiveness than the NR CPCs. The CR composite with 150 phr PANI gives the highest shielding effectiveness of 24.1 at 7 GHz and, considering the NR composites, the maximum SE obtained is 16.1 at 140 phr PANI loading. In addition to the types of the fillers [40], the matrix [41] can also affect the behavior of EMI SE. From equations (6.13) and (6.14), the absorptivity, reflectivity and transmittivity can be computed. For the CR CPC CP<sub>3</sub>, the transmittivity, reflectivity and absorptivity are 0.003, 0.262 and 0.733, respectively. Thus, the contribution of absorption to the total EMI shielding effectiveness is much larger than that from reflection. The shielding efficiency of the CR based composite CP<sub>2</sub>

(21.3 dB) at 7 GHz is higher than that reported by a silicone rubber based PANI composite with same PANI loading [46]. In this report, Yuping *et al.* has reported a maximum SE of 19.3 dB at 1 and 1.5 GHz. Hence, the prepared CPCs can act as efficient shields of electromagnetic radiation. Even though the composites with lower SE cannot be used for shielding of electromagnetic waves, studies have shown that such composites can be used for static charge dissipation [42, 43]. Hence, the lower loaded CPCs with lower SE may be used for the dissipation of static charge.

*Table 6.4 Shielding efficiency of the CPCs at 7 GHz*

NR based CPCs	SE	CR based CPCs	SE
NP <sub>0</sub>	2.62	CP <sub>0</sub>	4.3
NP <sub>1</sub>	4.52	CP <sub>1</sub>	13.1
NP <sub>2</sub>	15.4	CP <sub>2</sub>	21.3
NP <sub>3</sub>	16.1	CP <sub>3</sub>	24.1
NF <sub>1</sub>	12.8	CF <sub>1</sub>	22.2
NF <sub>2</sub>	11.3	CF <sub>2</sub>	18.1
NF <sub>3</sub>	10.8	CF <sub>3</sub>	13.5

## 6.4 Conclusions

The dielectric properties at microwave frequencies of the prepared CPCs were measured in the X and S band frequencies using the cavity perturbation technique. The dielectric permittivity and loss tangent of the composites increase with frequency and loading for both NR and CR based CPCs except for the composites of F series, which show a decreasing trend with loading. In the microwave range, better dielectric properties are exhibited by the CR composites, compared to the NR composites. The CR based composites has a dielectric permittivity of 96 at 150 phr PANI loading and at 12.7 GHz. At the same frequency, the NR based composite gives a permittivity of 35 at 140 phr PANI loading. The F series CPCs shows lower permittivity values compared to composites of P series. The 40 phr PANI-N-loaded CPC of CR records a dielectric permittivity of 23.6 whereas the NR based CPC gives a value of only 11.6. With frequency and loading, the loss tangent of the composites



increases. CPCs of CR are a better choice for high frequency heating applications. At 12.7 GHz and 150 phr PANI loading, CR has a  $J$ -value of 0.05 and at 120 phr PANI-N loading, the value is 0.18. The F series CPCs exhibits poorer heating properties than P series composites for both matrices studied. The CPCs are found to have appreciable SE depending on loading of PANI and in turn, the conductivity. The SE of the CPCs depends on the resistance loss and interfacial polarization loss.

## References

1. Unsworth J, Kaynak A, Lunn B, Beard GE. J Mat Sci 1993;28:3307.
2. Singh P, Babbar VK, Razdan A, Srivastava SL, Goel TC. Mater Sci Eng B 2000;78:70.
3. Xinagcheng Li, Gong R, Feng Z, Yan J, Shen X, He Huahui. J Am Ceram Soc 2006;89:1450-1452.
4. Sung-Soo Kim, Sun-Tae Kim, Yeo-Choon Yoon, Kyung-Sub Lee. J Appl Phys 2005;97:10F905.
5. Kim SS, Jo SB, Gueon KI, Choi KK, Kim JM, Churn KS. IEEE Trans Mag 1991;27(6):5462-5464.
6. Verma A, Mendiratta RG, Goel TC, Dube DC. J Electroceram 2002;8:203.
7. Musal Jr HM, Hahn HT. IEEE Trans Mag 1989;25:3851.
8. Naito Y, Suetaki K. IEEE Transactions on Microwave Theory and Techniques, MTT-19 1971;65.
9. Barba AA, Lamberti G, Matteo d' Amore, Domenico Acierno. Polym Bull 2006;57:587.
10. Lee CY, Song HG, Jang KS, Oh EJ. Synth Met 1999;102(1-3):1346-1349.
11. Luo XCH, Chuan DDL. Composites Part B 1999;30(3):227-231.
12. Nakamura E, Furuichi J. J Phys Soc Japan 1960;15(11):1955-1960.
13. Champlin KS, Krongard RR. IRE Trans Microwave Theory Tech 1961;MTT9:545-551.
14. Kupfer K, Kraszewski, Knochel R. Sensors Update Vol 7 and Microwave sensing of moist materials, food and other dielectrics. Wiley-VCH, Germany, 2000;186-209.

15. Ku CC, Liepins R. Electrical properties of polymers: Chemical principles. Hanser Publishers, Munich, 1987, p. 92.
16. Ezquerra TA, Kremmer F, Wegner. Dielectric properties of heterogeneous materials: Progress in electromagnetic research. Vol 6, Elsevier, New York, 1992.
17. Bradford LS, Carpentier MH. The microwave engineering handbook, Chapman and Hall, London, 1993.
18. Stephen CW, Frederic HL. Microwaves made simple: Principles and applications. United States Bookcrafters, Chelsea, 1985.
19. Abbas SM, Chandra M, Verma R, Chatterjee R, Goel TC. Composites Part A; 2006;37(11):2148-2158.
20. Dimri MC, Kashyap SC, Dube DC. Ceramic International 2004;30:1623.
21. Koops CG. Phys Rev 1951;83:121.
22. John H, PhD Thesis, Cochin University of Science and Technology, India, 2003.
23. MacCallum RJ, Vincent CA. Polymer electrolyte reviews II, Elsevier Applied Science Publishers Ltd, London and New York, 1987, chapter 2.
24. Kyritsis A, Pissis P, Grammatikakis J. J Polym Sci Part B Polym Phys 1955;33:1737-1750.
25. Maxwell JC. Electricity and magnetism. Oxford University Press, Oxford, 1892.
26. Sillars RW. IEEE Journal 1937;80:371.
27. Joo J, Lee CY. J Appl Phys 2000;88:513.
28. Chung DDL. Carbon 2001;39:279.
29. Olmedo L, Hourquebie P, Jousse F. Adv Mater 1993;5:373.
30. Joo J, Epstein AJ. Appl Phys Lett 1996;68:894.
31. Chandrasekhar P, Naishadhan K. Synth Met 1999;105:115.
32. Das NC, Khastgir D, Chaki TK, Chakraborty A. Composites Part A 2000;31:1069-1081.
33. Ott HW. Noise reduction techniques in electronic systems. Wiley, New York. 2<sup>nd</sup> edition, 1988.

34. Hund E. Microwave communications-Components and circuits. McGraw Hill, New York, 1989.
35. Colaneri NF, Shacklette LW. IEEE Trans Instrum Meas 1992;41:291.
36. Joo J, Epstein AJ. Appl Phys Lett 1994;65:2278.
37. Schulz RB. IEEE Trans Elec Comp 1968;EMC-10:95.
38. Kayanak A. Mater Res Bull 1996;31(7):845-860.
39. Yuping D, Shunhua L, Hongtao G. Sci Technol Adv Mater 2005;6:513-518.
40. Osaka Z, Kuwabara S. J Mater Sci 1987;22:4381.
41. Osawa Z, Kuwabara S. Polym Degrad Stab 1992;35:33.
42. Koul S, Chandra R, Dhawan SK. Polymer 2000;41:9305-9310.
43. Dhawan SK, Singh N, Rodrigues D. Sci Technol Adv Mater 2003;4:105-113.

# Chapter 7

## Summary and conclusions

Among conducting plastics, polyaniline stands out due to its interesting properties. It is one of the so-called doped polymers, in which conductivity results from a process of partial oxidation or reduction. Polyaniline compounds can be designed to achieve the required conductivity for a given application. The resultant blends can be as conductive as silicon and germanium or as insulating as glass. Another advantage is that, it is both melt and solution processable. This means that the compound can be easily mixed with conventional polymers and that it is easy to fabricate polyaniline products into required shapes.

The main target of conductive polymer technology development has been to combine the electrical and optical properties of these materials with the mechanical and processability properties of commodity bulk polymers. New conductive materials that offer significant application potential as substitutes, and new products having properties difficult or impossible to achieve by existing materials, can now be produced.

Textile materials as substrates and reinforcing materials for many polymers have wide industrial applications. In the present venture, an attempt has been made to prepare conducting composites by adding conducting polyaniline coated short Nylon fiber in insulating elastomer matrices. Polyaniline coated short Nylon fiber provides simultaneous reinforcement and conductivity to the elastomers. Two different elastomers, nonpolar natural rubber (NR) and polar chloroprene rubber (CR) were selected due to their industrial importance and attractive properties.

Conducting fibers were prepared by *in situ* polymerization of aniline on Nylon fibers. An etching treatment using chromic acid was done prior to *in situ* polymerization on

the fibers. The etching treatment was found to be effective in improving the adhesion of PANI to the fiber surface and conductivity. The etching conditions were optimized with reference to concentration of chromic acid and time of etching. The etching process involved hydrolysis of the amide linkages. By giving an etching treatment for 4 h, 8 times increase in conductivity was attained. The etching process roughened the fiber surface, reduced the strength of the fiber and resulted in marginal decrease in the crystallinity and thermal stability. PANI deposition on the etched fibers did not further lower its strength.

The conducting polyaniline coated short Nylon fiber (PANI-N) thus prepared was employed in the preparation of conducting polymer composites (CPCs) with two different elastomers, NR and CR. Elastomer composites with sufficient mechanical properties could be prepared by mechanical mixing. Addition of pristine PANI to NR accelerated the cure reaction whereas; the cure reaction of CR was slightly retarded. The cure reaction of both elastomers was accelerated by the addition of PANI-N. The shear modulus and viscosity of the CPCs increased with both PANI and PANI-N addition in both matrices. The cure reaction followed first order kinetics. Higher loadings caused agglomeration, which was predominant for PANI-loaded composites. The tensile strength of the CPCs could be improved by adding PANI coated short Nylon fibers. The addition of PANI coated short Nylon fiber not only brought about a significant improvement in the mechanical properties, but also increased the conductivity and thermal stability. The PANI particles and the uniformly oriented fibers linked with each other to form conductive chains or network in the matrix. The thermal degradation process followed first order kinetics.

In the latter part of the work, the dielectric properties of PANI and the CPCs were measured in the frequency range 0.1 to 8 MHz and in the temperature range 303 to 393 K. The dielectric permittivity of pristine PANI decreased with increase in frequency revealing that PANI exhibit interfacial polarization at low frequencies. At low frequencies and temperatures, the loss factor of pristine PANI decreased linearly with increasing frequency suggesting that at these frequencies and temperatures, DC conductivity process is more significant than interfacial polarization. The dielectric permittivity of the CPCs decreased with frequency owing to a decrease in interfacial

polarization and increased with PANI and PANI-N loading. With increasing temperature, it increased, reached a maximum value and then decreased. At 303 K and 0.1 MHz, a dielectric permittivity as high as 177 was obtained for 150 phr PANI-loaded CR CPC, which was almost double the value obtained for NR composite. The dielectric dispersion could be fitted well with the well known empirical equations. The effective permittivity of the CPCs can be predicted by utilizing one of these equations.

The conductivity in the CPCs is mainly due to hopping of charge carriers. AC conductivity increased with increase in frequency and temperature due to an increase in hopping conduction. The AC conductivity was found to be higher for CR based CPCs compared to NR composites. Better dielectric properties were exhibited by CR based composites due to its polar nature. Thus, the dielectric properties of the rubber matrix can be modified by appropriate loadings of PANI and PANI-N according to the temperature and frequency of interest.

In the last part, the dielectric properties at microwave frequencies of the CPCs were measured in the X (7-13 GHz) and S (2-4 GHz) band frequencies. The dielectric permittivity and loss tangent of the composites increased with frequency and loading for both NR and CR based CPCs except for the PANI-N-loaded composites, which showed a decreasing trend with loading. In the microwave range, better dielectric properties were exhibited by the CR based composites, compared to the NR composites. The PANI-N composites showed lower permittivity values compared to PANI CPCs. The loss tangent of the CPCs increased with increasing frequency and loading. The PANI-N-loaded CPCs exhibited poorer heating properties than PANI-loaded composites for both matrices studied.

The world is now facing a serious environmental pollution that we cannot see, hear or feel i.e. electromagnetic interference (EMI). Since the CPCs had good microwave absorption properties, the EMI shielding effectiveness of the CPCs were also determined in the range 7-13 GHz. The CPCs were found to have appreciable shielding effectiveness depending on loading of PANI and in turn, the conductivity.

But compared to PANI composites, the shielding effectiveness is found to be less for the PANI-N composites.

The use of polyaniline coated Nylon fiber in the conducting elastomer composites can certainly improve the mechanical properties of the composites. But the dielectric properties decrease on addition of polyaniline coated Nylon fiber. Better dielectric properties were observed at the highest polyaniline loading employed in both elastomers. But lower loadings of the conducting fiber gave dielectric properties very close to these polyaniline loaded composites. Hence preparation of polyaniline composites with low loadings of the conducting fiber can result in composites with desirable dielectric and microwave characteristics with good reinforcement.

## *Index of abbreviations and symbols*

---

ABS	Acrylonitrile-butadiene-styrene
AC	Alternating current
AFM	Atomic force microscopy
ASTM	American society for testing and materials
ATR	Attenuated total reflectance
CBH	Correlated barrier hopping
CPC	Conducting polymer composite
CR	Chloroprene rubber
CRI	Cure rate index
DBSA	Dodecyl benzene sulfonic acid
DC	Direct current
DPMB	Direct polymerization in mixed bath
DPSB	Direct polymerization in separate bath
DSC	Differential scanning calorimetry
DTG	Differential thermogravimetry
EMI	Electromagnetic interference shielding
EPDM	Ethylene-propylene-diene monomer
ESCA	Electron spectroscopy for chemical analysis
ESD	Electrostatic charge dissipation
ESR	Electron spin resonance
FTIR	Fourier transform infrared spectroscopy
ICP	Intrinsically conducting polymer
LabVIEW	Laboratory virtual instrument engineering workbench
MIC	Microwave-integrated circuit
ML	Mooney viscosity-large rotor



### *Abbreviations and symbols*

---

NBR	Acrylonitrile butadiene rubber
NR	Natural rubber
PANI	Polyaniline
PANI-N	Polyaniline coated etched short nylon fiber
PET	Poly(ethylene terephthalate)
phr	Parts per hundred rubber
PMMA	Poly(methyl methacrylate)
PMN-PT	Lead magnesium niobate-lead titanate
PPy	Polypyrrole
PTh	Polythiophene
PU	Polyurethane
PVA	Poly(vinyl alcohol)
PVDF	Poly(vinylidene fluoride)
RAM	Radar absorbing material
RCS	Radar cross section
RL	Reflection loss
RPA	Rubber process analyzer
SAXS	Small angle X-ray scattering
SBR	Styrene-butadiene rubber
SBS	Styrene-butadiene-styrene
SCLC	Space charge limited conduction
SE	Shielding effectiveness
SEM	Scanning electron microscopy
SIPN	Semi interpenetrating network
TG	Thermogravimetry
TGA	Thermogravimetric analysis
TSA	Toluene sulfonic acid
UTM	Universal testing machine
VRH	Variable range hopping
XPS	X-ray photoelectron spectroscopy
XRD	X-ray diffraction analysis

A	Area/Pre-exponential factor
c	Velocity of light
C	Capacitance
d	thickness
dB	decibels
D	Torque
$D_{\max}$	Maximum torque
$D_{\min}$	Minimum torque
$d\Omega$	Complex frequency shift
E	Electric field
$E_a$	Activation energy
f	Frequency
$G_{\text{spec}}$	Specific conductivity
$\Delta H_f$	Heat of fusion
I	Current
J	Current density/Heating coefficient
k	Boltzmann's constant/Rate constant
l	Length
L	Lee's parameter
$M_r$	Relative modulus
$m_f$	Mass fraction of filler
$m_p$	Mass fraction of polymer
n	Order of reaction
P	Power
$pK_a$	Acid dissociation constant
q	Quantity of electricity
Q	Quality factor
r	Rate of reaction
R	Universal gas constant
t	Time
T	Temperature

### *Abbreviations and symbols*

---

$T_{10}$	Scorch time
$T_{90}$	Cure time
$T_m$	Melting point
$\tan \delta$	Loss tangent
$V$	Voltage
$V_f$	Volume fraction of filler
$V_c$	Volume of the cavity
$V_s$	Volume of sample
$W_f$	Weight fraction of filler
$Z_{in}$	Impedance
$\alpha_f$	Filler specific constant/Absorption coefficient
$\beta$	Heating rate
$\varepsilon^*$	Complex permittivity
$\varepsilon'$	Real part of complex permittivity
$\varepsilon''$	Imaginary part of complex permittivity
$\eta_r$	Relative viscosity
$\mu$	Magnetic permeability
$\pi$	pi
$\sigma$	Conductivity
$\tau$	Relaxation time
$\chi_c$	Degree of crystallinity
$\omega$	Angular frequency

## *Author index*

---

- Abraham D 65, 69  
Anbarasan R 35, 42, 68  
Armes SP 11, 34, 69
- Balke ST 81, 100  
Byun SW 35, 66, 68
- Cao Y 11, 32, 34, 69, 168  
Carroll B 80, 100  
Chandra R 19, 35, 37, 196  
Chan JH 81, 100  
Chwang CP 129, 147, 165  
Coats AW 82, 100
- De Paoli MA 16, 36, 37, 100, 101, 125  
Dhawan SK 19, 35, 37, 38, 39, 196  
Diaz AF 3, 32  
Dutta P 129, 165
- Faez R 37, 90, 100, 101, 125, 113  
Freeman ES 80, 100  
Genies EM 42, 62, 67  
Goswamy A 132, 166
- Green AG 3, 32
- Haba Y 50, 68  
Heeger AJ 3, 15, 32, 33, 34, 68, 69, 168
- John 176, 195  
Jonscher AK 155, 167  
Jozefowicz M 3, 32
- Kim B 14, 36  
Kim SK 42, 68  
Koul S 18, 19, 35, 37, 196  
Koops CG 166, 176, 195  
Kupfer K 173, 194
- Lee BL 76, 87, 100, 106, 111  
Lennartz W 92, 101  
Letheby H 3, 32  
Leyya ME 18, 19, 37, 130, 166  
Logan JA 3, 32
- MacDiarmid AG 3, 32, 33, 34, 69, 165  
Macedo PB 138, 166  
Maxwell J 27, 141, 150, 166  
Mecoy HN 3, 6  
Moon YB 53, 69  
Moore WC 3, 32  
Mott NF 22, 33, 37, 156, 167
- Oh KW 35, 43, 51, 58, 62, 64, 66, 68, 69
- Pinho MS 20, 37  
Poughet JP 52, 69  
Pud A 62, 69
- Ramasasthry C 133, 166  
Ram MS 52, 68  
Redfern JP 82, 100  
Reghu M 156, 168

*Author index*

---

Shirakawa H 3, 32, 33  
Soares BG 20, 37, 166  
Survile R 3, 32

Tabellout M 69, 129,  
166

Wagner K 27, 150,  
166  
Willstatter 3, 32  
Wolf S 77, 100, 106  
Woodhead AE 3, 32

Yigit S 16, 36  
Yuping D 193, 196

Zilberman M 92, 101  
Zoppi R 16, 36

## *Subject index*

---

- Absorption Coefficient 174, 182, 183, 187, 205  
AC conductivity 131, 153-164, 199  
Adhesion 14, 41, 42, 43, 56, 62, 67, 104, 113, 114, 116, 128, 198  
Atomic polarization 25, 26, 175
- Bipolaron 8, 9  
Blends 11, 15-20, 23, 60, 88, 91, 92, 128-130, 147, 197
- Calendering 17  
Cavity perturbation 171  
Chloroprene 20, 103, 104, 130, 161  
Chemical polymerization 10, 17, 20, 42  
Complex permittivity 24, 130, 134, 136, 138, 169, 173, 174, 182  
Composites 1, 2, 11-13, 14-20, 23, 30, 48, 60, 62, 72, 73, 84, 85, 88, 107, 128, 129, 130  
Conducting fibers 1, 2, 12, 13, 31, 42  
Conduction 3, 7-10, 13, 20-29, 31, 116, 130, 153, 155, 160, 182  
Cure  
    Kinetics 75, 85, 106, 109  
    Rate constant 75, 76, 86, 106, 110  
    Rate index 75, 84, 86, 106, 107, 110  
    Time 74, 75, 83, 84, 106, 107, 110
- DC conductivity 50, 61, 78, 92, 92, 117, 129, 137, 138, 153, 154, 178  
Degree of crystallinity 43, 49, 59, 60, 66, 67  
Dielectric  
    Behavior 23, 128, 130, 135, 140  
    Constant 16, 20, 24, 27, 127-131, 138, 139, 142, 144, 149, 170, 174, 184, 187  
    Loss 174, 178, 182, 184  
    Loss factor 24, 130, 136, 182  
    Permittivity 24, 25, 131, 134-150, 174-180, 183, 184, 193  
Differential scanning calorimetry 17, 49, 53, 54, 58, 59, 60, 66  
Dipolar polarization 25, 175  
Dipolar relaxation 138
- Elastomers 15, 72, 103, 104, 157  
Elastomer composites 15-20, 72, 73, 84  
Electric modulus 138, 139

## *Subject index*

---

- Electrochemical blending 17
- Electrochemical coating 13
- Electronic polarization 25, 26, 176
- Electropolymerization 13, 17
- Elongation at break 19, 89, 114, 115
- EMI shielding 13, 28, 29, 30, 170, 187-193
- Etching 43, 44, 54-63, 65
  
- Filler dispersion 76, 87, 110
- Filler specific constant 77, 87, 88, 111, 112
- Grafting 13, 42
  
  
- Heating coefficient 174, 180, 181, 185
- Heat of fusion 49, 59, 60, 66, 67
- Hopping 9, 20, 22, 23, 129, 155-157, 159, 160, 162, 164
  
  
- In situ* polymerization 13, 17, 41, 43, 44, 60, 67, 129, 197
- Interfacial polarization 25-27, 129, 130, 134, 137, 138, 141, 146, 148, 175, 176, 184, 192
- Ionic polarization 25
- IR 42, 47, 51, 52, 57, 63
  
  
- Lichtenecker equation 150
- Loss tangent 174, 175, 178, 179, 184, 185
  
  
- Maxwell-Wagner model 134, 136, 137, 138, 141, 146, 154, 160,
- Mechanical properties 11, 14, 15, 17, 45, 73, 77, 88, 105, 127, 128,
- Mechanical mixing 17, 20, 130
- Melting temperature 49, 59, 60, 66, 67
  
- Melt mixing 19
- Microwave
  - Absorbers 28, 30, 169
  - Applications 28
  - Characterization 173
  - Conductivity 182
  - Heating 28, 187
- Microwaves 30
- Modulus 72, 73, 75, 76, 84, 87, 89, 90, 108, 115
- Morphology 2, 45, 50, 51, 55, 62, 77, 90, 91, 92, 116
  
- Natural rubber 16, 71-73, 84
  
  
- Orientation polarization 26, 140, 145
  
  
- Plasma treatment 43, 62
- Polarization 24-27, 129, 140, 145, 146, 170, 174
- Polaron 8, 9
- Polyaniline
  - Conduction 7, 9, 10, 13, 20-23
  - Charge storage 7
  - Doping 6, 7, 9, 10, 13
  - Structure 3, 4, 7, 8, 9
  - Synthesis 2, 10, 11
- Polymerization 2, 3, 5, 10, 11, 12, 14, 41, 42, 43, 44, 50, 54, 74
- Protonation 4-6, 9, 10
  
  
- Quality factor 173, 175
  
  
- Radar absorbing materials 28, 30, 187

SCLC 21  
Scorch time 75, 83, 84, 106, 107,  
108  
SEM 17, 45, 46, 50, 55, 78, 90, 91,  
106, 116  
Skin depth 175, 182, 183, 187, 189  
Solution mixing 17, 129  
Static charge dissipation 13, 16,  
193  
Surface coating 13, 14

Tear strength 78, 88, 89, 90, 114  
Tensile strength 19, 45, 60, 88, 89,  
112, 113, 114, 115, 116, 120  
TGA 48, 53, 58, 59, 64, 78, 79, 93,  
95, 96, 120, 121  
Thermal degradation kinetics 96,  
121  
Torque 75-77, 82-85, 88, 90, 107,  
108, 112

Viscosity 11, 76, 85, 87, 90, 98,  
108

Wave-guide 28, 171-173, 189  
Wet spinning 15

XPS 46, 56, 57  
XRD 47, 48, 52, 58, 64





## *Publications and presentations*

---

1. An elastomeric conducting composite based on polyaniline coated nylon fiber and chloroprene rubber  
A. Saritha Chandran, Sunil K. Narayanankutty  
***European Polymer Journal*** 2008;44(7):2418-2429.  
DOI: 10.1016/j.eurpolymj.2008.05.012
2. Dielectric behaviour of polyaniline/polyvinyl chloride/nylon fiber composites at microwave frequencies  
A. Saritha Chandran, Sunil K. Narayanankutty  
***Polymer-Plastics Technology and Engineering*** 2008 (*in press*).
3. Preparation and characterization of conducting nylon-6 fibers  
A. Saritha Chandran, Sunil K. Narayanankutty  
***Composites Part A: Applied Science and Manufacturing*** (*communicated*).
4. Polyaniline coated short nylon-6 fiber/natural rubber conducting composite  
A. Saritha Chandran, Sunil K. Narayanankutty  
***European Polymer Journal*** (*communicated*).
5. CR/PANI coated nylon fiber conducting composites  
Saritha Chandran A., Sunil K. Narayanankutty. International symposium, Polymers-Prospect and Challenges, **POLYMSYM'08**, April 4-5, 2008, National Institute of Technology, Calicut, India.

6. Cure and mechanical properties of PANI-PANI coated nylon fiber-CR conducting composites  
Saritha Chandran A., Sunil K. Narayanankutty. International Conference on Materials Science Research and Nanotechnology, **ICMSRN-2008**, February 27-29, 2008, Department of Physics, Mother Teresa Women's University, Kodaikanal, India.
7. Conducting nylon fibers based on polyaniline  
Saritha Chandran A., Sunil K. Narayanankutty. International Conference **POLYCHAR-16**, World Forum on Advanced Materials, 17-21 February 2008, World Unity Convention Center, Lucknow, India.
8. Preparation of conducting nylon fibers with special reference to the effect of etching treatment  
Saritha C. A., Kutty S. K. N. 17<sup>th</sup> Annual General Meeting of Materials Research Society of India- **AGM-MRSI**, February 13-15, 2006, University of Lucknow, India.
9. Preparation of polyaniline coated nylon fibers-Effect of etching medium  
Saritha Chandran A., Sunil K. N. Kutty. National Conference on Frontiers in Polymer Science and Technology- **POLYMER 2006**, February 10-12, 2006, Indian Association for the Cultivation of Science, Jadavpur, Kolkata, India.